Fakultät für Medizin

Friedrich-Schiedel Institut fur Neurowissenschaften

Analysis of cortical processing of sound-evoked inputs: from single spines to cortical populations

Diana Deca

Vollständiger Abdruck der von der Fakultät für Medizin der Technischen Universität München zur Erlangung des akademischen Grades eines

Doctor of Philosophy (Ph.D.)

genehmigten Dissertation.

Vorsitzende/r: Univ.-Prof. Dr. Claus Zimmer

Betreuer/in: Univ.-Prof. Dr. Arthur Konnerth

Prüfer der Dissertation:

1. apl. Prof. Dr. Helmuth Adelsberger

2. Prof. Dr. Israel Nelken, The Hebrew University of Jerusalem / Israel

Die Dissertation wurde am 03.08.2015 bei der Fakultät für Medizin der Technischen Universität München eingereicht und durch die Fakultät für Medizin am 18.09.2015 angenommen.

Abstract

Mammalian cortical neurons compute sensory information that arrives through numerous synaptic inputs located on their dendrites. Single neurons integrate these functional inputs into one functional output which is more or less tuned to sensory stimulation. How does a neuron compute all these functional inputs? How does a functional neuronal network compute? These two questions are fundamental to neuroscience and other fields as they could represent the starting point for reconstructing brain function.

In order to better understand this process, we have combined in vivo two photon calcium imaging and electrophysiology in order to look at the inputs and the outputs of layer 3 cortical neurons in the mouse auditory cortex at the same time. Sound-evoked dendritic events could be observed also in the absence of firing as well as preceding the firing output. Furthermore, population imaging in unanesthetized mice revealed the tonotopy in deep cortical layers.

Together with my colleagues, I have established the method of targeted multi-cell electroporation (TMTE) which allowed us to explore tonotopy in deeper cortical layers as well as single cell electroporation combined with cell-attached recordings which then allowed us to explore the connection between spine and dendrite signaling in vivo together with the cell's output.

Table of contents

1) Introduction

1.1. What is functional computation?

Mammals have the ability of processing information coming from the environment, and a large part of this processing is done by cortical neurons. Information arrives at single neurons through thousands of excitatory and inhibitory inputs. Some of these inputs have been observed during sensory stimulation, and for these reason I will call them functional inputs. Single neurons have the ability of integrating all these functional inputs into one single output. The exact way in which a single neuron performs such a computation is not completely known. Other units of computation in the brain have also been postulated, such as neuronal networks, dendrites, and even spines. They are all interconnected parts of a computing machine, and I will refer to each of these computational units in the following chapters. In the results section, I will show how each of these units performs different operations, and how these can be examined by using different methods.

1.2. The neuron as a computational unit

Many of the difficulties in understanding the functioning of a neuron stem from the fact that a neuron must be conceptualized at more than one single level at once. On the one hand, there is electrical conductance and resistance and one could oversimplify a neuron as a mere switch that selectively allows electrical signals coming from other neurons, and at the same time there is diffusion of different molecules through various biochemical processes. This complex biophysical machinery which we call a neuron allows for computation of incoming sensory signals into a single output. Things get even more complicated at the level of neuronal populations and integration of sensory stimuli.

1.3. Input processing in dendritic spines

Excitatory inputs usually arrive at dendrites of cortical excitatory neurons via dendritic spines, which are highly plastic small protrusions arising from the dendritic shafts. These dendritic spines also take an active part in input integration by means

of complex biochemical processes.

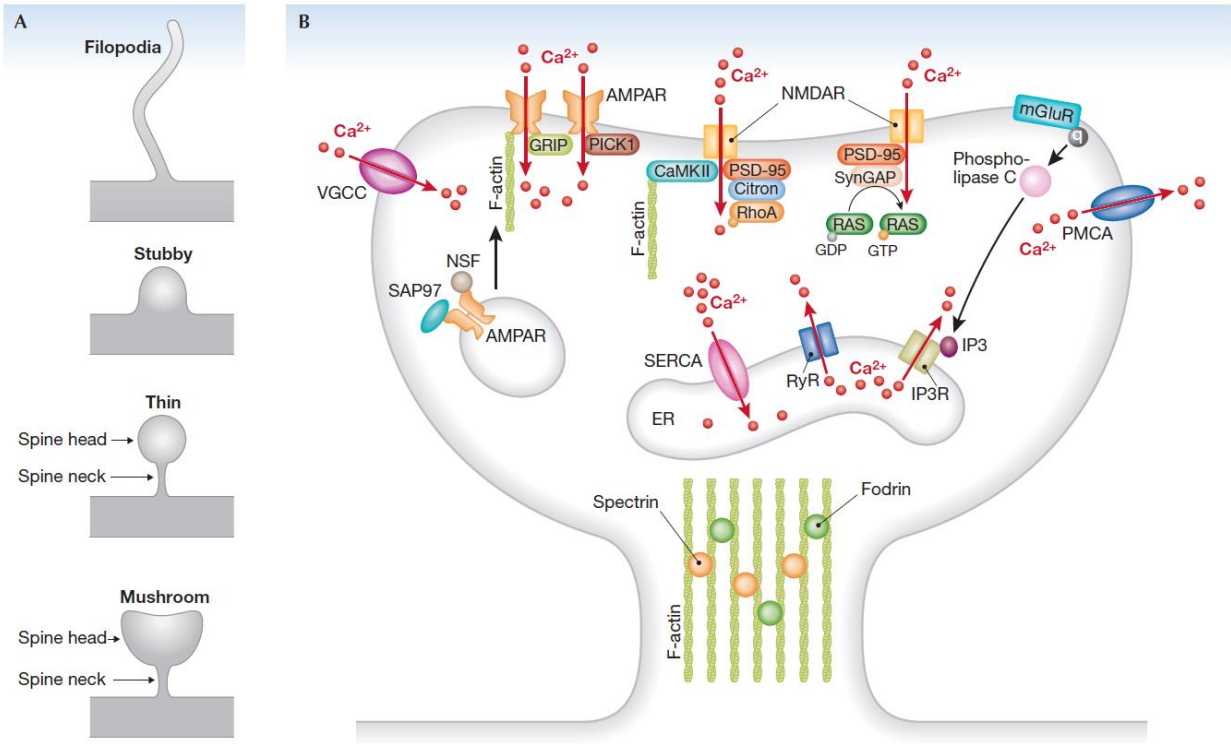

(adapted from Rochefort and Konnerth[1])

Fig.1. Structural and molecular organization of spines. (A) Schematic of four categories of spine morphology. The same spine can take any of these four shapes due to plasticity changes. (B) Sketch of main receptors and signaling molecules which take a role in Ca^{2+} signaling in dendritic spines. The red arrows mark the direction of Ca^{2+} Ions. Glossary: AMPAR, α-amino-3-hydroxy-5-methyl-4-isoxazolepropionic acid receptor; CaMKII, Ca^{2+} /calmodulin-dependent kinase II; ER, endoplasmic reticulum; GAP, GTPase-activating protein; GRIP, glutamate-receptor-interacting protein; IP3(R), inositol trisphosphate (receptor); mGluR, metabotropic glutamate receptor; NMDA, N-methyl-D-aspartate; NSF, N-ethylmaleimide sensitive factor; PICK1, protein interacting with C kinase; PMCA, plasma membrane Ca^{2+} -ATPase; PSD, postsynaptic density; RyR, ryanodine receptor; SAP97, synapse-associated protein 97; SERCA, sarco/endoplasmic reticulum Ca^{2+} -ATPase; VGCC, voltage-gated calcium channel.

Dendritic spines contain various types of Ca^{2+} channels. Dendritic spines have been observed for the first time in 1888 by neuroanatomist Ramon y Cajal[2]. Since then, many studies have been dedicated to a better understanding of their structure and function[3]. Their function could only be speculated until recently, when the first

stimulation-induced calcium transients were observed in dendritic spines in the living animal[4].

Understanding the main biochemical structure behind Ca^{2+} signaling in dendritic spines is important for understanding calcium imaging in vivo. Ca^{2+} is a secondary messenger which regulates the function (and in the long term the structural changes) of dendritic spines.

Ca^{2+} entry is first achieved through two main classes of ionotropic glutamate receptors present in most neuronal cell types that mediate postsynaptic calcium influx in dendritic spines are NMDA receptors and AMPA receptors. NMDA receptors are largely responsible for the observed Ca^{2+} transients observed in vivo. In most cases, dendritic spines are depolarized first by AMPA receptors, which remove the extracellular Mg^{+} ions that normally block NMDA receptor channels, which then continue to depolarize and allow for more Ca^{2+} ions to enter. Voltage-gated calcium channels (VGCCs) can further amplify this depolarization and generate Ca^{2+} entry together with sodium channels and are categorized into high (HVA) and low voltage-activated (LVA) channels. In the dendritic spines of most central neurons, VGCCs are activated by backpropagating action potentials (bAPs) and also by dendritic spine depolarization. Dendritic spines, therefore, can detect the coincidence of pre- and post- synaptic activity in an NMDA receptor dependent fashion.

Ca^{2+} release, on the other hand, begins with metabotropic glutamate receptors (mGluRs) which are 7-transmembrane Gprotein-coupled receptors. As soon as mGlur1 receptors are activated by glutamate binding, phospholipase C begins to mediate the generation of inositol trisphosphate (IP3), which then binds to receptors in the endoplasmic reticulum (ER) to induce Ca^{2+} release. Ca^{2+} release from the endoplasmatic reticulum is also achieved through ryanodine receptors (RyR). The high Ca^{2+} level inside the ER is maintained by the sarco/endoplasmic reticulum Ca^{2+} ATPase (SERCA) pump which transports Ca^{2+} ions from the cytosol into the ER lumen. Neuronal SOCs (store-operated channels) are plasma membrane channels that are activated upon emptying of intracellular Ca^{2+} stores and mediate Ca^{2+} influx from the extracellular space independently of surface receptors or IP3.

Spine necks also have a high input resistance and can mediate the propagation of a given input. This is one of the reasons why calcium imaging has revealed fairly high amplitudes of depolarizing potentials in spines compared to the amplitudes of calcium transients in dendrites in the absence of firing (Fig. 2,3).

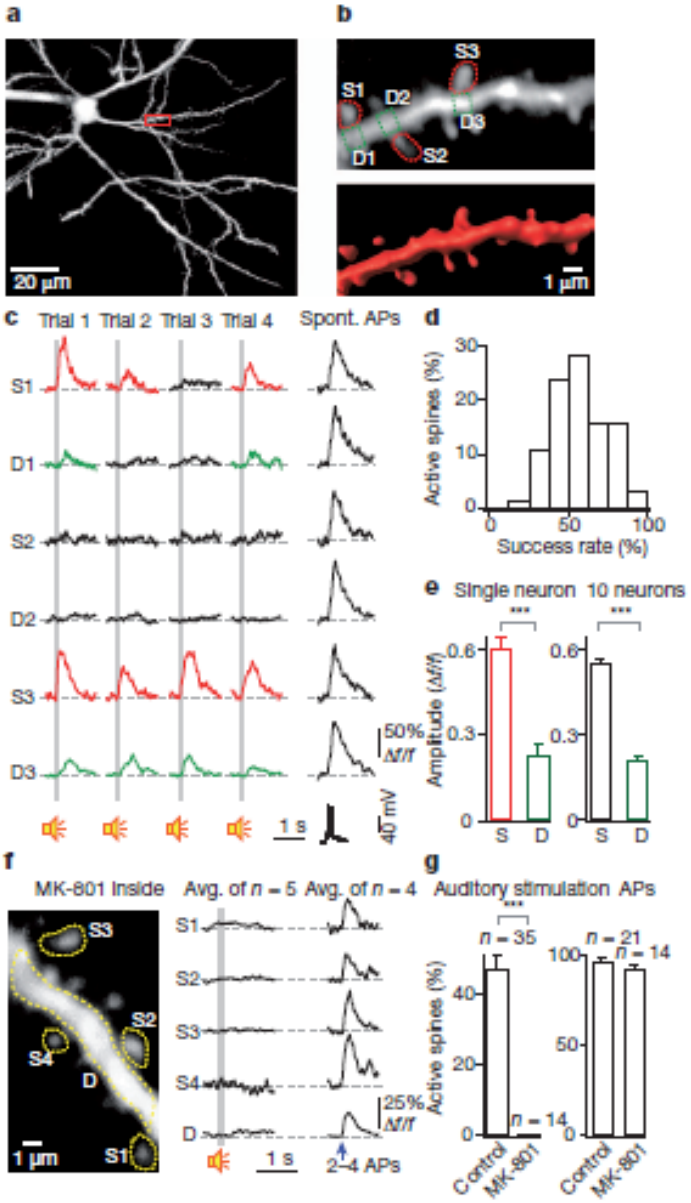

(adapted from Chen et al 2011)

Fig.2. Sound-induced calcium transients in single spines. a, z-projection of a layer 2/3 neuron of the primary auditory cortex, labelled with OGB-1. The red rectangle indicates the area magnified in b. b, Upper panel: image at high magnification of the dendritic segment indicated in a (average of 6,250 frames). Three spines of interest (S1–S3) and the adjacent dendritic shaft regions (D1–D3) are indicated by dashed lines. Lower panel: three-dimensional image reconstruction of the dendritic segment. c. Subthreshold calcium transients evoked by auditory stimulation in spines (red) and corresponding dendritic shaft regions (green), as indicated in b. Four consecu-

tive trials of auditory-stimulation-evoked subthreshold calcium transients, followed by an action-potential-evoked calcium transient. APs, spontaneous action potentials, are shown. The spontaneous action potentials occurred while the neuron was at resting membrane potential. d, Reliability of auditory-evoked calcium responses in spines, calculated for each active spine during seven consecutive trials (broadband noise, 0 dB attenuation) (n = 178 spines, 10 neurons). e, Mean amplitude of auditory-evoked calcium responses in active spines (S) and active dendritic shafts (D). Left panel: data from the neuron shown in a–c. Right panel: data from ten neurons (n = 178 spines, n = 142 dendritic shafts). f, Left panel: image of a dendritic segment (average of 6,250 frames). Right panel: average (Avg.) calcium signals in the spines (S1–S4) and dendritic shaft (D) indicated in the left panel, in response to broadband noise and to action potentials (APs) in the presence of MK-801 (1 mM). Action potentials (2–4) were evoked by brief depolarizing pulses. g, Summary of MK-801 experiments. The fraction of active spines per dendrite was calculated by normalizing the number of active spines to the number of all spines. The number of dendrites for each condition is indicated on the top of each column. Unpaired t-tests, ***, $P < 0.001$. Error bars show s.e.m. Grey bars in c and f indicate sound stimulation (broadband noise, 100 ms duration, 0 dB attenuation).

The spine Ca^{2+} transients recorded in the mouse auditory cortex in layer 2/3 pyramidal neurons (Fig. 2) appear only in some spines and do not invade the nearby spines, indicating that there was no clustering of inputs on that dendritic segment or any dendritic event. These calcium transients were recorded with OGB1 and whole cell recordings in anesthetized animals.

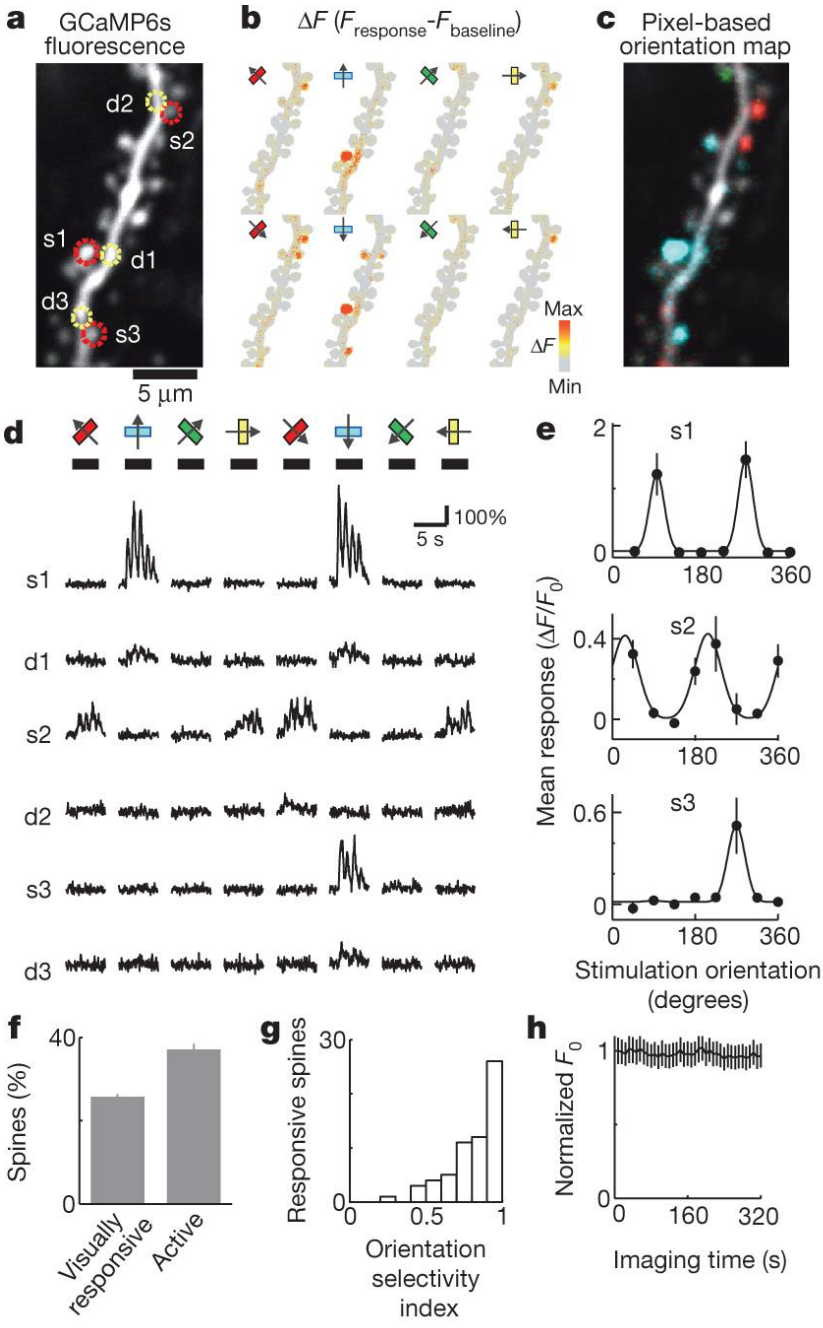

(adapted from Chen et al 2013)

Fig.3. Single spine calcium transients in the mouse visual cortex in response to drifting gratings together with their corresponding dendritic segment. a, Image of an L2/3 dendritic branch expressing GCaMP6s. Regions of interest (ROIs) are indicated as dashed circles (red, spines; yellow, dendrites). b, Map of fluorescence change (ΔF = Fresponse – Fbaseline) in response to drifting gratings of 8 different orientations. c, Pixel-based map of orientation preference. d, Responses of dendrit-

ic spines (s1–s3) and neighbouring dendritic shafts (d1–d3) to drifting gratings with different orientations (corresponding to ROIs indicated in a). e, Orientation tuning of individual spines (s1, s2, s3). Error bars correspond to s.e.m. (n = 5 trials). f, Fraction of spines that show detectable calcium transients (active) and respond to visual stimulation (responsive) (228 spines; 15 dendrites; 4 mice). g, Distribution of the orientation selectivity index across visually responsive spines (62 spines). h, Baseline fluorescence across individual dendritic spines over 320 s of continuous imaging (228 spines; 15 dendrites; 4 mice; error bars reflect s.e.m. across spines).

A similar example (Fig. 3) shows calcium transients in response to drifting gratings in the mouse visual cortex using the GCaMPP6. Here, earby spines show very different direction selectivity, also indicating a lack of clustering of inputs or dendritic events. These recordings were performed in the anesthetized animal.[5]

1.4. Input processing in neuronal dendrites

A single neuron receives thousands of excitatory and inhibitory inputs from the axons of other neurons. During sensory stimulation, these inputs (which are nothing but the outputs of other neurons) can be tuned for a specific sensory stimuli, and therefore contribute to the overall tuning of the cell. The axons of these neurons contact a cell on its spiny dendrites. Since my project was based on reporting the activity of subcellular compartments by means of Ca^{2+} imaging, I will present a sketch of calcium signaling in the neuronal spines, dendrites and the neuronal somata.

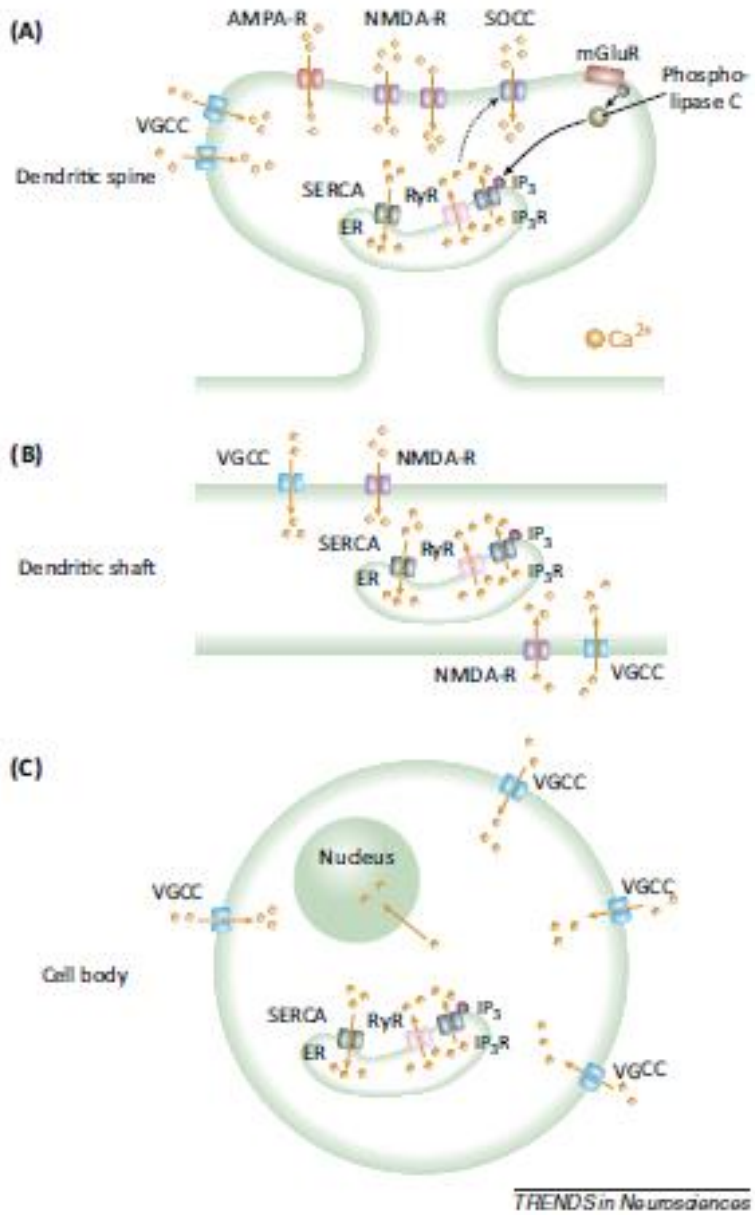

(adapted from Grienberger et al.,[6])

Fig.4. Neuronal Ca^{2+} signaling in dendritic spines (Fig.5A), dendritic segments (Fig. 5B) and the cell somata (Fig. 5C).Dendritic spines (A) contain various Ca^{2+} - permeable channels. The main source of calcium entry in dendritic shafts (B) are VGCCs. Similar to the VGCCs in dendritic spines, these Ca^{2+} channels are activated by bAPs. The neuronal somata (C) are richly endowed with VGCCs. Somatic Ca^{2+} signals are responsible for the induction of gene transcription in the nucleus through activating multiple signal processing pathways[7].

During the past years, it has become increasingly evident that dendrites are more than passive cables, but rather take an active role in integration, be it

through linear or non-linear mechanisms. Neuronal spiny dendrites have been characterized extensively, both structurally[8] as well as functionally[9]. A number of studies[101112] show that dendrites themselves are capable of producing action-potential-like all-or-none events, thereby switching from a linear to a non-linear integration mode[1314].

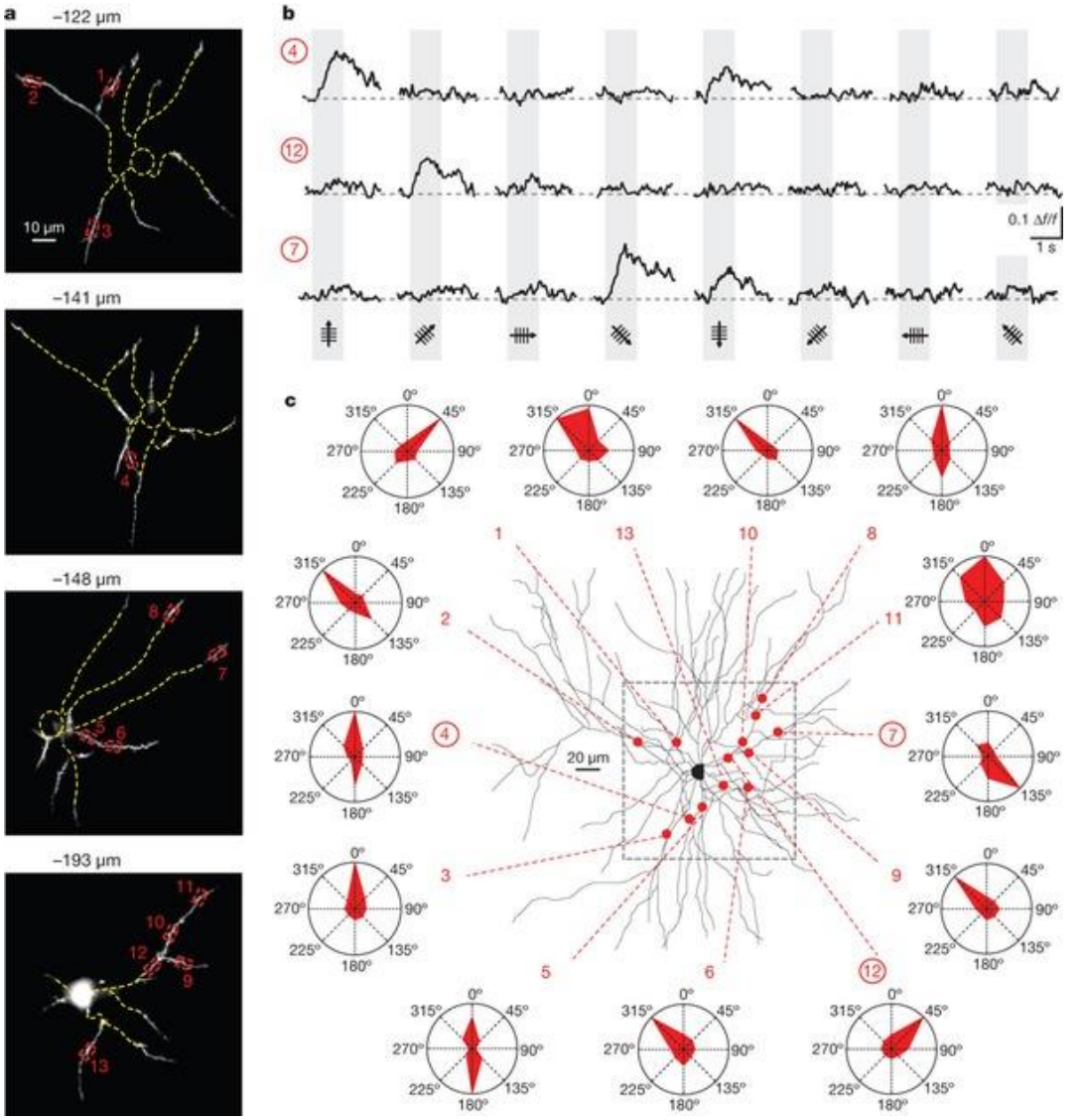

(adapted from Jia et al 2010)

Fig.5. Heterogeneously distributed direction-selective hotspots (subthreshold calcium transients on dendritic segments) on a layer 2/3 pyramidal neuron in the mouse visual cortex. a, Four two-photon images (each an average of n5100 frames) of a layer 2/3 neuron obtained at different depths under the cortical surface as indicated. Red dashed boxes indicate hotspots of local dendritic calcium signaling. b,

Local dendritic calcium signals evoked by drifting gratings of different orientations (average of six trials) at three different dendritic sites indicated in a. c, Location of each hotspot indicated as a red dot on the Z-projection of the reconstructed dendritic tree. Red dashed lines point to the polar plot obtained for the corresponding local Ca^{2+} signals. The frame (grey dashed line) indicates the area of imaging. The output signal of the neuron was tuned for the vertical orientation.

So far, different types of dendritic calcium transients have been reported in vivo in response to visual stimulation. One of the first such signals, called a 'hotspot' was reported by Jia et al[15] (Fig. 6). The name itself does not refer to a spine or dendritic spike in particular, but shows that there are dendritic segments showing calcium transients in the absence of action potential firing in response to drifting grating stimulation. The slow rise time of the calcium transients shown in Fig. 6 suggests that this might be a cluster of active spines rather than an all-or-none dendritic event.

NMDAr-dependent dendritic calcium transients have been observed also in tuft dendrites of layer 2/3 of the somatosensory cortex in response to hindpaw stimulation[16]. The presence of such subthreshold dendritic transients is much more likely in tuft dendrites, given the large difference in activity between the soma and the tuft. However, even in this condition, only one subthreshold calcium transient has been observed in this study in physiological firing conditions. These results, however, show that calcium signaling in the tuft can be very different from calcium signaling in the dendrites of non-tufted pyramidal neurons.

Large plateau potentials have also been observed in layer 5 neurons during active touch.[17] Since simultaneous action potential firing was not recorded during stimulation but only induced artificially in slices, it is still unclear whether these sensory-induced dendritic signals were indeed subthreshold or not.

Furthermore, dendritic spikes could also be recorded with patch electrodes on small dendritic segments. [18] Simultaneous dendritic Ca^{2+} imaging suggests that these changes in voltage recorded on dendritic segments correspond to higher amplitude Ca2+ transients in the respective dendritic segments. Furthermore, the spike waveform corresponding to calcium transients recorded only locally was different from that corresponding to global calcium transients, which would suggest that local calcium transients might not have a corresponding action potential at the soma.

One of the most important questions in neuroscience is how a neuron processes all the inputs it receives into one single output. What kind of temporal and spatial summation of inputs leads to the output a given cell has? Some major advances have been made towards answering that question. Some of them include mapping a large number of inputs by

hyperpolarizing a direction-selective cell just below its firing threshold and imaging different portions of its dendritic field (Jia et al 2010). This study showed that a single direction selective cell receives many inputs (seen as subthreshold calcium transients called 'hotspots') which are tuned to many different directions. This reflects the salt-and-pepper organization of the mouse visual cortex in terms of direction selectivity. Another study (Chen et al 2011) directly recorded spine calcium transients in vivo for the first time and showed that also neurons in the mouse auditory cortex receive highly heterogeneous inputs which are tuned to many different frequencies.

Other studies have aimed at understanding integration by blocking the output of a cell and estimating the sum of all inputs[19]. After the discovery that there are subthreshold calcium transients even in the absence of an action potential which are tuned to many different directions, frequencies or other modes of sensory stimulation, a number of papers have also shown that there are so-called 'dendritic spikes', recorded either electrophysiology with calcium imaging.

Finally, there are even studies showing sensory-induced calcium transients in spines and the corresponding dendritic segment at the same time (Cichon et al 2015), suggesting a correlation between persistent activity in spines and dendritic calcium transients. However, one cannot be sure that these events appeared in the absence of an action potential given that there was no concomitant electrophysiological recording.

For this reason, the definition of a dendritic or calcium spike remains variable from one paper to another. In this thesis I will refer to a calcium spike as a local rise of calcium on a dendritic portion in the absence of action potential firing or preceding a somatic action potential. I will also define a single spine input as a local rise in intracellular calcium observed in only one or several spines in the absence or preceding action potential firing.

Given these considerations, we aimed at trying to get a more causal explanation of how spine-level sensory inputs affect the (electrophysiologically recorded) output of a given cell. Since we already had the conceptual knowledge needed for looking at inputs when a cell is hyperpolarized, I used electroporation and cell-attached recordings to look at subthreshold inputs while the cell was firing in its physiological conditions and recorded the firing activity of the electroporated cell via cell-attached recordings while simultaneously examining different kinds of calcium transients. I have performed these experiments in non-tufted pyramidal cells in the mouse visual cortex as they are some of the simplest and most well-studied cell types.

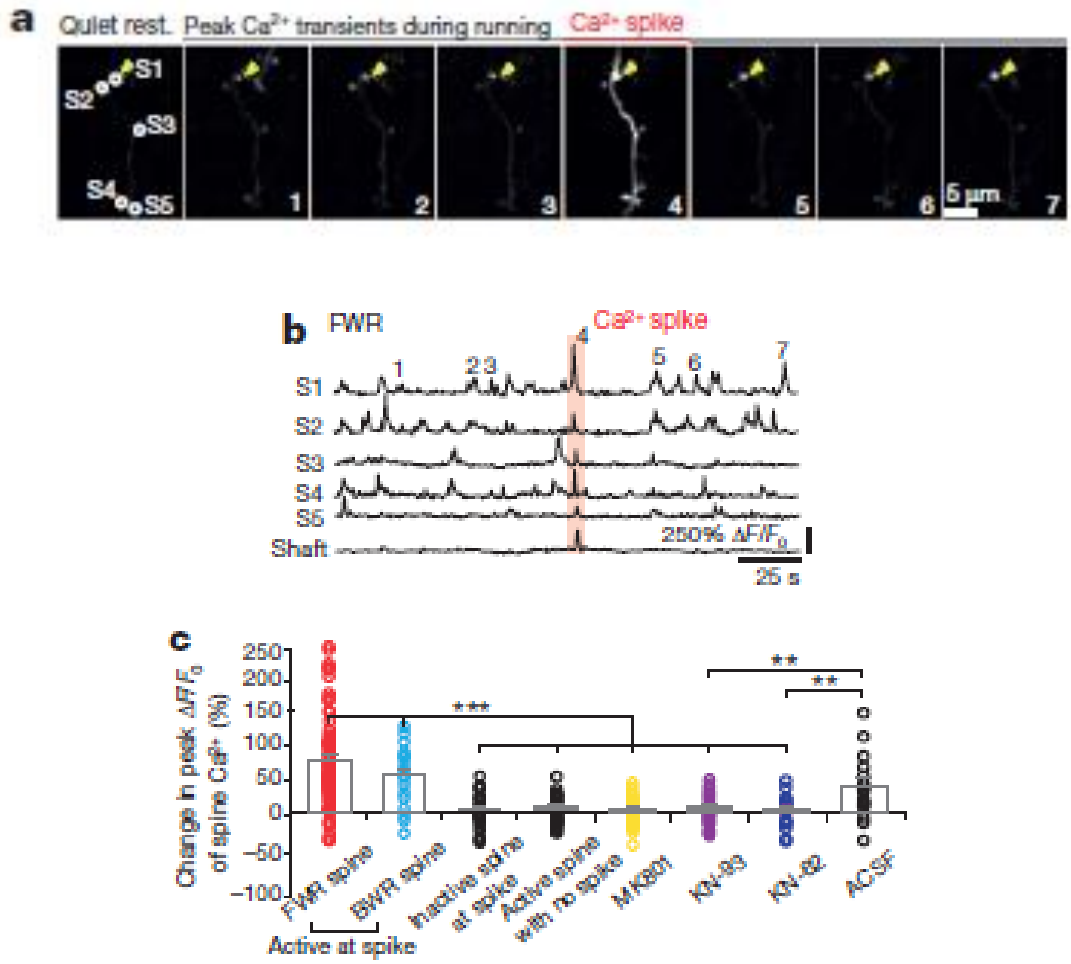

(adapted from Cichon et al 2015)

Fig.6.Locomotion-related spine Ca^{2+} transients in the mouse motor cortex, together with a corresponding dendritic calcium transient. a, b, Time-lapse images and fluorescent traces of a representative apical tuft branch and spines expressing GCaMP6s. Running-induced Ca^{2+} transients in spines (arrowheads point to peak Ca^{2+} signals for spine 1) and a Ca^{2+} spike (marked by red bar). c, Spines active during spikes showed a significant increase in the peak amplitude of Ca^{2+} transients after Ca^{2+} spikes during FWR (n = 80) and BWR (n = 18), whereas spines not active during spikes (P = 0.76; n = 22 spines), or active spines with no encounter of spikes (P = 0.15; n = 35), showed no increase. Local application of MK801 (n = 31), KN-93 (n = 20) and KN-62 (n = 18), but not artificial cerebrospinal fluid (ACSF), blocked potentiation of spine Ca^{2+} transients (P> 0.05).

Finally, calcium transients were observed in dendritic spines and corresponding dendritic segments in the motor cortex (Fig. 6), this time in an awake behaving animal, both before, during, and after a dendritic signal was ob-

served, suggesting that there might be a correlation between spine and dendritic activity during movement[20]. This last finding paves the way for understanding the correlation between sensory-induced spine transients and the corresponding dendritic transients that they can generate.

The dendritic transients reported in vivo and in awake behaving mice support the notion of dendrites having an active role in neuronal integration, rather than acting as mere cables. Figure 4 shows calcium transients or hotspots (which at this point could be either averaged signals from multiple spines or some form of dendritic signals) which are tuned to very different directions, reflecting the salt-and-pepper organization of the mouse visual cortex. Although these studies suggest that these transients might not be backgpropagating action potentials and would have an effect on action potential firing through different methods, it is imperative to prove that this is indeed so by actually performing dendritic calcium imaging together with electrophysiology under physiological conditions. For this reason, I have chosen to combine the LOTOS method described in the subsequent chapters together with cell-attached recordings and electroporation, in order to prevent cell dialysis or interact with the physiological firing of the cell in any way. My results show spine and dendritic signals observed in neurons during, before and in the absence of backpropagating action potentials during sensory stimulation.

1.5. Input processing in cell bodies and neuronal populations

The final step in integration is done in the neuronal somata. Since the somata are also where electrophysiological recordings have been performed in order to understand the output, I will focus on this section in more detail. Because the neuronal somata have also been used as a direct reporter of the neuronal output by means of calcium imaging, population imaging has been used to estimate the sensory response of large cell populations. In order to understand that process, I will begin by focusing on the biochemical substrate of neuronal Ca^{2+}signaling.

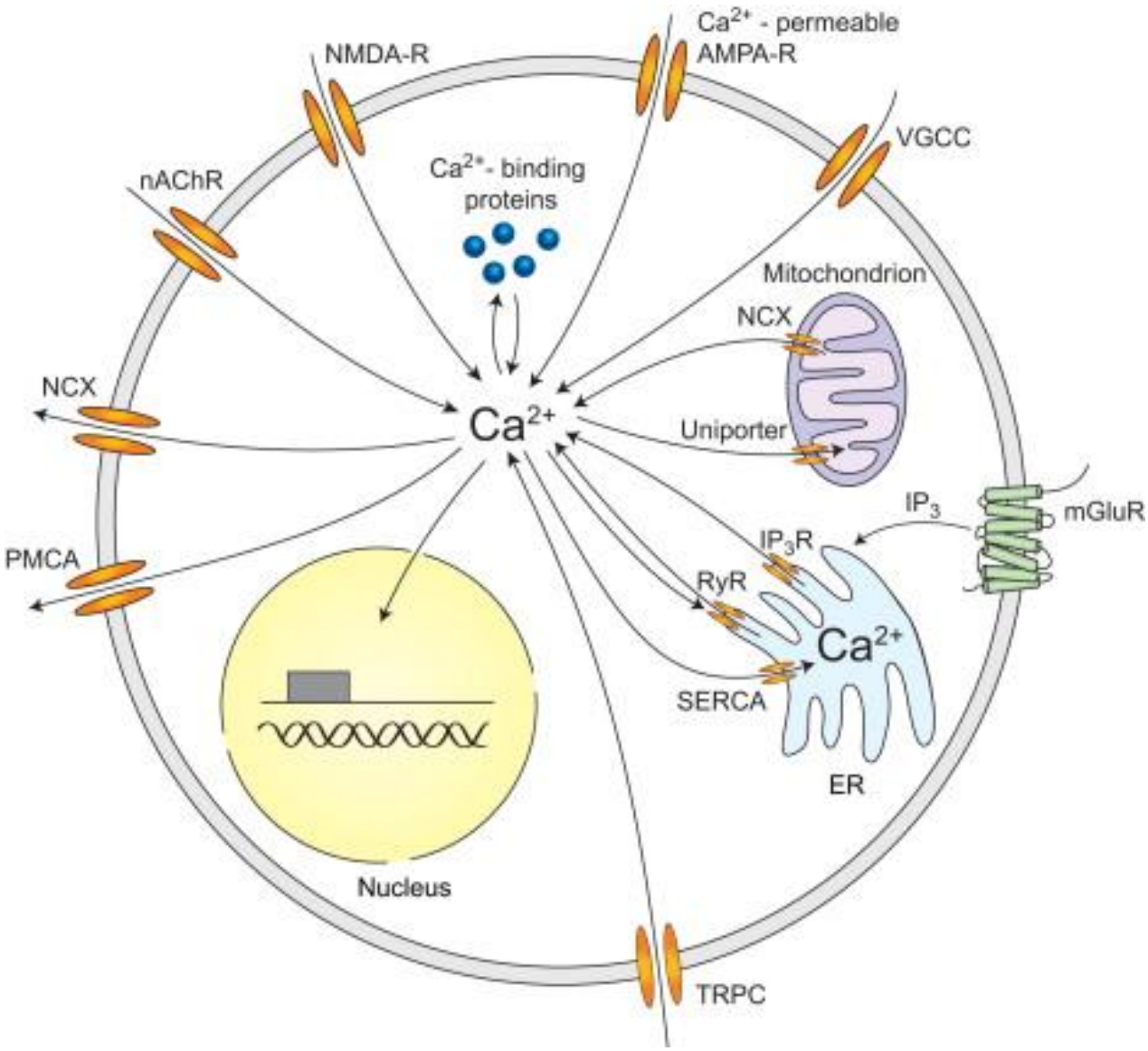

(adapted from Grienberger et al.,)

Fig.7. Calcium signaling in the neuronal somata. Sources of calcium influx are calcium-permeable α-amino-3-hydroxy-5-methyl-4-isoxazolepropionic acid (AMPA) and N-methyl-D-aspartate (NMDA) glutamate-type receptors, voltage-gated calcium channels (VGCC), nicotinic acetylcholine receptors (nAChR), and transient receptor potential type C (TRPC) channels. Calcium release from internal stores is mediated by inositol trisphosphate receptors (IP3R) and ryanodine receptors (RyR). Inositol trisphosphate can be generated by metabotropic glutamate receptors (mGluR). Calcium efflux is mediated by the plasma membrane calcium ATPase (PMCA), the

sodium-calcium exchanger (NCX), and the sarco-/endoplasmic reticulum calcium ATPase (SERCA).

As in the case of dendritic and spine Ca^{2+}signaling, the main entry points for Ca^{2+} ions are mostly regulated by NMDA and AMPA receptor channels, as well as VGCCs. In addition, Ca^{2+}entry in the soma is also mediated by nAChR and TRPC channels. Ca^{2+} release from internal stores is mediated by IP3 receptors and ryanodine receptors. IP3 is generated my mGluR and the calcium efflux that is quantified in Ca^{2+} imaging is mediated by the plasma membrane Ca^{2+} ATPase, the Na^{+} - Ca^{2+} exchanger and the SERCA pump.

Since my projects have focused both on single cell imaging as well as population imaging, it is important to know whether there is a way to dissect the synaptically-driven somatic signals from the signals which combine backpropagation and input integration. The above figure[21] summarizes the potential pathways that presynaptically-driven Ca^{2+} ions may enter the neuronal somata. Synaptically released glutamate may activate mGlurs, which are bound to PLC.

Haegenston et al[20] suggest four pathways by which information arriving onto synapses may be conveyed to the nucleus. The first hypothesis goes as follows: As mentioned before, the activation of NMDA and AMPA receptors on dendritic spines by glutamate leads to increases in Ca^{2+} (this has been also shown experimentally in vivo by means of Ca^{2+} imaging on spines, Fig.2 and Fig.3). These increases in Ca^{2+} might be locally amplified by RyR calcium release, which would then trigger the activation of cargo-NLS and therefore diffuse Importin/cargo complexes through the dendritic cytosol until they reach the soma. According to the second hypothesis, which is one of the most popular ones, synaptic activity evokes EPSPs, which then reach the soma. If the summation of inputs is above firing threshold, then an action potential is produced. At the Ca^{2+} imaging level, the EPSP-induced membrane depolarizations activate somatic VGCCs, which then allow Ca^{2+} to flow down its concentration gradient from extracellular space into the soma and invade the nucleus. The third hypothesis claims that synaptic stimulation activates mGluRs, which triggers the production of IP3. When IP3 binds to IP3 receptors on the ER membrane, it causes Ca^{2+} to flow into the cytosol, triggering regenerative waves of Ca^{2+} release. Finally, according to the fourth hypothesis, stimulation VGCCs on dendritic spines would evoke local currents which would in turn evoke an electrotonic signal across the ER membrane, and thereby allowing these currents to flow toward the soma. This then would also result in backgpropagating action potentials throughout the dendritic tree.

In the past years, there have been major technological advancements in calcium imaging in populations of neurons. For example, Andermann et al show

GCaMP3 Ca^{2+} transients in single cells across an entire cortical column of the barrel cortex in awake mice running on a linear trackball[22]. These recordings were obtained by implanting a microprism and imaging the reflection in z of cells in such a column. This allows for performing calcium imaging across all layers in an entire cortical column. While the possibility of imaging in all layers at the same time could be an important step forward for functional imaging, the field of view for each depth is limited, thereby making it difficult to look at the tonotopy of a large field of view.

Jennings et al also performed deep imaging in neuronal populations, this time with the aid of an implanted microendoscope together with a miniscope in order to observe somatic calcium transients in distinct cellular populations during feeding behaviors[23] in freely moving mice.

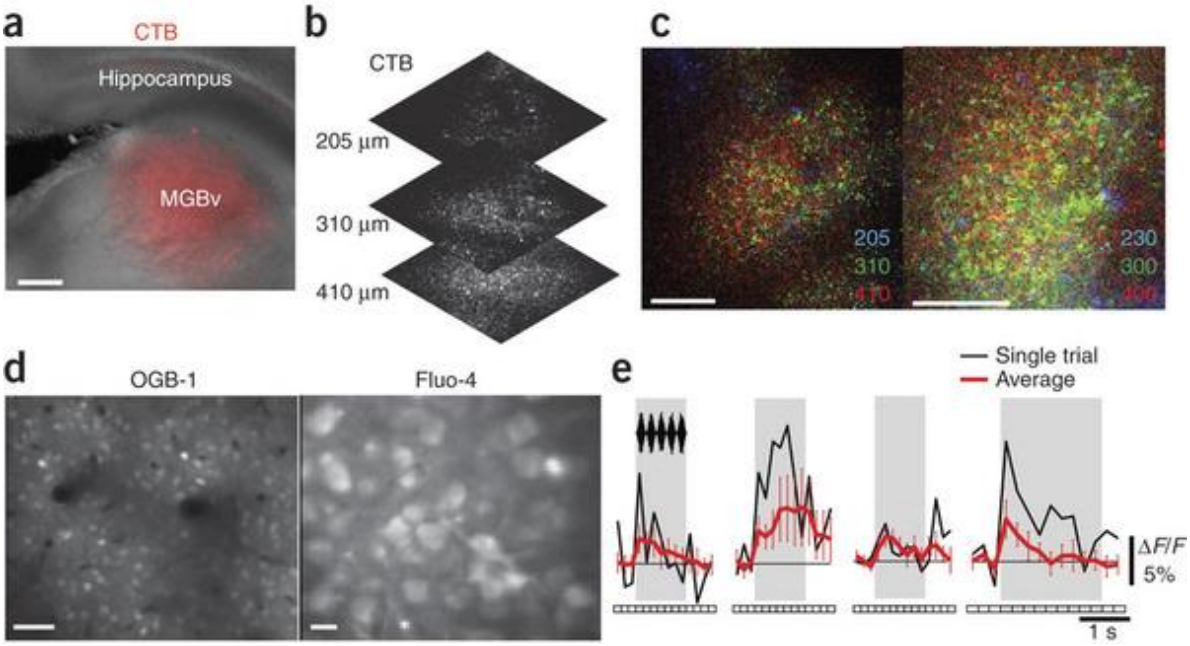

(adapted from Bandyopadhyay et al 2010)

Fig.8. Calcium transients in the anesthetized mouse auditory cortex recorded at different depths. a,b. Confirmation of craniotomy and imaging site in ACX by anterograde labeling. Choleratoxin-B (CTB) was injected into the medial geniculate body (MGB) stereotactically a. A craniotomy was performed at our imaging locations. Fluorescently labeled terminals were imaged at three depths of 205, 310 and 410 µm from the cortical surface b. Following imaging of terminals in vivo, slices were cut to confirm tracer injection in the MGB a. c Images taken at different depths in two mice are

superimposed. Note that most signals originated at a depth of 300–400 µm, indicating the thalamo-recipient layer. Thus, our imaging location was in A1. Scale bars represent 100 µm a,c. d Images of bulk-loading ACX with OGB-1 (left) and Fluo-4 (right). The area over which cells were loaded varied in experiments from 200-µm- to 1-mm-diameter regions. Scale bars represent 50 µm (left) and 10 µm (right). e Single trial (black) and mean (red) fluorescence changes (ΔF/F) with SAM broadband noise from four different cells. Error bars represent 95% confidence intervals, indicating a significant fluorescence change. Frame timing is shown below the fluorescence trace.

Fig. 8 shows calcium transients obtained with OGB1-AM and Fluo-4 bulk loading at different depths in layer 2/3[24]. This study has focused on the differences in tonotopy in the mouse auditory cortex in different layers, and it will be referred to again in the results section for comparison with my own results.

Finally, Issa et al show the tuned Ca^{2+} responses of a single neuron in the unanesthetized mouse auditory cortex. In this study[25], the auditory cortex was previously identified by imaging the GCaMP-based Ca^{2+} signals under the thinned skull with a standard camera during the presentation of low, middle and high frequency pure tones. This allowed the experimenters to map low, middle and high frequency brain regions and then do subsequent Ca^{2+} imaging on single cells on a predefined area. Similarly to the study presented in Fig.8, these results aim at understanding tonotopy in the mouse auditory cortex. There has been a long ongoing debate as to the tonotopy in the mouse auditory cortex is dominated by homogeneous or heterogeneous responses, and whether there is clustering of similarly tuned neurons or not. I will focus on both of these studies in more detail and the connection with my own findings in deep layers of the mouse auditory cortex in the Results section.

As the above summary suggests, there are many different techniques available for measuring Ca^{2+} in neuronal somata, both Ca^{2+} indicators and microscopy techniques. I will continue with describing the methods I used and adapted in order to look at functional integration in dendrites, spines and neuronal population. Since my aim was to get a better understanding of functional integration, I decided to continue studying this in the mouse auditory cortex with single cell and population imaging. I chose frequency tuning as a paradigm, and I decided to look at the tonotopy of subcellular compartments and neuronal populations in different cortical layers and see if there are any patterns.

2) Methods

Two photon microscopy is by now the method of choice for imaging neuronal activity in living animals [26] and has therefore made an enormous contribution to cellular neuroscience[27] over the past 25 years. Its major advantage is that it limits photo bleaching and photodamage, by maximizing the chance of detecting a single photon per excitation event. During two photon excitation, two low energy photons cooperate to generate a higher-energy electronic transition in a fluorescent molecule. The excitation volume with 2P is very restricted, thereby reducing nearby phototoxicity, as well as giving better resolution and contrast, since the image is not limited by scattering of the emitted photons (very focused emission means that most photons will come from the point of interest).

2.1. Set-up

A standard two photon microscope consists of a laser beam that is raster scanned over the imaged sample. When fluorescent, the imaged sample will emit photons which will be detected with different kinds of detectors (ranging from standard cameras to highly sensitive photomultipliers). In Ca^{2+} imaging of in vivo neuronal activity, the sample should be fluorescent whenever there is an increase in a cell's electrical activity. The detected signals are then summed based on the pixel dwell times and mapped back onto individual pixels for each image by the software. In order for the laser beam to produce the two photon effect in the living sample without damaging it, it is broken into very fast pulses (80-120 femtoseconds) with long breaks inbetween every two pulses (in the range of nanoseconds). Most fluorophores used allow for two-photon excitation at wavelengths between 700-1100 nm, and that is therefore the tuning range of a standard two photon laser. A large proportion of commercially available two photon microscopes use galvanometric mirrors for scanning. Finally, the emitted light obtained this way is collected with a detector. An ideal detector for a two photon microscope should have large photosensitive areas, high quantum efficiency and low dark noise. For this reason, many labs use photomultiplier tubes (PMTs). In my experience, it has also been extremely important to have as much live feedback during the experiment as possible, especially when studying functional integration in single cells. Live feedback during the experiment can modify the actual scientific question, and allow for a more bottom-up approach to understanding integration. It is therefore important that live imaging is combined with a way of visualizing the calcium activity, and if applicable the electrophysiological activity at the same time. Furthermore, when applying sensory stimulation it is very useful if the software

can show whether the neurons are indeed responsive to the sensory stimulation (by generating color coded Δf/f maps during the stimulation time for example). This means that it is necessary for the experimenter to have immediate feedback on whether the brain tissue is healthy and stable (especially during awake experiments), whether neurons are indeed responding to the stimulation and show tuning, and whether the calcium activity reports on the electrophysiological activity accurately (the so-called one action potential resolution of a calcium transient). Experiments which did not comply with these requirements were stopped immediately.

As previously mentioned, there have been very significant advances in the past few years regarding tools for understanding functional integration in neurons. One of the most notable techniques which had shaped the field of cellular neuroscience to a large extent is the development of two photon microscopy. The next sections will describe the technical developments made in order to look at both single spines and neuronal populations and describe the technical improvements that were made specifically for my projects. My colleagues and I have written a protocol for anyone who wishes to use the LOTOS two-photon imaging technique[28].

The LOTOS method implies data acquisition at high frame rates and low excitation laser power, thus the name – low power temporal oversampling (LOTOS). This leads to high sensitivity for detecting incoming photos from the fluorescently labeled samples and reduced phototoxicity, which allows for longer and more stable calcium imaging in the living mammals. The entire protocol, going from mouse surgery up to the analysis of the results, can be completed in few hours. Although calcium imaging of dendritic spines has been performed extensively in vitro[29], in vivo spine imaging has been limited by movement due to heartbeat and respiration-induced brain pulsations, high density of blood vessels which cause more scattering of emitted photons and phototoxicity cause by imaging within a very small volume of tissue. Some of the advantages of the LOTOS include the use of a high-speed two photon microscope and optimized animal surgery. One of the limitations of this method at the time was the depth limit, making these recordings possible only in layers 2/3 and only in anesthetized animals.

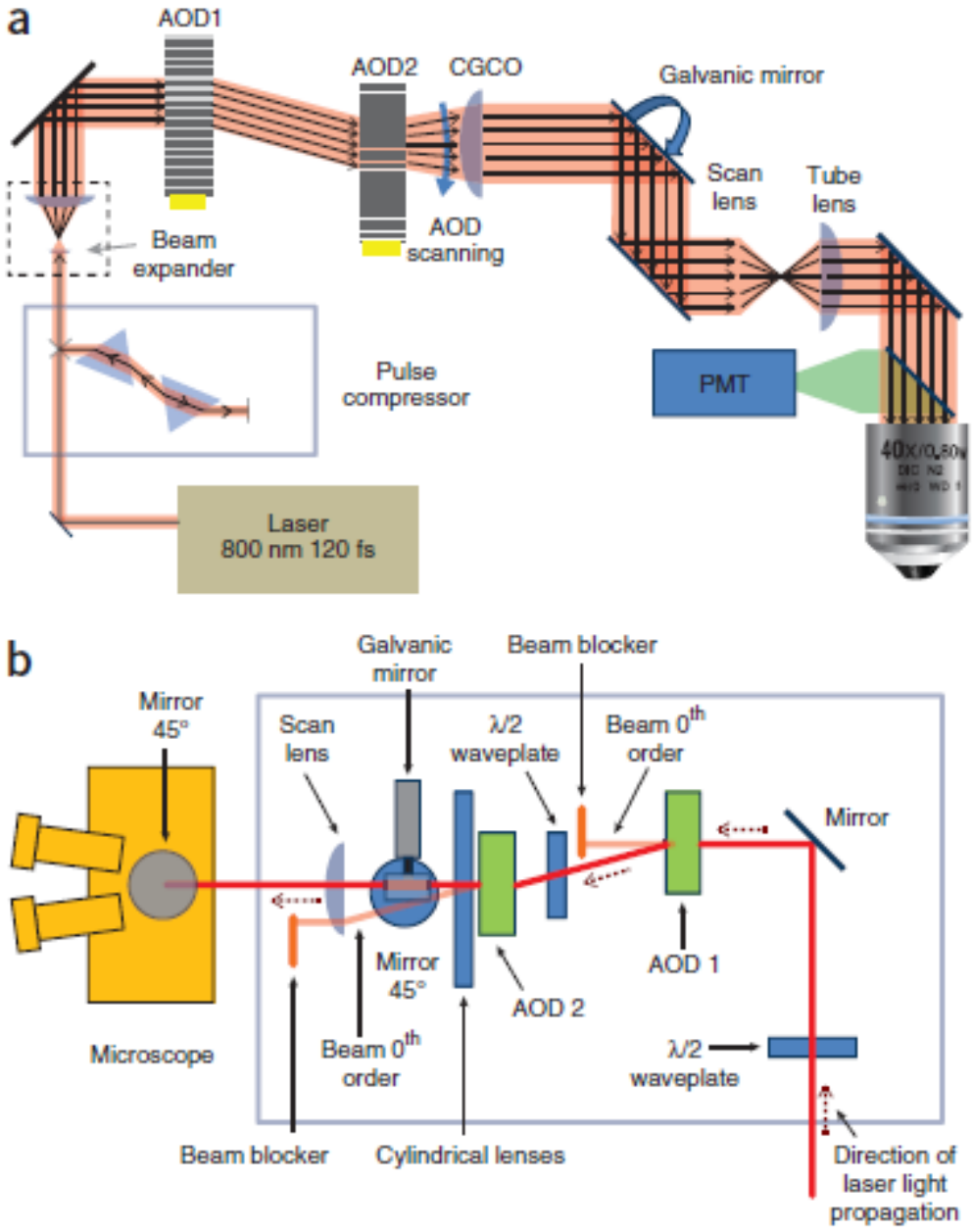

Fig.9. Schematic of an AOD-based high-speed two-photon microscope used for dendrite and spine imaging. (a) Schematic illustration of the two-photon imaging setup. AOD, acoustic-optic deflector; CGCO, chirped grating compensation optics; PMT, photomultiplier tube. (b) Schematic of the layout of the scanner. AODs cause two major beam distortions, namely the cylindrical lens effect and the chromatic dispersion. The cylindrical lens effect is compensated with a set of cylindrical lenses mounted in an automated filter wheel (CGCO), and the chromatic dispersion is compensated with an identical AOD (AOD 1), thereby generating the same disper-

sion in the opposite direction. Each AOD additionally requires a halfwave plate to adjust the polarization, and a beam blocker for the fraction of 0th-order light that is not deflected. After the light passes the AOD scanner and all optical elements for compensation of AOD-based distortions, the light is directed onto a galvanic mirror oriented in 45° for the deflection in the slow horizontal scan direction, toward a static 45° mirror to direct the light through the scan lens onto one additional mirror and through the camera entry toward the optics of the microscope.

The LOTOS version that is most fit for spine imaging is done with a high-speed two photon imaging device. This device consists of an acousto-optical deflector (AOD) for the fast x-scan running in continuous straight lines at 100 kHz repetition rate and a galvanic mirror for the y-scan running in sawtooth waveforms at either 80 Hz (maximmum field-of-view, full-frame mode) or 1,000 Hz (zoomed-in, LOTOS mode). Detailed configurations of each mode are as follows: (a) full-frame mode, frame rate = 80 frames per s, pixel resolution = 500 × 500 pixels, field of view = 90 × 90 µm (for zoom factor ×1; 1 pixel = 0.179 µm); (b) LOTOS mode, frame rate = 1,000 frames per second, pixel resolution = 250 × 80 pixels, field of view = 28 × 9 µm (for zoom factor ×2; 1 pixel = 0.11064 µm). In this mode, the actual illumination time per µm in the fast direction = 1 µm/(Δx/Δt) = 1 µm/(28 µm/12.5 µs) = 446 ns, where Δt is the time for scanning one line in the fast direction with AOD and Δx is the total length of the scan line. For both modes, pixel dwell time is fixed to be 50 ns by the image acquisition system. The chromatic dispersion is compensated by another AOD device; although a prism can also be considered for this compensation. A set of cylindrical lenses mounted into a rotating wheel and placed between AOD2 and the galvanic mirror, and is used for compensating beam distortions caused by a chirped optical grating. AOD2 and the galvanic mirror are controlled by signal generators and are synchronized by a high-speed data acquisition digitizer. The detection channel is used by a PMT. The scanning system is mounted on a standard commercial upright microscope. Excitation light at a wavelength of 920 nm is obtained by a Ti:Sapphire pulsing laser. A long working distance (3.5 mm) and water-immersion objective is needed for placing patch electrodes easily. This setting allows for imaging at a sampling rate of up to 1000 frames per second, a short pixel dwell time of 50ns and a low intensity of laser power for measuring 1-action-potential-induced calcium transients reliably (as low as 18mW in Layer 2/3). Since the temporal resolution of the system greatly exceeds the speed of the neuronal events related to integration (in order to visualize a spine input reaching the soma one does not need a temporal resolution much higher than 50 frames per second). The main difference between such a system and an AOD-based one is that the imaging time, especially for spine events, will be shorter until photodamage occurs. In

the described experiments, the first signs of photodamage appear on a resonance scanner-based system after around 2 minutes of continuous spine imaging at around 20mW of laser excitation under the objective, while on an AOD setup they would appear after 10 min or so (considering the lower laser excitation intensity needed for AOD system imaging). Although high frame rates allow for long term imaging of spines and dendrites, lower frame rates can easily be achieved with more conventional imaging devices, such as those involving resonant scanner–based two-photon microscopy, which also allow for fast changing of the laser wavelength for imaging different calcium indicators. The LOTOS procedure can also be efficiently performed on a resonant mirror–based high-speed two-photon laser scanning microscope, at a frame rate of 200hz. This alternative two-photon laser scanning system that can achieve high-speed frame scanning is based on a resonant mirror. In this system, the fast x-scan unit is a 12-kHz resonant mirror. The actual frame-repetition rates are configured to be 40 Hz for an image consisting of 512 lines (full-frame mode) and 200 Hz for 64 lines (LOTOS mode). Optical zoom factors (×1 to ×20) in both the x axis and y axis can be arbitrarily adjusted by controlling the amplitude of the mirrors, such that the aspect ratio of pixels can differ from 1:1. Pixel dwell time depends on the location of a given pixel because of the sinusoidal characteristic of the resonant mirror, varying from 40 to 250 ns. Configurations of imaging modes are as follows: (i) full-frame mode, frame rate = 40 frames per second, pixel resolution = 512 × 512 pixels, field of view = from 300 × 300 µm to 50 × 50 µm (zoom factor from ×1 to ×6) and (ii) LOTOS mode, frame rate = 200 frames per s, pixel resolution = 256 × 64 pixels, field of view = from 50 × 13 µm to 15 × 4 µm (zoom factor from ×6 to ×20). In contrast to the AOD-based setup, the resonant mirror does not require wavelength-dependent optical adjustments, and thus the wavelength of excitation laser that can be used (from 700 to 1,050 nm) is not necessarily confined to a specific value. It is possible that the maximum depth of imaging (in single-spine resolution) may be deeper, because the resonant mirror system may have fewer optical aberrations.

Spine and dendrite imaging as well as deep population imaging involve a technically challenging and complex version of two photon imaging, which require not only the use of the correct imaging devices, but also advanced skills in microsurgery, electroporation, bolus loading and electrophysiology. My first project was therefore to adapt the LOTOS method to electroporation and cell-attached recordings in the mouse visual cortex in order to see sensory-evoked spine inputs and their role in generating a tuned output. For more details on the specific adjustments made for these studies, please see the Results section.

2.2. Materials

2.2.1. Reagents

Mice aged 28–40 days; we have used C57BL/6.

Isoflurane (Abbott Laboratories) Anesthesia was performed in accordance with the relevant animal care regulations. Isoflurane is a volatile liquid; therefore, an effective ventilation of the experimental room is needed. Lidocaine hydrochloride, a local anesthetic agent (20 mg/ml ; e.g., Xylocaine, AstraZeneca), and the same amount of Metamizol. The cell-impermeant fluorescent calcium indicator used was Oregon Green 488 BAPTA-1 hexapotassium salt (OGB-1).

A low concentration of Alexa Fluo dye 594 for loading the pipette for juxtacellular recordings and targeting an electroporated cell.

The materials we used were: NaCl, KCl, NaHCO3, NaH2PO4, $CaCl^{2+}$, $MgCl^{2+}$, glucose, potassium d-gluconate, HEPES, Mg-ATP, Na^2GTP, Na^2-phosphocreatine, low-melting-point agarose, cyanoacrylate glue, borosilicate capillaries, distilled water and carbogen.

The ACSF solution contains 125 mM NaCl, 4.5 mM KCl, 26 mM NaHCO3, 1.25 mM NaH2PO4, 2 mM $CaCl^2$, 1 mM MgCl2 and 20 mM glucose. The ACSF was bubbled with carbogen (95% oxygen, 5% carbon dioxide) in order to adjust the pH to 7.4 and freshly prepared for each experiment.

The ACSF perfusion system was used to circulate fresh, oxygenated ACSF into the recording chamber. The perfusion system consists of a perfusion pump, inlet and outlet tubing and a heating bath for keeping the ACSF temperature at 36.5–37.5 °C. I kept the temperature of the ACSF stable by placing a thermometer inside the recording chamber and adjusted it on an experiment-by-experiment basis. The isoflurane anesthetic unit includes a pure oxygen supply, an isoflurane vaporizer, an airflow meter and a respiration mask for the mouse.

For the agarose preparation, I dissolved 20 mg of agarose powder in 1 ml of ACSF solution and boiled for a few seconds. After this, the solution was cooled down to a temperature of 38 °C just before applying it onto the surface of the cortex. For spine calcium imaging, I often applied a thick layer of agarose (about 2 mm) on the top of the cortical surface. The agarose solution was freshly prepared before every experiment.

2.2.2. Equipment

The components are the following: high-speed two-photon microscope (For the initial spine imaging in the visual cortex I used a custom-built AOD-based system; I also used other resonant scanner-based systems that can run at high-speed frame-scanning mode, e.g., image repetition rate of 200 Hz), tunable Ti:Sapphire pulsing laser (Chameleon, Coherent; pulse width 80-120 fs, repetition rate 80 MHz), galvanic mirror (Cambridge Technology, cat. no. 6215 H), AOD (Crystal Technology, cat. no. 4150), CGCOs (a set of cylindrical lenses mounted into a rotating wheel; a modified version of AFW-65 from PI-Micos), signal generators, high-speed data acquisition digitizer, PMT, standard upright microscope, microscope objective (water immersion, ×40/0.8, WD 3.5 mm; Nikon). The software for imaging data acquisition was custom-written with LabVIEW 8.5. The software modules for controlling the AOD scanner are freely available. Furthermore, a patch-clamp amplifier was used (e.g., EPC9/10, HEKA), motorized micromanipulators for controlling the patch pipette, patch pipette puller, manometer for monitoring pressure and suction changes; available from many providers, pressure valves for holding pressure in the patch pipette, animal monitoring system to control the body temperature and breathing rate, heating plate to keep the body temperature of the animal at 36.5–37.5 °C, isoflurane vaporizer, airflow meter, surgical equipment, including a dissection microscope, drill, scissors and forceps, recording chamber (diameter = 38 mm; see ref. 16) with center-access opening (diameter = 4 mm;); custom-made from a standard cell-culture dish, perfusion pump, electrostatic speaker driver, free-field speaker, sound card.

2.2.3. Sound stimulation

Sounds were presented in free-field using an electrostatic speaker driver (ED1, Tucker Davis Technologies) with an ES1 free-field speaker (TDT) placed about 2 cm away from the contralateral ear of the mouse. Because sound stimulation was not peformed in a sound-proof chamber, we measured the background noise using a 1/4-in microphone (Microtech Gefell) connected to a B&K measuring amplifier (Type 2636), and then sampled at 240 kHz on a PCI 6731 sound card (National Instruments) for additional offline analyses. Background noise was dominated by low-frequency components, going up to 2kHz, which is the lowest frequency used for sound stimula-

tion.

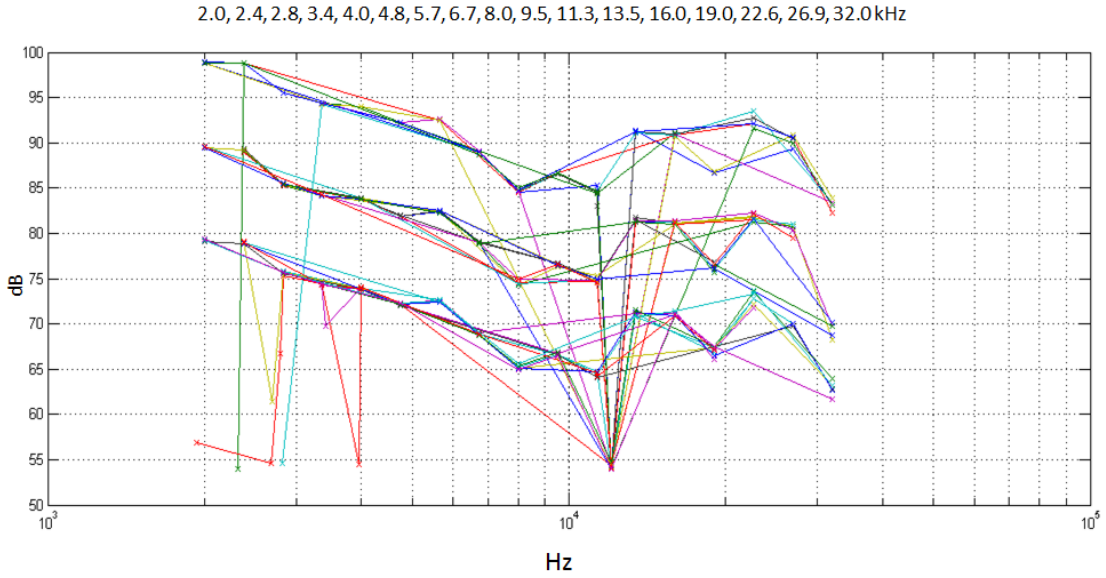

Fig.10. Calibration curves at 3 different attenuation settings for assessing background noise contribution to the sound stimulation. The panel above shows the frequency range for pure tones (2-32kHz) and the correlation with the background noise at different intensities. The x axis shows the frequency in Hz and the y axis shows the sound intensity in decibels.

We calibrated the sound levels by placing the microphone near the loudspeaker and the ear of the mouse, measuring the resulting sound levels. To avoid harmonic distortions, the gain of the ED1 driver was always set no higher than 9 dB attenuation. Typically, this attenuation level corresponded to a sound level of 73 dB sound pressure level (SPL) for frequencies between 1 kHz and 10 kHz, and to a sound level of about 65 dB SPL for frequencies up to 32 kHz. The resulting sound levels were verified by the B&K sound meter level; linearity was confirmed over a range of 30 dB. Bursts of broadband noise had a bandwidth of 0–50 kHz, and had the same overall energy as a tone at the same sound level. Thus, at 0 dB attenuation, the noise had a spectrum level of about 25 dB/√Hz.

For auditory stimulation, broadband noise and pure tones were generated with custom-written software based on LabVIEW (National Instruments), and transduced to analogue voltage through a PCI 6731 (National Instruments) sound card. For testing the tuning properties of single spines, 17 frequencies (2.00, 2.37, 2.82, 3.36, 4.00, 4.75, 5.65, 6.72, 8.00, 9.51, 11.31, 13.45, 16.00, 19.02, 22.62, 26.90, 32.00) all in the range of 2–32 kHz, were applied. Each frequency or broadband noise stimulus was applied 7-10 times, for both single cell and population imaging. The duration of each auditory stimulus was 30 ms (5-ms rise/fall time). The inter-stimulus interval was either 1 s (multiple-

frequency experiments) or 4 s (broadband noise and 2-tone experiments). Two types of sound stimuli, broadband noise (from 2 to 50 kHz) and pure tones, can be generated by a custom-written program based on LabVIEW, and they can be transduced to analog voltage via a PCI 6731 sound card. The start of the sound stimulation program was synchronized with the start of two-photon imaging and, when needed, with the electrophysiological recordings. The frequencies used cover 4 octaves at a resolution of 4 frequencies/octave in order to allow for an efficient mapping of tonotopy.

2.2.4. Calcium indicators

Calcium imaging is a very versatile and efficient method for estimating a neuron's electrical activity partly due to the large difference in concentration intra- versus extracellularly. The downside of calcium dyes however is the fact that they report on electrical activity only indirectly, by means of coupling to calcium ions which move in and out of a cell as a result of opening and closing of ion-permeable channels during changes in membrane voltage. Intracellular calcium signals regulate processes over different time ranges, from neurotransmitter release at the microsecond scale to gene transcription, which lasts for minutes and hours[30]. The time course, the amplitude, and, most importantly, the local action site in spines, dendrites and the neuronal somata are essential in helping experimenters understand the underlying electrical changes.

The choice for a particular calcium indicator can affect the quality of the data tremendously, depending on the scientific question. For looking at functional computation, it is important that the calcium indicator of choice reflects the electrophysiological activity reliably (the one AP resolution) for population imaging. For single cell imaging, an extra requirement is that the calcium indicator is sensitive enough to detect isolated calcium transients and spines in the absence of action potential firing.

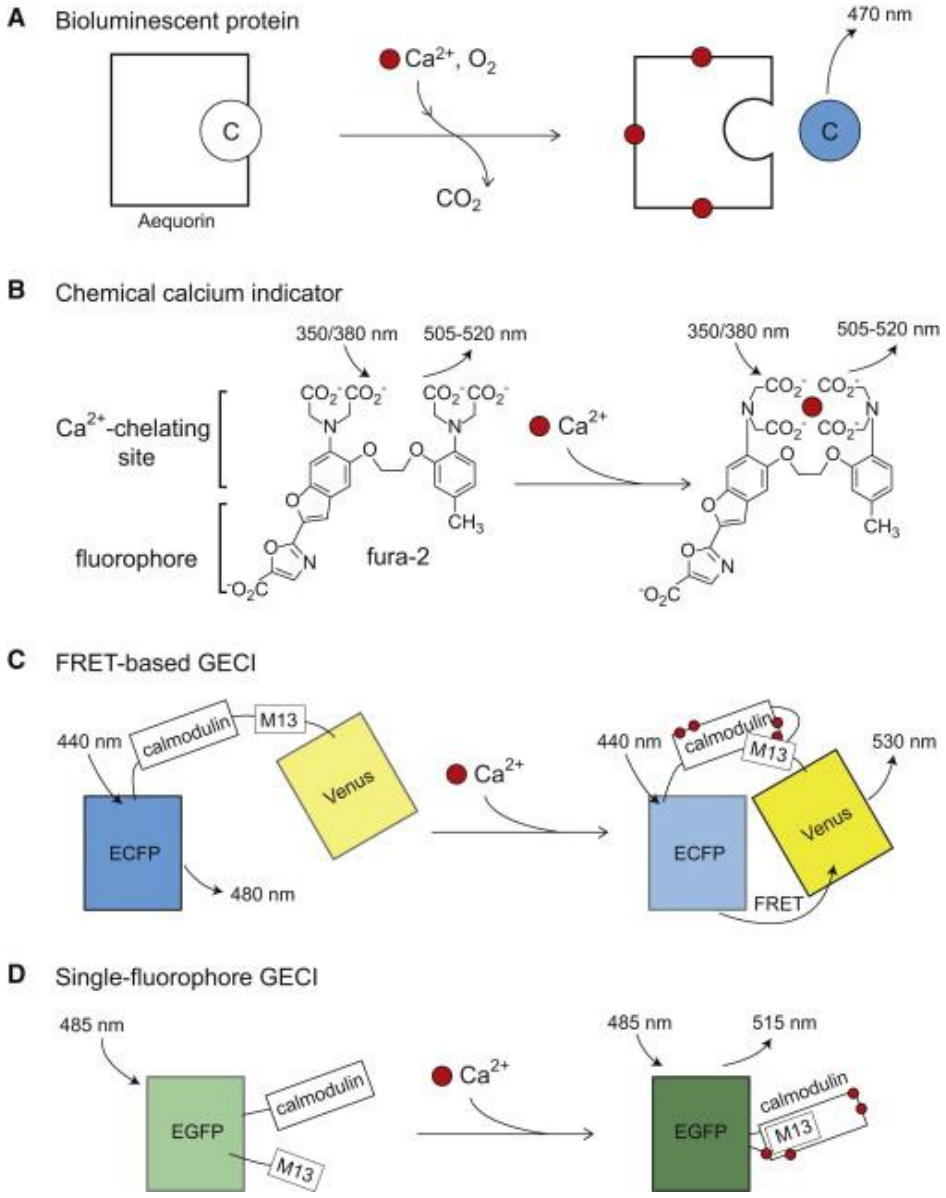

(adapted from Grienberger et al.)

Fig. 11. Different types of calcium Indicators. (A) Bioluminescent protein. Binding of calcium ions to aequorin leads to the oxidation of the prosthetic group coelenterazine (C, left side) to colenteramide (C, right side). Colenteramide relaxes to the ground state while emitting a photon of 470 nm. (B) Chemical calcium indicator. Fura-2 is excitable by ultraviolet light (e.g., 350/380 nm) and its emission peak is between 505 and 520 nm. The binding of calcium ions by fura-2 leads to changes in the emitted fluorescence.(C) FRET-based genetically encoded calcium indicator (GECI). After binding of calcium ions to yellow chameleon 3.60 the two fluorescent proteins, ECFP (donor) and Venus (acceptor), approach. This enables Förster resonance energy transfer (FRET) and thus, the blue fluorescence of 480 nm decreases, whereas the fluorescence of 530 nm increases. (D) Single-fluorophore genetically encoded calcium indica-

tor (GECI). After binding of calcium to GCaMP conformational intramolecular changes lead to an increase in the emitted fluorescence of 515 nm.

It is also important to keep in mind that calcium indicators are calcium buffers which can affect physiological signaling themselves. Ideally, an indicator would be calibrated so that it has a minimal concentration to reach a desired signal to noise ratio.

A bath concentration of 1-5 µM gives a dye concentration inside the cells of up to 100 µM.

We used chemical calcium indicators for my projects. OGB1 in both its AM and salt version has a low affinity (around 20 µM inside the cell for the cell-impermeant version) but which does allow the experimenter to use relatively lower concentrations, thereby limiting its phototoxicity and making it advantageous for detecting small changes in intracellular Ca^{2+} [31].

For imaging single cells, I electroporated the salt version of OGB1 into a single cell within every craniotomy in order to make sure that the subthreshold signals observed belong to a single neuron, whose firing activity is also monitored by a separate electrode. The OGB1 concentration inside the pipette was around 9 mM. This gave in most experiments a reasonable 1AP resolution and allowed for monitoring inputs at the spine and dendrite level.

For population imaging, I used a recently developed calcium indicator for AM loading. This dye, called Cal520, showed better signal to noise than OGB1-AM[32] both in the anesthetized and awake conditions, allowing for a better detection of tone-induced calcium transients in single cells and therefore allowing for a more accurate tonotopy in layers 4 and 5 of the mouse A1, as well as having a good 1 action potential resolution. This could be partially due to its lower baseline fluorescence, which makes it more fit for AM loading, I used the same concentration of Cal520 as for OGB1 AM, namely 9 mM. This should give a final dye concentration inside the cytosol of about 20µM.

In order to calibrate the laser power and PMT gain with the aim of obtaining the highest signal to noise ratio without causing phototoxicity, I looked at the fluorescence trace of a given cell and raised the laser power until I observed a drop in the baseline fluorescence. This is a clear sign of photodamage. I then lowered the laser power just below this value and then adjusted the PMT gain until the image was crisp, without much background fluorescence.

3) Results

Single neuron electroporation with the membrane-impermeable dye Oregon Green under two-photon guidance was first established together with the shadow-patching method[33] and was later developed for other types of indicators.[3435] The LOTOS procedure was designed by my colleagues, and I have contributed to it by applying it on electroporated cells and combining it with cell-attached recordings (in short, EC). The main idea behind this combination is that whole-cell recordings involve dialysis of the solution inside the pipette into the intracellular medium, and might therefore affect intracellular signaling. While whole-cell recordings have their advantages, such as the possibility of injecting certain drugs inside the cell or hyperpolarizing the cell, however electroporation allows for recording in more physiological conditions after the cell has completely processed the calcium dye. The same electroporated cells were then targeted for cell attached recordings which allow for reliable recording of single action potentials. The aim of using this method was therefore to explore neuronal calcium signaling in more physiological conditions. Targeted multi-cell electroporation (TME) is similar to single cell-electroporation, but involves staining multiple cells within the same field of view in order to allow population imaging in the trunks, which are known to give a reliable single action potential resolution. The following subchapters will describe the adapted procedure in detail and will show its applications for single cell (EC) and population (TME) imaging.

3.1. Adapted LOTOS procedure of two photon imaging for single cell analysis

Mouse surgery (45–60 min)

1. The mouse was anesthetized with 1–1.5% (vol/vol) isoflurane in pure oxygen (O2) and placed it onto a heating plate (set to 37.5–38 °C). I checked the depth of the anesthesia by assessing the tail-pinch reflex.

2. The hair was from the skull and 50 µl of lidocaine hydrochloride were injected under the skin. We waited for about 2 min for the local anesthetic to take effect.

3. The skin and muscle tissue above the skull were removed using fine scissors.

4. For craniotomies on the auditory cortex, we turned approximately 70–80° away from the midline to expose the skull above the left auditory cortex, and then carefully removed the muscle and connective tissue above this part of the skull using a new needle. It was critical at this point to not damage any blood vessels during muscle removal. When the bleeding persisted, I stopped the experiment as this could affect the neuronal response to auditory stimuli. The visual cortex was located 2.5 mm laterally from the lambda, and the auditory cortex was 2.5mm medial and 4.5mm lateral to the bregma. For locating the auditory cortex, I examined the blood vessel configuration and checked the location based on the coordinates. The opening was made when the location based on coordinates and the one based on the blood vessel configuration corresponded.

5. For visual cortex imaging, the recording chamber was adhered to the skull with cyanoacrylate glue, while making sure the opening of the chamber is parallel and close to the center of the visual cortex. For the auditory cortex, and in particular for the unanesthetized experiments, a more complicated procedure is necessary. First, after removing the muscle covering the auditory cortex, I added a bonding agent on the skull and recording chamber. Then, I used dental cement to make a bridge around the auditory cortex which is located underneath the lateral part of the skull. After this, I added dental cement on the recording chamber and pressed gently. The dental cement was dried instantaneously with UV light (2 pulses x 40s). This also prevented detachment of the recording chamber while the unanesthetized mouse was moving.

6. Once the chamber has adhered, a small craniotomy was made (approximately 2 × 2.5 mm) using a high-speed drill with a small-tip steel burr (0.5 mm in diameter) above the visual or the auditory cortex.

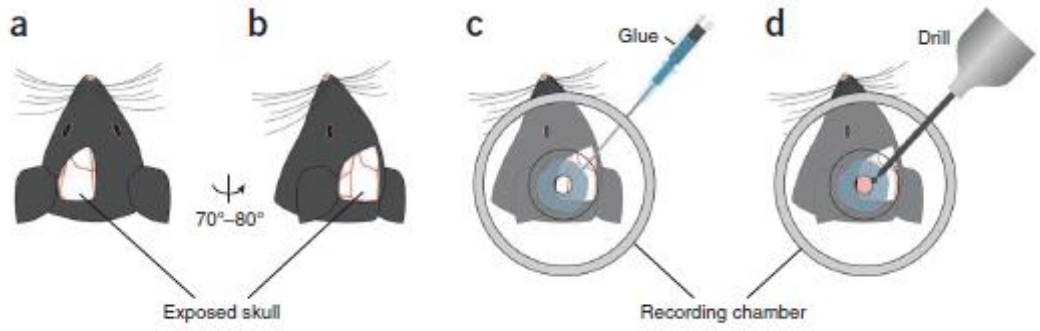

Fig.12. Mouse surgery, recording chamber and craniotomy procedure. (**a**) Schematic illustration showing the top view of the exposed skull after removal

of the skin and muscle. (**b**) The top view of the exposed skull above the auditory cortex turned 70–80° away from the midline. (**c**) The recording chamber is glued to the skull. (**d**) The craniotomy is made by a high-speed drill with a small-tip steel burr (0.5 mm in diameter).

7. The bone debris and blood were then gently washed away with fresh ACSF.

8. After this, the ACSF was removed from the recording chamber and warm agarose solution was added (20 mg/ml) on the surface of the exposed cortex and the surrounding skull. The agarose was left to dry for 10 minutes until a compact and solid layer of agarose was formed with a thickness of ~2 mm, after which the chamber was filled with ACSF again.

Preparation for recording (30min)

9. When the agarose dried, the mouse was carefully transferred to the recording apparatus on a heating plate (set to 37.5–38 °C), and the isoflurane concentration was reduced to 0.8–1.2% (vol/vol).

10. The speaker for auditory stimulation was placed relatively near (~2 cm away) to the right (contralateral) ear for experiments made with sounds stimulation in the auditory cortex.

11. While doing so, the respiration and rectal temperature of the mouse were constantly monitored. Stable status of the mouse is crucial throughout the period of recording, as variations in temperature as small as 2 degrees may affect neuronal signaling irreversibly. The isoflurane flow and heating plate temperature were constantly adjusted constantly until the rectal temperature was around 37 °C and the breathing rate was in the range of 90–120 breaths per min.

12. The patch pipettes had open-tip resistances of 3-5 MΩ for electroporation and AM loading, and with resistances of 5-7 MΩ for cell-attached recordings.

.

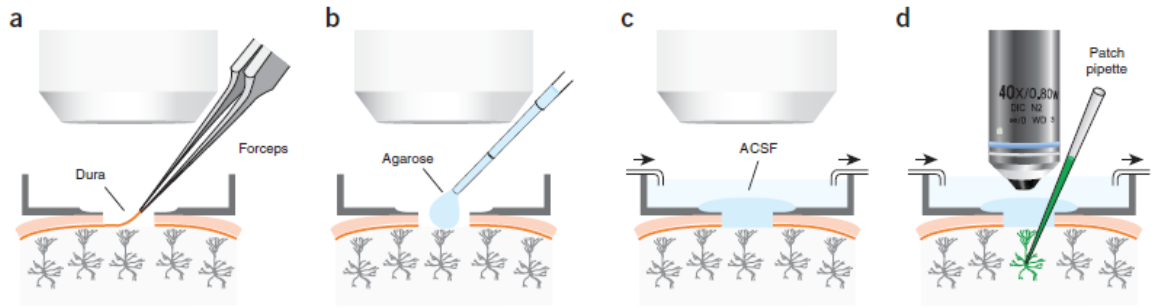

Fig. 13. Craniotomy preparation and stabilization before imaging. (**a**) The removal of the dura in the craniotomy window by forceps with fine tips under the dissecting microscope. (**b**) Agarose solution is applied to the craniotomy window with a plastic pipette. (**c**) Side view of the craniotomy with agarose on the top and with the perfusion of ACSF. (**d**) Switch from the dissecting microscope to the two-photon imaging setup for the patch-clamp recording and imaging.

Calcium imaging of dendritic spines and combined electrophysiological recordings (30-60min)

13. Two hours after electroporating the cell, we checked the quality of the recording and the stability of the brain. If the size of the transients was reasonable, I then proceeded to insert a pipette filled with a low-concentration Alexa dye. In order to approach an already labeled cell with another pipette for cell-attached recordings, it is useful to calculate the angle of the pipette, which in my case was around 40 degrees, and use trigonometry law to decide how far the pipette should be in order to reach that particular cell. A more straightforward way to do this is to simply enter the brain in the same place as the electroporation pipette and look for the cell once the desired depth is reached. The difficulty of this varies with increasing the cortical depth, and therefore performing a cell-attached recording on an electroporated cell in layer 2/3 will be less demanding then approaching one in layer 5. While advancing the pipette in the brain, it is important to avoid contact with other cells or even penetrating them, as this will block the pipette tip and make electrophysiological recordings noisy. One approach for avoiding this is monitoring the pipette resistance under two-photon guidance and applying gentle positive pressure when this increases, while slowly retracting the pipette until it reaches its initial resistance value. Another approach, which is useful when targeting cells which are located deeper under the cortical surface, is to avoid imaging and only monitor the resistance. It is crucial to avoid

large movements inside the brain during the approach, as this can cause mechanical damage and even bleeding.

14. Once the pipette was close to the cell, we used positive pressure until I saw dye coming out and the resistance of the pipette going back to the initial value it had while being outside the brain. For these pipettes, the resistance was around 5-7 MΩ. Just before touching the cell, the resistance was roughly the same as the initial one, and after touching the cell and causing a small dimple, the resistance increased by a few MΩ (up to 11). At the same time, I applied negative pressure at around 80mbars in order to bring the membrane into the recording pipette. The resistance rose slowly to around 30 MΩ. From my experience, if these conditions are fulfilled, then the quality of the electrophysiological recordings is good and allows the experimenter to observe clear single action potentials from the recorded cell alone. This approach is useful for looking at the connection between spine and dendrite inputs and the firing output in more physiological conditions.

15. After seeing single action potentials in the electrophysiological recordings, I then checked the cell responsiveness to stimulation, either to drifiting gratings in the visual cortex or white noise in the case of the auditory cortex. If evoked responses could be observed, then I proceeded to imaging the cell.

16. I then looked for a portion of a dendrite, adjusted the focus until the dendrite and its spines were in focus, and then adjusted the laser power and PMT gain until I could see calcium transients corresponding to single action potentials. Single action potential resolution has been a benchmark for high-quality recordings of single cells in these projects. However, since the goal of the project was to observe subthreshold events, I examined the fluorescence value of a dendrite, and raised the laser power until a small drop in the baseline fluorescence could be seen in the online analysis, which is a sign of photodamage. I then adjusted the laser power just below this value, and then adjusted the PMT gain for maximum signal and low background. This method allows for seeing the best possible signal in a given cell, which includes single action potential-related calcium transients as well as subthreshold transients.

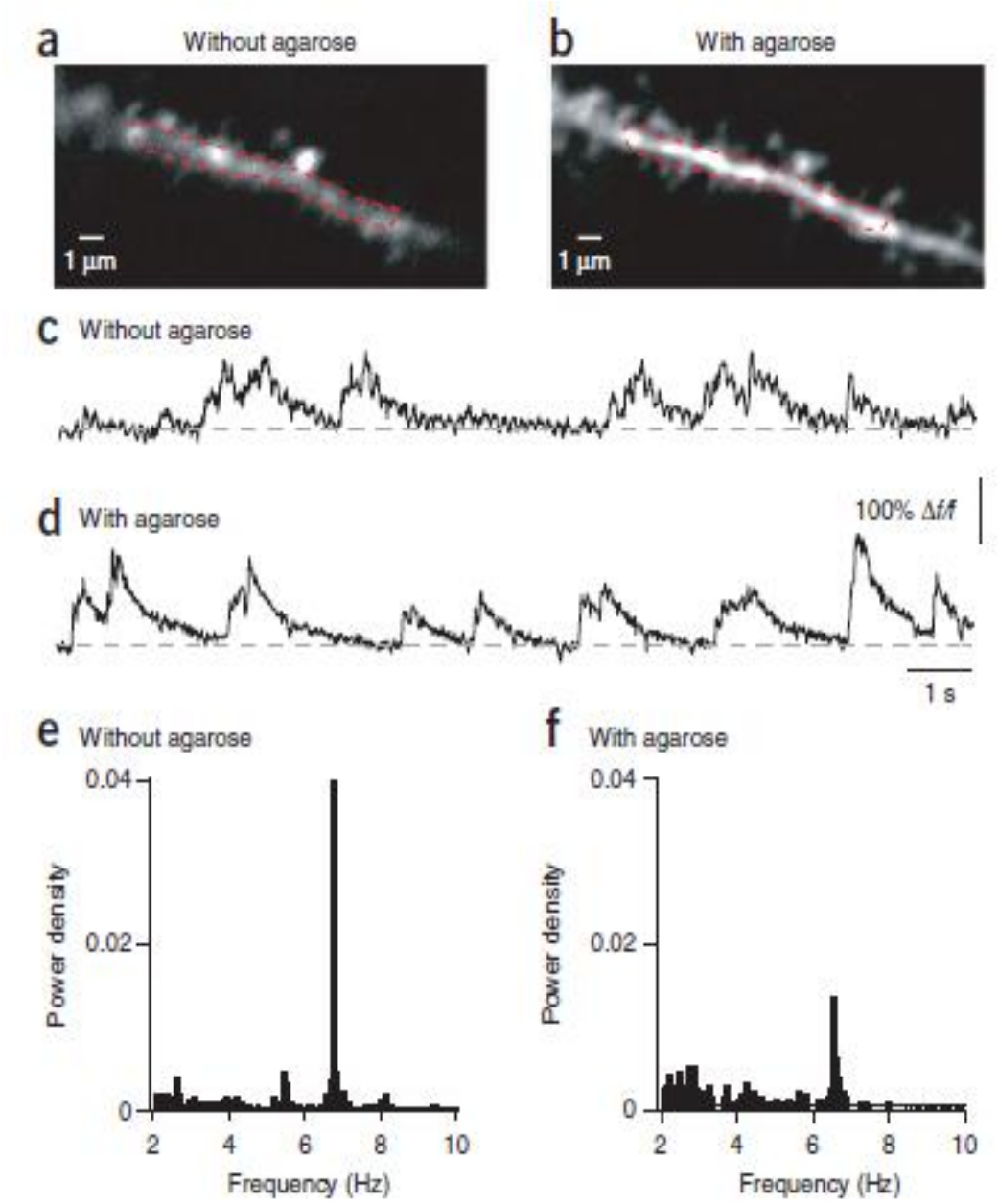

Fig.14. Reduction of heartbeat-induced noise by agarose application. a,b. Two-photon images (average of 6,250 frames) of a dendritic segment of a L2/3 neuron before (a) and after applying agarose b. Note that more dendritic spines are visible after the application of agarose. c,d. Calcium signals from the ROIs indicated by red dashed lines in a and b, respectively. e,f. Power spectra of the calcium traces in c and d, respectively. The peak around 6–8 Hz is consistent with the heartbeat frequency of the mouse under isoflurane anesthesia. Note the clear reduction in the peak after applying agarose. Because of mechanical disruption, addition of agarose into the craniotomy easily causes a loss of whole-cell recording if the electrode is present. In order to keep a stable recording before and after agarose application, OGB-1 was injected into

the neuron by electroporation instead of whole-cell patch-clamp recording, and the pipette was completely removed in this experiment.

17. We then went on to look for another appropriate region of the dendritic field of the neuron with two-photon imaging, and continued imaging in this way at high zoom (with around 10 to 20 spines in the same field of view) and high temporal resolution (between 200 and 1000 frames per second). For systematic mapping of spine calcium signals, I found the following order to be efficient: from the left side of dendrites to the right (left-to-right), and from the apical dendrites to basal ones for tufted neurons. For this full-frame imaging mode, the average power delivered to the tissue is usually in the range of 20–30 mW under the objective.

18. The amount of laser power needed to obtain subthreshold spine and dendrite signals was adjusted based on the quality of the microsurgery.

19. We then began to perform the auditory stimulation, cell-attached recording and spine calcium imaging simultaneously. Spontaneous spine calcium signals and the corresponding somatic electrical activity can also be recorded. The recording time is limited by the onset of the first signs of phototoxicity. With the above-mentioned LOTOS settings, typically six to ten trials of spine imaging (duration of each trial = 30 s) can be safely performed. In order to correct for mechanical movement which is often present when trying to image spines in the auditory cortex, it is important to realign the imaged dendrite to the focal plane before starting each stimulation trial.

20. After 5-6 trials of imaging, with 30s each, I acquired a z-stack of images of the dendritic branch for post hoc three-dimensional reconstruction of the recorded spines using the LOTOS mode (z-scanning step size = 0.25 µm, scanning range = 30 µm, step dwell time = 2 s).

21. After this, we moved to another dendritic branch for spine calcium imaging and continued the protocol.

22. At the end of the experiment, I acquire a z-stack of images of the neuron. While doing so, I placed as many dendrites as possible in the field of view using the full-frame mode (z-scanning step size = 0.5 µm, scanning range = covering all visible dendrites, step dwell time = 1 s). Depending on the maximal available field of view in one z-stack, multiple z-stacks at different locations may be acquired. The laser power was higher than for dendrite imaging, and was reduced gradually while acquiring z-stack images from the bottom portion of the neuron to the top portion.

23. Having acquired the z-stack, I carefully retracted the pipette.

Off-line analysis of spine calcium signals (hours to days)

24. The data was smoothed and then downsampled from 1,000 frames per second to 80 frames per second. In the case of imaging on the resonance scanner, imaging data acquired at 200-500Hz was not downsampled. The downsampling was done by using a lowpass filter to smooth the time series of each pixel, and then keeping the images at 80hz in a custom-written program for spine imaging data analysis based on LabVIEW 8.5.

25. An average template image of 500 consecutive frames (6.25-s recording period) was made from the downsampled data.

26. The brightness and the contrast of the average image were adjusted so that the dendritic spines are readily visible.

27. The regions of interest (ROIs) were drawn manually on both spines and corresponding dendritic shafts.

28. The fluorescence changes were calculated for each such ROI and expressed as Δf/f.

29. Then noise filtering (an exponentially weighted moving average) was applied in order to obtain the final results.

30. Steps 23–29 were repeated for all the trials from the same dendritic branch.

31. We visually examined the features of spine calcium signals in detail using a software called Igor for display, e.g., the reliability of the responses, the relationship with electrical activity, the frequency and intensity tuning properties, and the spatial and temporal patterns of the responses. These considerations helped in further reshaping the hypothesis after series of up to 5 successful experiments.

32. For quantifying the responses to auditory stimulation, the following procedure was applied in Matlab after the calcium traces were obtained in LabView for single spines, dendrites, trunks, and neuronal somata in the case of AM loading: Tone-responsive calcium transients were defined as significant if they had an amplitude that is at least 3 times the standard deviation of the 100ms calcium fluorescence just before auditory stimulation (the same pro-

cedure as for Chen et al 2011. In this case, the peak value was defined as the maximum amplitude of calcium transients within 500ms just after stimulus onset. In the figures showing average calcium transients in the 'Results' section, the red traces correspond to tone-responsive transients and the black traces show the transients which did not satisfy these criteria. The fraction of tone-responsive trials was also examined based on the ratio between the number of tone-responsive trials and the number of all trials. A significant response to a given frequency was therefore obtained when a ROI had a significant response in minimum 50% of the stimulation trials with a given frequency. The frequency sweeps were defined as the average values of the calcium signal amplitudes as a function of all frequency conditions tested (Chen et al, 2011). The amplitude of a calcium signal was determined as the average value for a period of 200ms around the peak of the calcium transient (25ms before and 175ms after), with the prestimulus calcium fluorescence of 100ms before the stimulus onset being subtracted. The best frequency (BF) was defined as the frequency with the maximum value in the frequency sweeps, which applies to both the significant larger calcium signal compared to the prestimulus calcium fluorescence value and the larger fraction of tone-responsive trials. The significance of calcium signals was verified with paired t-tests across trials between the time averaged calcium transients at 200ms just before as well as after tone onset. The baseline-corrected calcium signal in each ROI was obtained by subtracting the linearly fitted background fluorescence from the original fluorescence calcium trace of each neuronal somata. Finally, the difference between the best frequency of each cell somata in the tonotopy map was plotted as a function of the distance between the given pairs of ROI. With these parameters, the Matlab analysis of the fluorescent traces for each neuronal somata gave the following information: average responses to each frequency for each ROI, as well as the single trial responses for each ROI, frequency tuning curves for each ROI based on the average calcium traces, as well as a significance test for the responses of each cell to each frequency. In order to obtain the coordinates for each ROI and the distances between them, an average map of the xy coordinates for the center of each ROI was obtained in LabView. This xy map was then combined with the tuning information for each ROI and displayed as a tonotopy map with a color code ranging from 2 to 32 khz (blue is 2khz, and red is 32 khz). The xy ROI coordinate map was further used to assess the distance between similarly tuned cells. Further statistical analyses were performed in Excel. The exact same procedure was applied to trunk imaging of multiple electroporated cells.

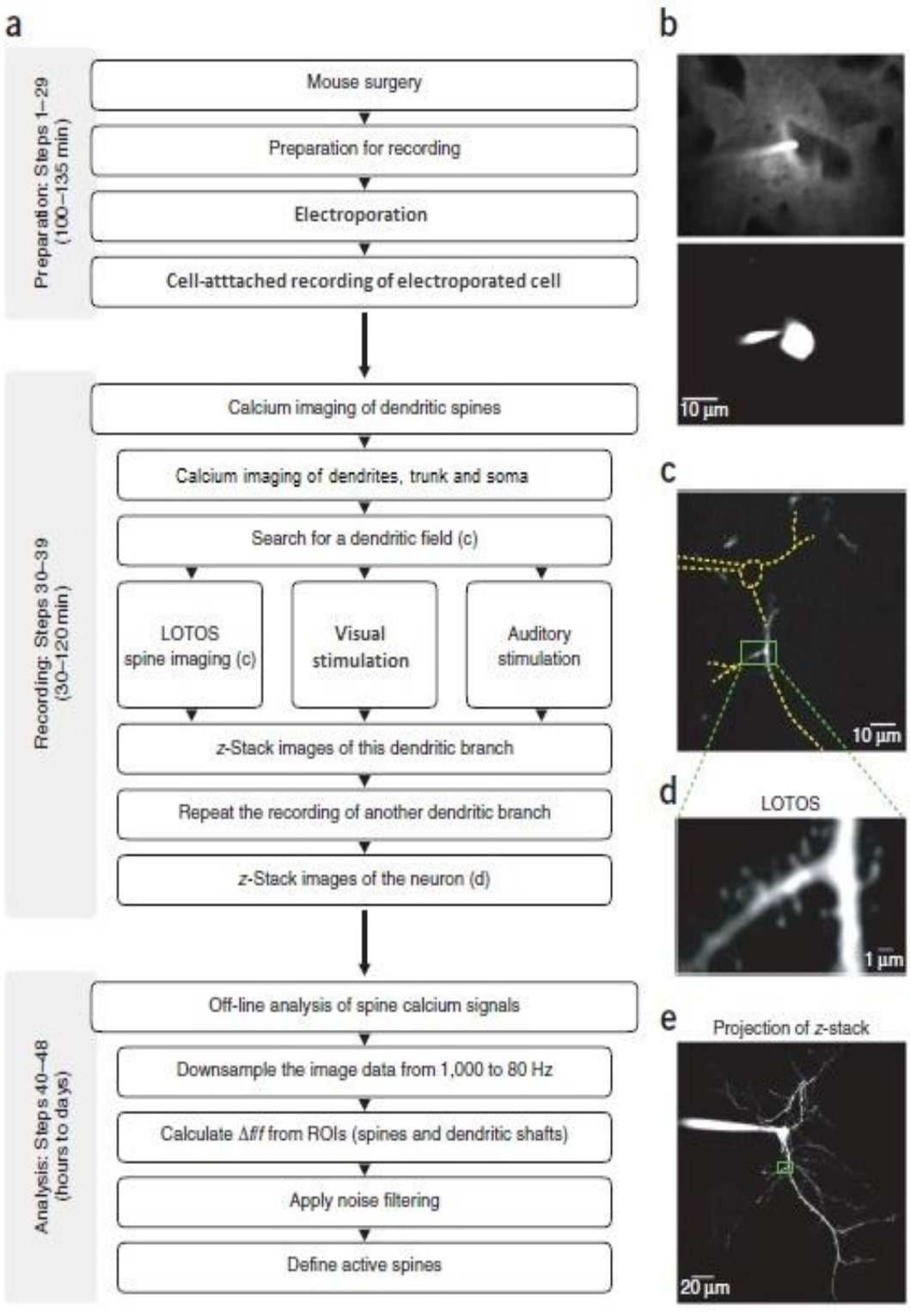

Fig. 15. Flowchart for the entire experimental procedure. a. Flowchart showing all steps of the procedure. (b) Two-photon images showing a L2/3 neuron before and after electroporation. Top, the cell before the approach and after releasing a calcium dye into the soma. Note the electroporation pipette on

the left side. (c) Two-photon image of one focal plane of another L2/3 neuron, acquired with the full-frame mode (frame rate = 80 frames per s). This step allows for searching dendritic fields. Yellow dashed lines indicate out-of-focus portions of the neuron and the electrode. (d) Two-photon image of a dendritic segment indicated by the green box in c (average of 6,250 frames), acquired with the LOTOS procedure. (e) Projection of a *z*-stack of two-photon images of the same neuron in c and d. This image is merged from multiple stacks from different portions of the dendritic tree.

Table 1. Troubleshooting table for combined electroporation and cell-attached recordings.

Step	Problem	Possible reason	Solution
1	Persistent bleeding	Damaged blood vessels	Gently puff fresh ACSF to the craniotomy.
			If this does not work, completely remove ACSF
			from the chamber and keep the craniotomy dry
			for 20 s or longer (max duration: 2 min)
2	Bubbles in the agarose	There are air bubbles	Shake the glass tube for several

		inside the agarose after it is boiled.	times after the agarose is boiled. If there are still some bubbles, cool down the agarose and boil it again
3	Very low breathing rate	Isoflurane overdose	Keep the breathing rate at 90–120 breaths per min by constantly adjusting isoflurane level. Keep body temperature at 37 °C.
4	The need of large lateral movements of the pipette	A large blood vessel is present in the way of	Retract the pipette back to the surface of the brain and slightly shift to a new location

		the target neuron	to avoid the blood vessel
5	Cannot form a cell-attached seal	There is no clean contact between the pipette tip and the cell membrane	Change to a new pipette and approach another cell
6	Whole-cell configuration is formed	The pipette is pushed too much into the cell body	Reposition the pipette tip with two-photon imaging guidance and apply brief suction again
7	Poor visibility of dendritic spines	Dye loading time is too short	Wait until the spines are visible
8	Electroporated cell is hyperactive	Electroporation was too agressive	Electroporate another cell with a lower pulse intensity and duration
9	No Ca^{2+} signal in electroporated cell	Too much dye was injected	see above
		Tissue is not	Restart ex-

		healthy	**periment**
10	**Ca^{2+} signals are too small**	**Too much dye was injected in the neuropil**	**Re-electro-porate in a different ar-ea**
		Photodamage	**Move to an-other den-dritic seg-ment**
11	**Large motion artifacts**	**The imaged dendrite is close to large blood vessels**	**See above**

The version of the LOTOS for combined electroporation and electrophysiology with the aim of imaging spine and dendrite calcium signaling is, in my view, the most appropriate for understanding in vivo neuronal functional integration in single cells.

Its main advantage compared to loading cells with a calcium dye via whole-cell recordings is that there is no dialysis of the solution inside the pipette into the recorded cell, which may mean that the spiking activity recorded from the electroporated cell may be closer to its physiological one.

The AOD-based or resonance scanner-based LOTOS procedure we described here allows reliable and long-term imaging calcium transients with a robust signal-to-noise ratio in dendritic spines of cortical neurons in vivo, which can be clearly distinguished from the signals in the neighboring dendritic shafts. The prolonged recording time before photodamage (up to 350 s of total illumination; mean = 241 s) allows for stable recording of multiple trials of spontaneous and stimulus-evoked spine calcium signals, thereby providing a method to explore the sensory functions of such small structures, as well as their integration throughout the dendritic tree.

Moreover, spine calcium imaging using the resonant mirror–based LOTOS procedure running at 200 frames per second usually lasts for at least 300 s before photodamage. This procedure for spine calcium imaging allows for a number of new applications.

The application I used in the visual cortex allowed for simultaneous mapping of spine and dendritic inputs together with the firing output of a cell, by performing cell-attached recordings on electroporated neurons. This way the physiological activity of neurons could be recorded, without the need of hyperpolarizing the cell or generating cell dialysis. By recording spine and dendrite calcium signals in the presence as well as absence of backpropagating action potentials, I was able to distinguish sensory-evoked single spine inputs together with dendritic events which appeared in the absence of action potentials.

For electroporation, it is important to consider the possibility of damaging a cell while injecting the dye. For this reason, I have chosen a pulse strength around 270nA, and used 2-3 such pulses for injecting the calcium dye, depending on cell size. An electrical pulse that is too strong can cause irreversible damage to the cell. The best way to test for this is to measure the spiking rate of the cell 2 hours after the injection, and compare the spiking rate with that of similar non-electroporated cells. A damaged cell will have a higher spiking rate than other similar cells, and event burst continuously. The two hour recovery time allows for recording under physiological conditions, provided that this condition is met. Apart from mechanical damage during electroporation, it is also important to consider whether the amount of calcium indicator loaded inside the cell is large enough to provide the best calcium transients, again without overloading the cell with calcium dye. For OGB1, the intracellular concentration for whole-cell dye loading is around 20 µM, as measured by Stosiek et al[36] when performing a whole cell recording on an AM-loaded cell and measuring the concentration at a similar fluorescence value for the nearby cells. For electroporation, the experimenter can use the fluorescence of the calcium dye-filled pipette tip as a standard. After 2-3 pulses of 270nA for 30s with a pipette containing a 9 mM OGB1 hexapotassium salt calcium dye, the fluorescence of the soma should be comparable to that of the pipette tip.

Another important consideration for an experimenter who wishes to perform an electroporation of a pyramidal neuron is the position of the pipette relative to the cell. In this situation, the pipette should be juxtacellular in that it barely touches the cell membrane, without entering or breaking it. However, should the pipette be too far away from the cell, the dye loading will not be complete and it will be very difficult to obtain a single action potential resolution.

Since the brain is a 3D space which is viewed by the experimenter as a 2D space, the pipette may often be above or below a certain cell but look as if it is touching it. When the cell fails to load with dye despite multiple pulses, it is better to restart the process on a different cell, while monitoring the re-

sistance of the pipette and lowering the pipette up to 1 µm. Once the cell has been loaded successfully and appears to have a spiking rate close to the physiological range, the cell can be targeted for cell-attached recordings. The main difference between cell-attached and juxtacellular recordings is that the 'grip' of the membrane is stronger, and does now allow for the possibility of recording action potentials or local field potentials from nearby cells as in the case of juxtacellular recordings.

As in the case of electroporation, a grip that is too strong may damage or even break the cellular membrane. Should the recorded resistance be above 100MΩ, the change of the pipette breaking through the membrane is very high. Since the cell-attached pipette contains extracellular solution, breaking into the cell will result in strong depolarization and potentially the death of the cell. It is therefore important to monitor the resistance recorded from the pipette throughout the experiment. One of the advantages of cell-attached recordings is that during brain movement the pipette can be slightly retracted without damaging the quality of the recording.

I have also applied this method to both superficial and deeper neurons in the mouse auditory cortex while stimulating with pure tones as well as the visual cortex while stimulating with drifting gratings. Small dendritic calcium events could also be observed in the distal as well as proximal dendrites of superficial neurons in the auditory cortex.

In the case of targeted multi-cell electroporation in deeper layers, the procedure is the same as for single cell electroporation, except the aim is to electroporate multiple cells in the same field of view which are close enough to each other in order to have all their apical trunks within a field of view of 150-200 µm. Apart from the experimental adjustments made for deep imaging (larger craniotomy that allows for collecting more photons), increasing the frame rate and keeping the laser power low allows for reliable recordings while preventing scattering.

Apart from LOTOS imaging of dendrites and spines of electroporated neurons during simultaneous cell-attached recordings and sensory stimulation, we also performed population imaging in unanesthetized animals with bolus loading of Cal520 as well as population imaging of trunks of electroporated cells using the targeted multi-cell electroporation approach. The mouse surgery and the preparation for recording are the same for both of these methods. The pipettes used for AM loading have the same tip diameter as the ones used for electroporation, and in the case of targeted AM loading specifically for layers 4 and 5, the injection was monitored by adding a small concentration of Alexa594 dye to the Cal520 AM dye. The dye was applied with a small positive pressure at around 550 µm in the brain, and the pressure was stopped as soon as the fluorescence labelling reached 450 µm. Imaging was

then performed on the AM-loaded cells during sound stimulation at low zoom (with a field of view of 150-200 µm) in the unanesthetized mouse. During removal of anesthesia the breathing rate and movement of the mouse were constantly measured. Recordings began 15 minutes or more after the anesthesia was stopped, and after the breathing rate was over 180 breaths per min and after the mouse started moving. Base on visual inspection, were no significant changes in neuronal activity between 5 min and 1.5 hours after removing the anesthesia.

TIMING

Steps 1–8, mouse surgery: 45–60 min

Steps 9–12, preparation for recording: 30min

Steps 13–22, electroporation, cell-attached recordings, and calcium imaging of dendrites and spines: 30–120 min/AM loading, imaging of AM loaded cells/targeted multi-cell electroporation, trunk imaging

Steps 40–48, off-line analysis of calcium signals: hours to days

Using this experimental setup, I was able to measure spine and dendritic calcium transients together with the cell's spiking activity.

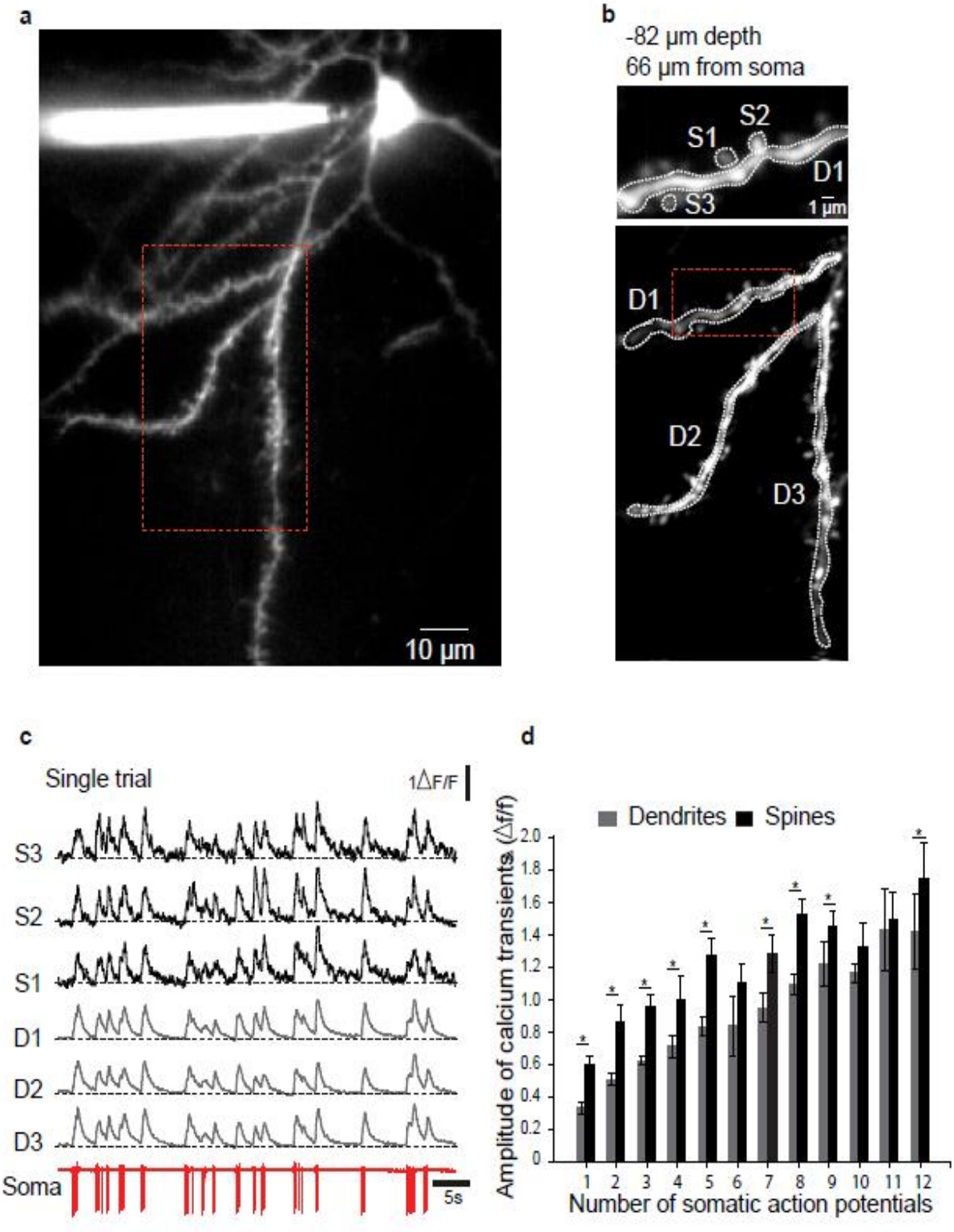

Fig. 16. Correlation between AP firing and Ca^{2+} activity in OGB1-6K electroporated layer 2 non-tufted neurons in the mouse V1 in vivo . (a) z-projection of a layer 2/3 neuron of the primary visual cortex, labelled with OGB-1. (b) Lower panel: low-magnification image of the area marked in a. Upper panel: high magnification image of the area marked by the red rectangle in the lower panel. (c) Spontaneous calcium transients recorded in the dendritic segments

(blue traces) and the spines (black traces) indicated in panel b. The corresponding somatic action potentials are shown below in red. (d) Average amplitude of the calcium transients in dendritic segments (black) and corresponding spines (blue) for different trains of somatic action potentials (1 to 12 APs, less than 50 ms apart). Error bars indicate SEM.

One of the first observations we made when looking at calcium transients of electroporated cells in combination with cell-attached recordings is that single backpropagating action potentials produced reliable calcium transients, and the correlation between the number of action potentials and calcium transients observed in dendrites is mostly linear in layer 2/3 non-tufted cells in the mouse visual cortex (Fig.17). Furthermore, the adapted LOTOS procedure could be used to map larger dendritic fields while keeping a resolution for imaging single spines. As fig. 17 shows, the linear correlation between single calcium transients and the relative number of action potentials recorded simultaneously at the soma is relatively clear. However, there are some small nonlinearities which are considered to be due to the combination of excitatory and inhibitory inputs the cell receives, as well as the combination of back- and forth-propagating action potentials. Importantly, the contribution of nonlinear integration is relatively small in non-tufted pyramidal cells. The next figures will show some of these nonlinearities, and focus more on the excitatory NMDAr-dependent inputs and their propagation, given the limitations of the method used.

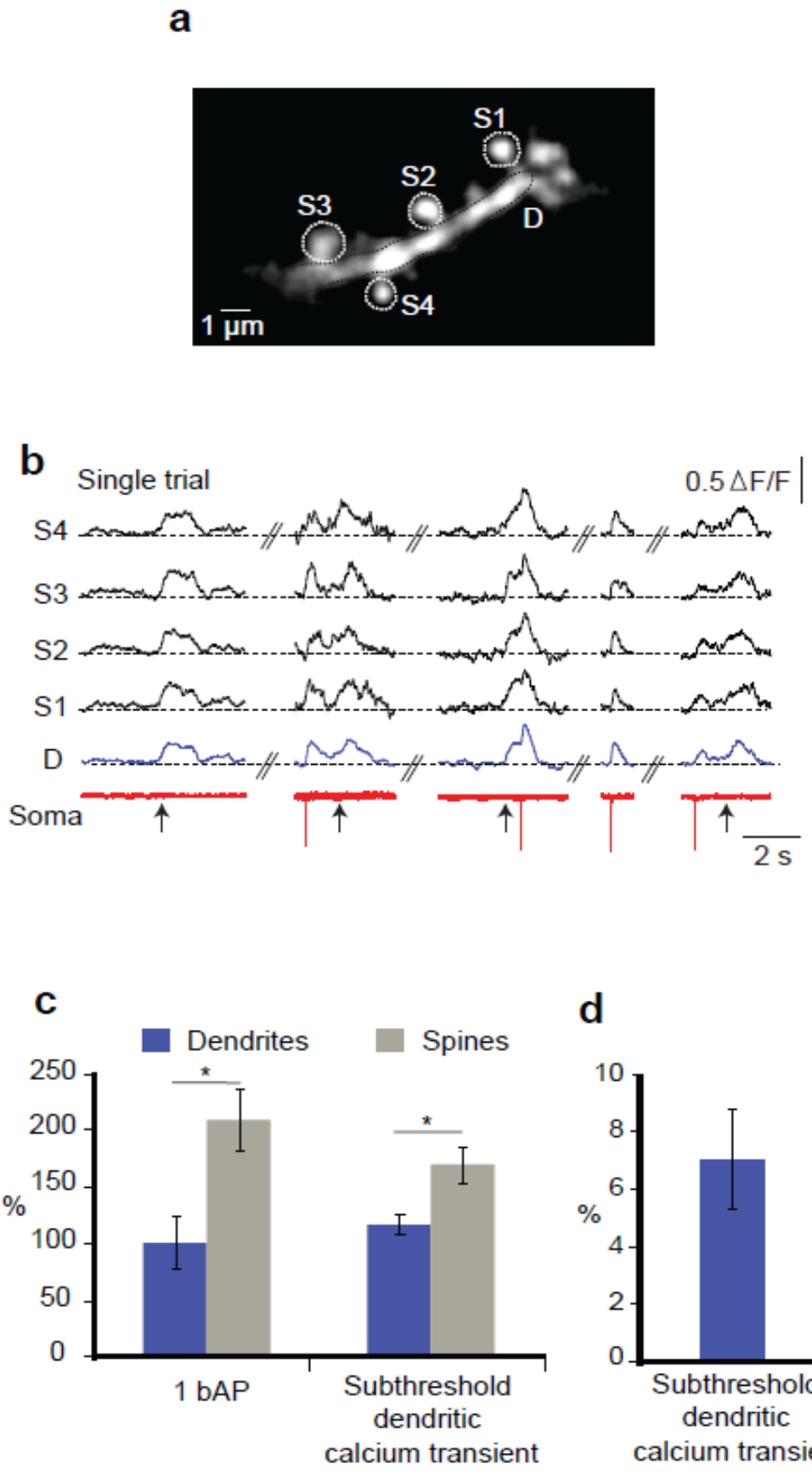

Fig.17. Dendritic Ca^{2+} transients in the absence of action potential firing in

OBG1-6K electroporated layer 2 non-tufted neurons in the mouse V1 in vivo. a. In vivo two-photon image of a dendritic segment of a layer 2 neuron in the primary visual cortex. b. Spontaneous dendritic and spine calcium transients recorded in the regions of interest indicated in panel c. Subthreshold dendritic calcium transients are indicated by black arrows. (c) Relative amplitudes of subthreshold dendritic calcium transients compared to calcium transients associated with 1 somatic action potential. d. Proportion of subthreshold dendritic calcium signals among all calcium transients (n=200 in 6 dendritic segments from 3 mice). Such dendritic transients occurred at a frequency of 0.007 Hz. Errors bars indicate SEM.

Apart from subthreshold single spine calcium transients, I could also observe subthreshold dendritic events, with a relatively lower rise time than the previously observed spine inputs. These events were observed together with single spine signals in the corresponding dendritic segment, and were relatively smaller than the spine signals. The relative difference between the spine signals and the corresponding dendritic signals was smaller when these events appeared in the absence of an action potential. The percentage of subthreshold dendritic calcium transients observed is around 7%. Again, these dendritic subthreshold calcium transients had a relatively slower rise time and a lower amplitude than their corresponding spine signals, suggesting that these inputs did not lead to an action potential-like all-or-none event in these cell types.

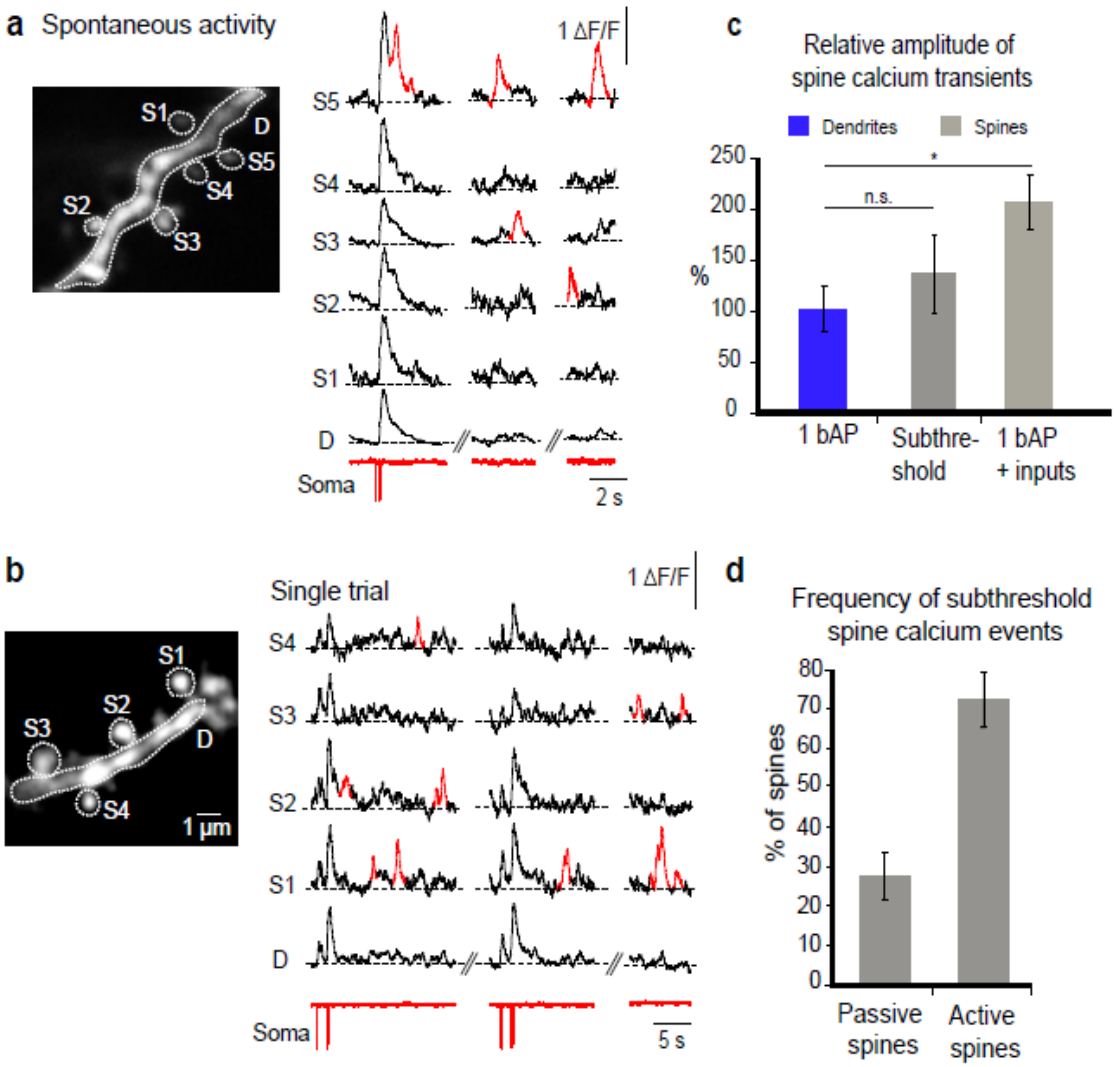

Fig.18. Single spine Ca^{2+} transients in the absence of AP firing in OGB1-6K electroporated layer 2 non-tufted neurons in the mouse V1 in vivo. a-b. Spontaneous calcium transients recorded in the dendritic segments and the spines indicated in the high-magnification images on the right panels. Subthreshold spine calcium transients are indicated in red. c.Relative amplitude of subthreshold spine calcium transients compared to calcium transients associated with 1 somatic action potential. d. Frequency of subthreshold calcium transients in spines. On average, 72 % of the spines displayed subthreshold calcium transients (n=100 spines from 13 dendrites of 4 mice).Errors bars indicate SEM.

Under these experimental conditions, single spine signals could also be observed in the absence of backpropagating action potentials, with different amplitudes (Fig.18). The percentage of such 'active spines' was around 72% of all the spines we recorded from (Fig.18c). The average amplitude of subthreshold single spine calcium transients was slightly larger than that of single-action potential induced spine signals. These subthreshold spine calcium transients were larger than those generated by a single action potential, and smaller than the ones generated by a single backpropagating action potential (bAP) and a simultaneous input.

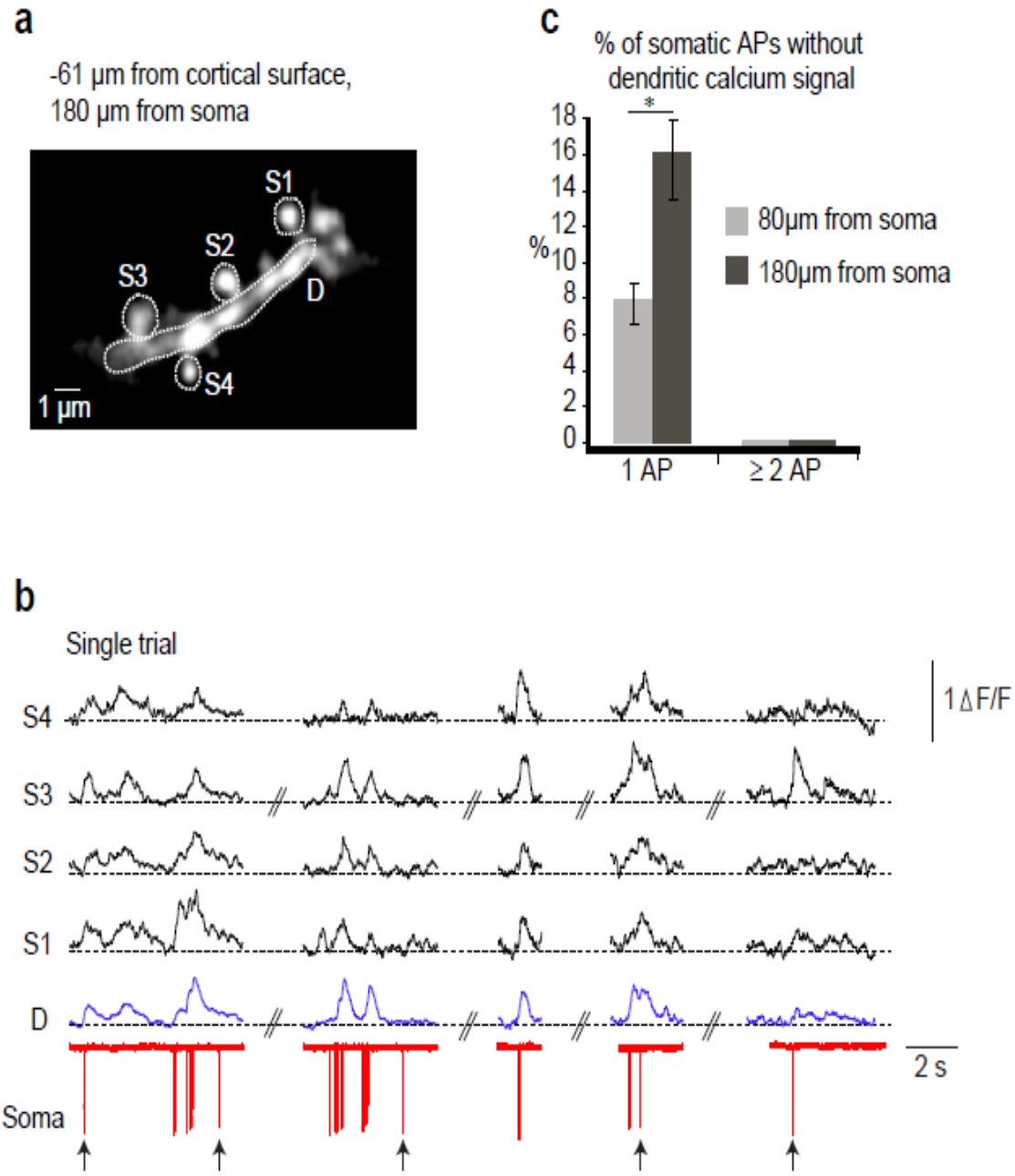

Fig.19. Action potential firing without associated calcium transients throughout the dendritic tree. High-magnification image of a dendritic segment of a layer 2/3 neuron in the primary visual cortex. (b) Spontaneous calcium transients recorded in dendrite and spines indicated in panel a. Single action potentials are indicated by black arrows. (c) Percentage of somatic action potentials without dendritic calcium signals. Around 16 % of single action potentials were not associated with dendritic calcium transients at distal (160-197 um) locations from the soma. Trains of action potentials were systematically generating dendritic calcium transients at both proximal and distal locations. Errors bars indicate SEM. (n=200 calcium transients in 6 dendritic segments in 3 mice)

Under the same conditions, we also observed that some action potentials failed to backpropagate in distal sites of the dendritic tree, despite the presence of subthreshold spine and dendritic inputs in the same recording (Fig.20b). The percentage of somatic action potentials that did not backpropagate in the dendritic sites I recorded from is 15% in the distal sites and 7% in the proximal sites. Only single action potentials failed to backpropagate, while 2 action potentials always produced calcium transients reliably throughout the dendritic field.

According to the literature, the shape and causal influence on the output of a dendritic spike depends very much on the morphology of the cell. For example, CA1 cells do show high amplitude NMDAr-dependent calcium spikes in intracellular calcium on different dendritic portions[37]. Furthermore, subthreshold calcium spikes have been observed in the tuft of some cortical neurons, which is probably due to the large difference in backpropagation of somatic action potentials between tuft and basal dendrites in such cell types.

In non-tufted neurons in the mouse visual cortex, we have observed such dendritic events, but their shape resembles a cumulative measure of a large number of spine signals. The figure above also demonstrates the large number of nearby spines that are activated simultaneously, without generating such a large dendritic event. It may be that if a large dendritic event was formed, it would propagate to the soma and generate an action potential. This suggestion is supported by the large number of calcium transients observed in dendrites which preceded the action potential firing, as in the figure above, suggesting that there might be a causal connection between the calcium spike and the cell firing.

To conclude on the results presented so far, we have applied the combined electroporation and cell-attached recording method to the mouse primary visual cortex non-tufted neurons in layer 2 of the V1 and have observed a number of events and modes of integration. The most common one is backpropagation of single action potentials, followed by single-spine inputs which do not propagate into the neighboring dendritic segment. We have also observed dendritic events together with these large spine inputs, suggesting that strong enough inputs to a dendritic segment (either in amplitude, number or amount of clustering) at the level of spines can lead to a dendritic event which still does not produce an action potential at the soma. Finally, we have also observed cases in which the action potentials did not invade the entire dendritic field, with events called failures being far more common in distal dendritic segments rather than in proximal ones. These preliminary results have helped us better understand which modes of integration may exist in a pyramidal neuron when a cell is not hyperpolarized and functioning within

physiological conditions. With this knowledge in mind, we could now move forward to understanding integration during sensory processing.

Given the observations made in layer 2/3 of the mouse visual cortex, a number of questions have arised. The first one is whether these events also appear in other brain areas, and whether these events are observed also in tufted neurons, in different layers of the cortex. There are many lines of evidence suggesting that integration may look very different in tufted neurons[38], given that tuft activity does not reflect the firing activity as linearly as in the case of non-tufted neurons. In fact, a number of studies suggest that the apical tuft of such neurons works as a separate compartment, without much evidence so far for a reliable sensory-driven response in the tuft. For example, Palmer et al 2014 have looked at calcium transients in the tuft of layer 2/3 tufted neurons in the somatosensory cortex during hindpaw stimulation, and observed calcium transients in the tuft during hindpaw stimulation only in 18% of the stimulation trials. In order to see a reliable response, they combined hindpaw stimulation with electrical stimulation of layer 1 of the somatosensory cortex veryvia an electrode. These data suggest that layer 1 activity might be responsible for the absence of reliable responses in the tuft of cortical neurons. Furthermore, since in our hands the mouse visual cortex shows a relatively small number of tuned cells under isoflurane anesthesia, and experiments with isoflurane-anesthetized mice had a much higher success rate in terms of finding neurons with an obvious response to auditory stimulation, we decide to explore spine and dendritic inputs on single cells in deeper layers with these same methods but this time in the mouse auditory cortex, with the aim of giving an integrative picture of sensory processes in tufted cortical neurons.

In order to electroporate in deeper layers, some adjustments had to be made to the resonant scanner two photon microscope setup. Some of these include: a larger craniotomy that allows for more photons to be detected, a better photomultiplier tube detector which has a lower dark noise and a higher sensitivity to detecting single photons, reducing the imaging time at high depths in order to reduce phototoxicity at the surface where the tuft is imaged, and also doing blind electroporation (advancing the pipette to the desired depth without imaging and only monitoring the pipette resistance). One main advantage of the auditory cortex when doing deep imaging is its curved surface, meaning that starting at the beginning of the surface curvature will yield a gain in depth of up to 200 µm in depth simply due to the curvature of the cortex. The downside of performing these experiments in the auditory cortex is given by the larger number of blood vessels in this cortical area, which can give a lower success rate due to heartbeat-related movement in the superficial tufts, as well as limited visibility in depth due to the shadowing

effect of multiple blood vessels. Such experiments therefore require a PMT detector with low dark noise and high gain, as well as a fast scanning rate that would allow for compensating with a larger amount of laser power.

The results below will show not only that populations of neurons process sound in different ways and depend on various factors, but that also single neurons have various levels of integration, and this is very much dependent with what their network is telling them to integrate. In order to do this, I have looked at the sound-induced responses in dendrites and spines of these neurons in combination with loose-patch recordings. These experiments are considered to be technically challenging, and for this reason, with a few exceptions, most imaging studies related to integration in the auditory cortex have focused on population rather than single cell imaging.

These results led to a lot of other questions: can the tuft be reliably activated by sensory stimulation? Can the tuft alone be activated as such? Are these events dependent on coincident input and backpropagating action potentials or are presynaptic events sufficient to generate dendritic events on their own? Can we modulate this process in order to get stronger or weaker effects?

In answer to the first question, tuft dendrites could be reliably activated by sensory stimulation. Based on the findings of Chen et al 2010, showing that increasing the sound intensity of white noise activates a larger number of dendritic spines in non-tufted neurons, we decided to test whether very loud white noise (93dB) would indeed elicit even more reliable responses in tuft dendrites of layer 3 neurons In the mouse auditory cortex. Importantly, the average number of tuft responses to the white noise stimulation trials is in fact larger than the action potential firing responses to the same stimulation trials. We used white noise rather than single pure tones in order to increase the response probability, based on the idea that white noise includes more than one frequency, and potentially including the neurons' preferred frequency as well.

As Fig.21 shows, the percentage of trials which elicited a significant response in the tuft dendrites recorded is higher than the percentage of trials which elicited an action potential response from the cell, suggesting a causal role between the tuft dendrites and the firing activity of the cells. Importantly, the percentage of successful stimulation trials is 92% in tuft dendrites and 75% in the firing activity of the recorded cells, which shows that it is indeed possible to obtain reliable responses from tuft dendrites to sensory stimulation. Palmer et al 2014 obtained a stimulation success rate of only 18% in tuft dendrites of layer 3 neurons of the mouse somatosensory cortex, which was later coupled in their study with artificial electrical stimulation of layer 1 in order to produce a reliable response, and this was then interpreted as a need

for tuft dendrites to receive coincident input. Here we show that tuft dendrites can act on their own and do not require coincident input in order to generate reliable responses to sensory stimulation. Furthermore, since these recordings were made in isoflurane-anesthetized animals and neuronal responses are dependent on up and down states, it may well be that the reliability of the responses goes up to 100% should the mouse not be anesthetized. Since now we had an answer to the question of whether tuft dendrites can indeed be activated reliably by a type of sensory stimulation, we decided to try and answer the next question on whether the tuft can be activated by sensory stimulation in the absence of coincident backpropagating action potentials, and whether we can modulate this process. In order to obtain proof of the tuft being activate on its own, we had to find tuft responses in the absence of action potential firing, which can be easily verified by again electroporating layer 3 tufted neurons and performing a targeted cell-attached recording.

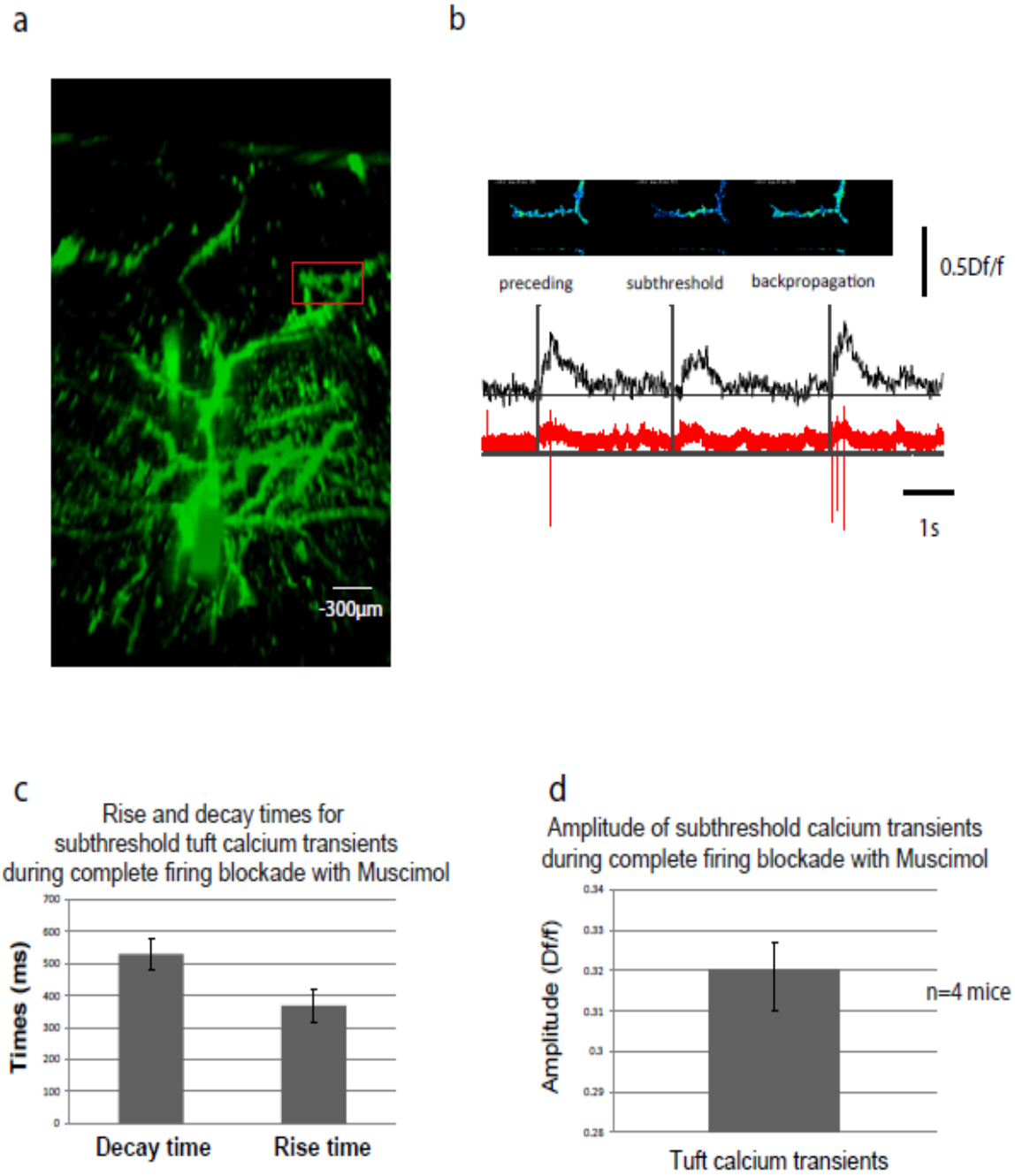

Fig.20. Sound-evoked subthreshold Ca^{2+} transients in tuft dendrites of an OGB1-6K layer 3 neuron in the mouse A1. a. z-stack projection of an electroporated neuron in layer 3 of the mouse auditory cortex. b. Dendritic calcium transients in a tuft dendrite located 140 µM below the cortical surface in response to white noise at 93dB during partial blockade with 30 µM Muscimol applied locally at the soma. c.. Rise and decay times of subthreshold tuft Ca^{2+} transients during complete firing blockade with GABAa agonist Muscimol. e. Rise and decay times for subthreshold tuft Ca^{2+} transients during complete firing blockade with Muscimol. d. Amplitude of subthreshold Ca^{2+} transients

during complete firing blockade with Muscimol. Error bars indicate S.E.M. n=4 mice, 20 subthreshold Ca^{2+} transients, 5 for each mouse.

Figure 22 shows an example neuron in layer 3 of the mouse auditory cortex during auditory stimulation with 100ms long white noise at 93dB. In order to modulate the tuft responses, I brought a second pipette 5-10 µm away from the neuronal somata filled with a solution of Muscimol diluted at 30 µM. Since Muscimol is a potent agonist for GABAa receptors, the expectation was that a very small amount injected at the soma would block the somatic firing activity while leaving the physiological tuft activity intact. We chose this drug because, like the electroporation and cell-attached recording method, it does not affect the intracellular signaling in the way QX would by affecting the impedance properties of the dendrites or provoking dialysis of the solution inside the pipette into the recorded cell as in the case of whole-cell recordings combined with hyperpolarization. By applying very small positive pressure (approximately 50mbars) of the Muscimol solution at the cell somata for a few seconds, a partial blockade of the somatic firing activity could be observed (Fig. 22b). In this configuration, calcium transients could be observed in the presence and in the absence of backpropagating action potentials, as well as preceding the action potential firing. In order to examine the contribution of different dendritic subcompartments more efficiently, we used a color code for the fluorescence of the dendrite yielding an average image of the calcium fluorescence in the imaged area 200ms after the onset of every stimulation trial (Fig. 22b). Around 3 min after the first local application of Muscimol, a complete blockade of the somatic firing activity could be observed (Fig. 22c). In this configuration, calcium transients could be observed reliably in the tuft in response to the white noise stimulation, indicating that there is no need for coincident backpropagating action potential firing. Finally, approximately 10min after the local application of Muscimol, a complete recovery of the somatic firing activity could be observed (Fig. 22d), revealing large calcium transients in the tuft correlated with the cell's firing activity in response to sound stimulation, as well as spontaneous action potentials which fail to invade the tuft. These Muscimol blockade results were confirmed and quantified in n=4 mice.

After having answered the questions on whether the tuft dendrites of these neurons can respond reliably in the absence of coincident backpropagating action potentials and having seen that we can modulate the ratio between tuft signaling and action potential firing of the cell, we decided that it was time to revisit the results found in non-tufted neurons in the visual cortex in terms of the percentage of subthreshold inputs and failures, but this time during auditory stimulation in the tuft dendrites.

Interestingly, as Fig. 21e shows, the percentage of significant sound-evoked tuft transients observed in the absence of action potential firing during physiological conditions was 10%, larger than the percentage of spontaneous subthreshold dendritic events found to appear spontaneously in non-tufted neurons in the mouse visual cortex.

There were also instances in which firing in the soma was not accompanied by a calcium transient in the recorded tuft dendrite. I will refer to this phenomenon as a failure. The occurrence rate of this phenomenon was found to be 12% (Fig.21f), which is closer to the percentage of failures we found spontaneously in non-tufted neurons.

Therefore, after comparing the numbers of evoked nonlinearities in tuft dendrites of layer 3 auditory cortex neurons with the numbers obtained in tufted neurons, it appears that the differences are not that pronounced even though we have examined very different cell types under different conditions.

The last remaining question for this project was then whether the results observed in the tuft dendrites are not only an effect of the anesthesia, and whether this is a result of activating layer 1 with loud white noise.

Therefore I decided to image tufts of cells that are located in deeper layers in the mouse auditory cortex, this time in the absence of anesthesia. I used Cal520 for performing a population-level loading of a large number of cells and imaged their tufts between 20 and 200µm. The first observation that I could make is that single tuft dendrites as well as fields of view as large as 200µm containing tuft dendrites overall respond very reliably in the awake condition.

Figure 23 shows the tuft responses in this configuration at different depths within the tuft areas. Interestingly, responses in the most superficial parts (up to 100µm below the cortical surface) are fairly sparse and appear every time the sound stimulus is presented. This tendency is kept also below 100 µm below the cortical surface, but the amount of activity that is not evoked is considerably higher. Since the deeper area of the tuft is considered to have a larger backpropagation component, these results further strengthen the idea that tuft inputs are indeed responding more reliably than the cell itself, and might therefore have an important functional role. In order to assess whether this is indeed true, I examined whether the percentage of spontaneous calcium transients during stimulation trials increases with the depth of the imaged tuft segments, as shown in Fig. 23 b-d.

The results show that not only is there a linear correlation between the two but it appears that there are no spontaneous calcium transients up to 100 µm, and there is a substantial increase in spontaneous activity below 100 µm. This then confirms the notion that as we get closer to the trunk, the amount of non-evoked activity increases compared to that of the evoked activity in

the tuft. The last remaining question is then whether the percentage of successful trials also decreases with depth.

Not very surprisingly, the percentage of successful white noise stimulation trials decreases linearly with increasing depth within the imaged tuft segments.

To conclude, we have shown that subthreshold dendritic and spine calcium transients can be elicited very reliably with sound stimulation in tufted neurons in the mouse auditory cortex. This effect can also be modulated with the GABAa agonist Muscimol via a local application in order to selectively block action potential firing. Moreover, this effect even more pronounced in unanesthetized animals. I have combined the method of single cell electroporation and cell-attached recordings with tuft imaging of Cal520 AM-loaded neurons in layer 3 of the mouse auditory cortex in order to verify whether these signals originate in the tuft and that they degrade as a function of distance from the trunk. These results confirm and are complementary to the findings of Palmer et al 2014 and Smith et al 2013 which both suggest that sensory-evoked dendritic events do affect the output signaling. The main novelties in this case are the following: the tuft was reliably (92-100%) activated by sensory stimulation, the effect was modulated without affecting intracellular signaling, these events were observed also in unanesthetized animals, and the reliability degraded as linearity increased with depth. Most importantly, single cell and population imaging were combined in order to answer a question about functional computation in single cells. The next project will aim at combining methods in order to understand functional computation at the population level.

3.2. Multi-cell targeted electroporation of layer 4 and 5 cells in the unanesthetized mouse A1

Since there are many lines of evidence pointing to a large scale-structure of the mouse auditory cortex that is homogeneous, we decided to check whether the structure is preserved at the level of single cells.

As previously mentioned, deep imaging has been considered technically challenging for a long time, among other things, due to the high laser power needed to excite photons emitted from depths below 450 µm. One way of going around this is to have a large opening, and to have a local AM injection, in order to prevent fluorescence above the images sample.

The location of the mouse auditory cortex was confirmed by post-hoc imaging of the injection site. In order to verify the position of the injection, I used a template from the Mouse Brain Atlas[39] and adapted it to the slice image. I then marked the location of the auditory cortex using the coordinates of the auditory cortex in the atlas.

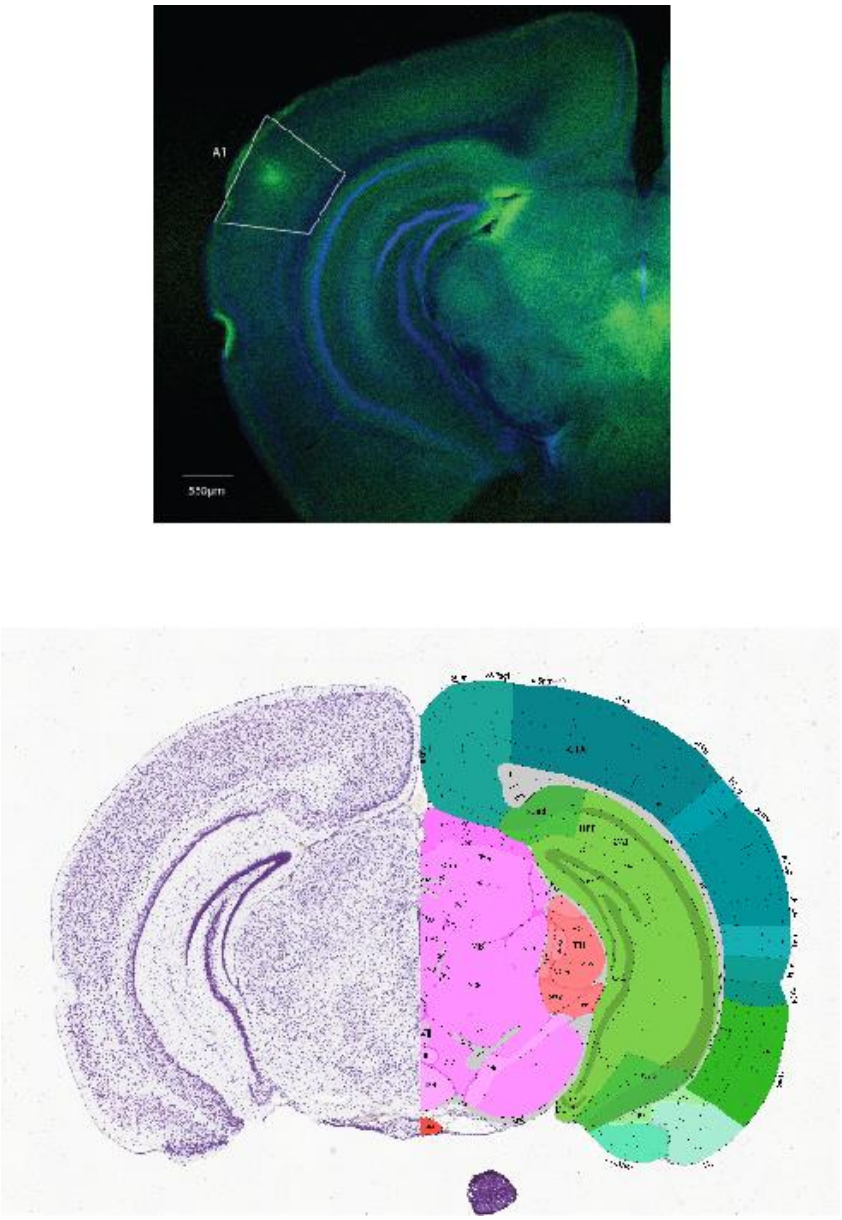

Fig. 21. Mouse coronal slice showing the location of the AM injection in the A1 with higher fluorescence. The borders of the mouse auditory cortex were drawn using coordinates from the mouse brain atlas. Scale bar is 550 µm.

For the Cal520 AM loading, the fields of view showing the highest fluorescence were located between 450 and 550 µm below the cortical surface, corresponding to layers 4 and 5 of the mouse auditory cortex.

The peak of the fluorescence is obtained within an area of approximately 300x300 µm within layers 4 and 5 of the mouse auditory cortex. This procedure allows for fast and efficient localization of the imaging site using stereotaxic coordinates which are freely available online and is particularly useful when immediate feedback is needed on finding the correct area to image, without the need for performing a recovery surgery and perfusing the animal with PFA.

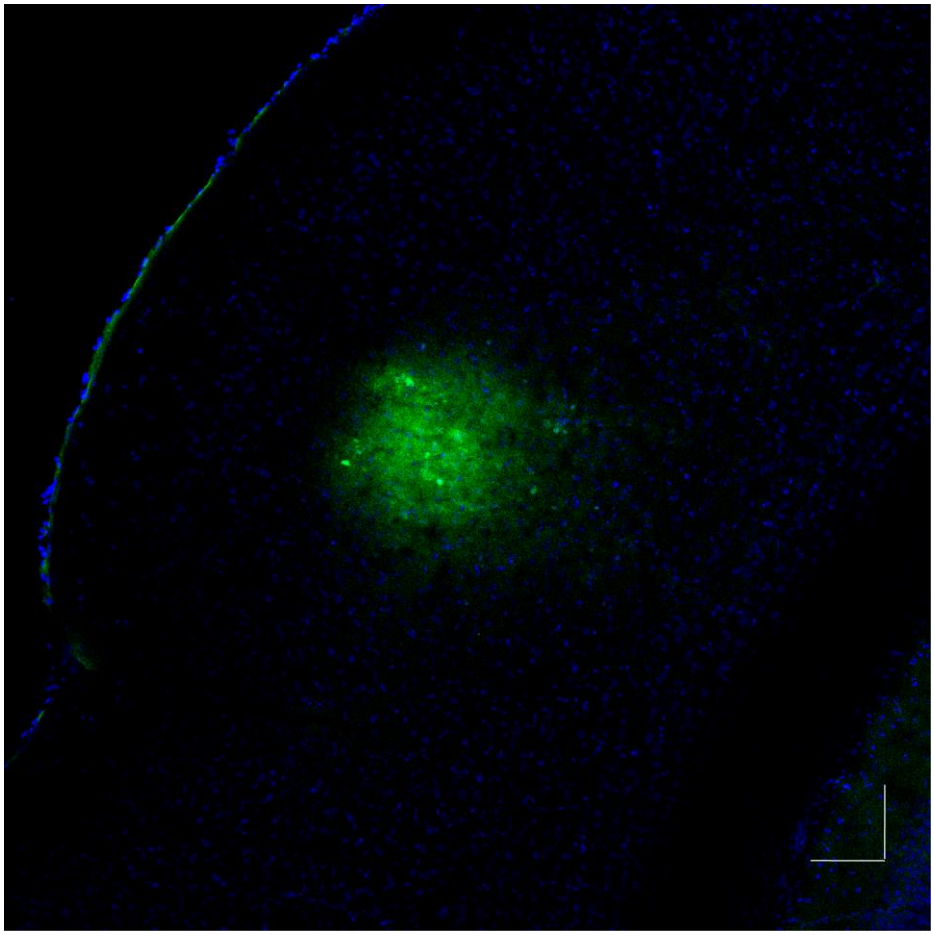

Fig. 22. Zoom-in on the location of the fluorescent OGB1-AM staining combined with a DAPI staining showing single cell somata stained in layers 4 and 5 of the mouse auditory cortex. Scale bar is 100µm.

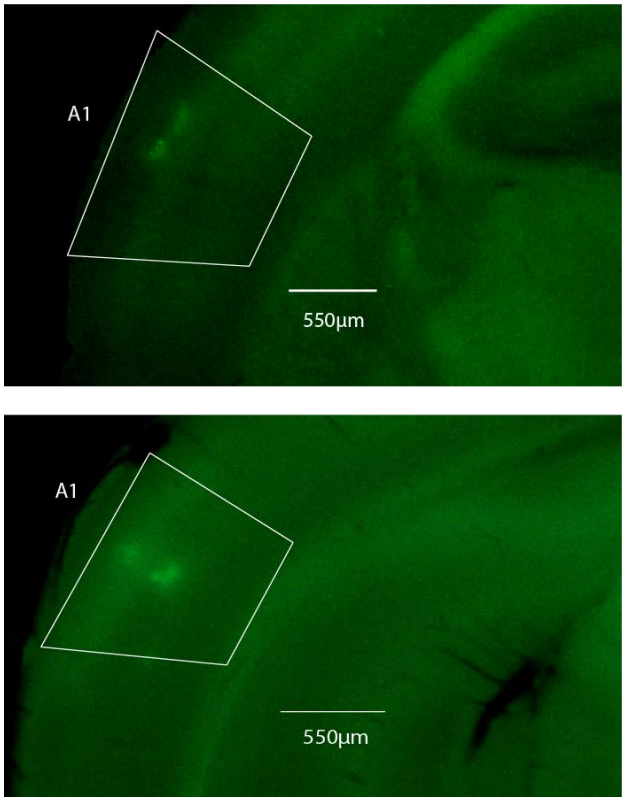

Fig.23. Further examples of staining locations of cells in layers 4 and 5 of the mouse auditory cortex electroporated with OGB1-6K.

Importantly, the electroporated cells can also be visualized post-hoc using the same procedure. Fig. 26 shows two examples of clusters of electroporated cells located within the mouse auditory cortex.

At first glance, large calcium transients could also be observed in the anesthetized condition in layers 4 and 5 and single, also corresponding to single action potentials. A striking observation is that large increases in the amplitude of the recorded calcium transients could be observed as soon as 10 minutes after removing the anesthetic gas. Consistently with Issa et al, no significant differences in activity were observed in the unanesthetized state between 10 min and 1h after removing the isoflurane anesthesia. I took this minimum time as a benchmark, while monitoring the breathing rate and movement of the animal (the breathing rate in most mice went above 180 BPM within 10 min and the first movement could be picked up by the spinning disk).

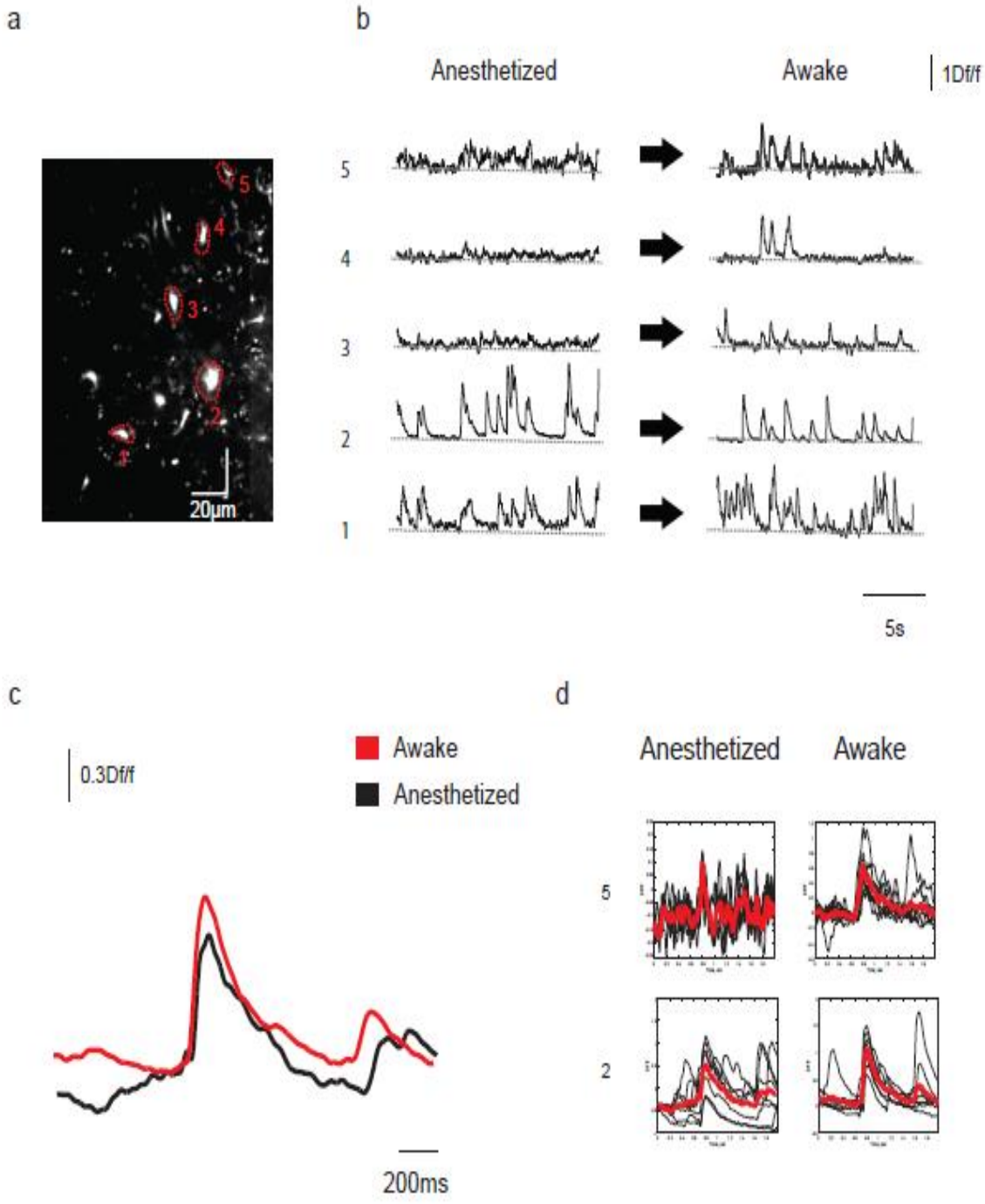

Fig.24. Comparison anesthetized vs. awake recordings in layer4 of the mouse A1. a. High-resolution image of trunks of layer 4 cells electroporated with the TMCE method. b. Single trials showing calcium transients in the ROIs marked in a in the anesthetized (left) and the awake (right) conditions. c. Average of calcium transients for a cell marked in b. in the anesthetized (black trace) and awake (red trace) conditions. d. Overlay of average and single trial responses for all cells marked in b. e. Average responses to pure tones in the same

ROIs during anesthesia and in the awake state. Black traces show average responses, and red traces show single trial responses.

The same cells imaged before and after the animal was woken up have shown slight changes in the amplitude of calcium transients, as well as changing their tuning properties, consistently with the findings of Issa et al. These results also suggest that the switch to the unanesthetized state might account for the differences found between Rothschild et al, Winkowski et al and Issa et al, with the later only performing experiment in the unanesthetized state. An obvious next step is of course to check whether this truly reflects the spiking activity of the images cells and to examine the differences between calcium traces and spiking activity with and without anesthesia.

a. Single ROI subtraction

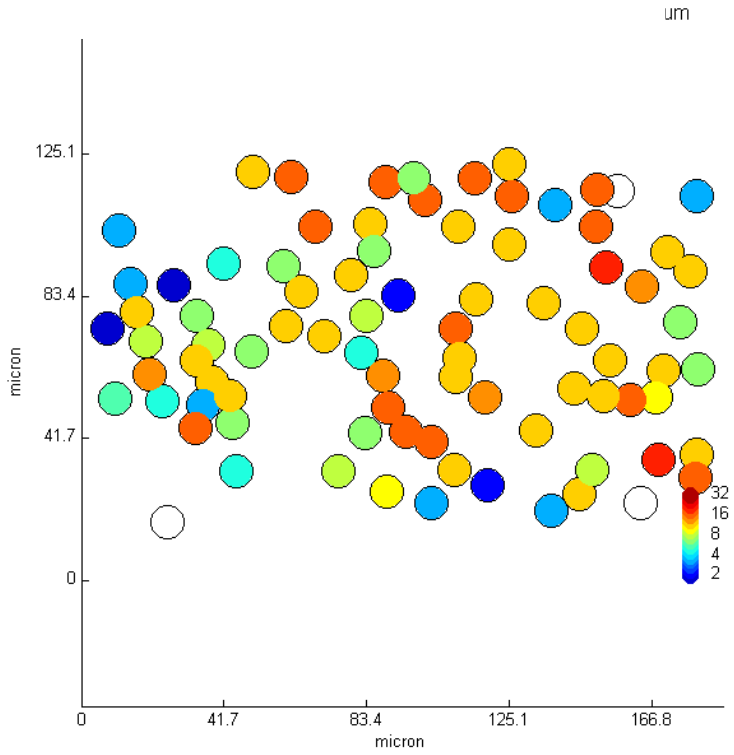

b. Multiple ROIs subtraction

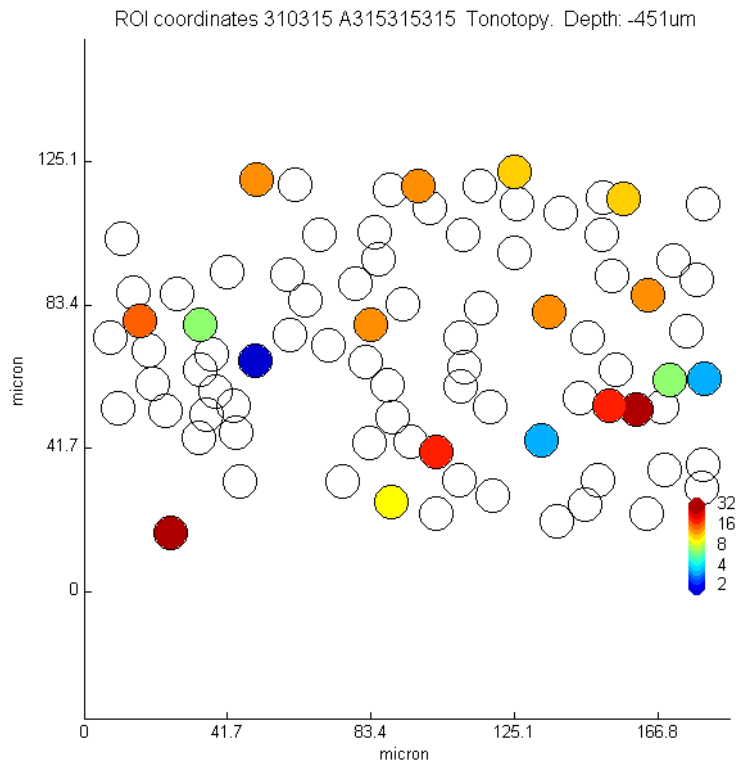

Fig.25. Example of tonotopy maps obtained with two different methods of background subtraction on the same data. a. Single ROI background subtraction whereby the fluorescent trace obtained from an ROI on the background was subtracted equally from all somatic ROIs. b. Multiple ROI background subtraction where a background circle was drawn around each ROI and subtracted from that ROI.

Importantly, background subtraction can be a major issue in population imaging, and can be crucial in the case of deep imaging. In the case of AM loading, the stained neuropil includes active dendrites and axons, and the amount of neuropil contribution to the somatic signals, may affect their responses to a very large extent. We therefore decided to go deep into this issue and makes sure we take all possible precautions for making sure that what we record is the true activity of neurons.

The method chosen for background subtraction in the case of population imaging-based tonotopy can go as far as changing the hypothesis from a fairly homogeneous tonotopic map to a highly heterogeneous one. This is illustrated very clearly by the difference between Fig.31 a and b, where two tonotopy maps were generated using two different methods of background subtraction on the same dataset. As Fig.31 a shows, the map generated with the single ROI background subtraction method shows a lot of cells tuned to similar frequencies, suggesting that there is quite a lot of homogeneity. On the other hand, Fig 31b shows a very heterogeneous map. In this case the multiple ROI subtraction method has canceled out most of the somatic signals.

The most common method for background subtraction for AM loaded cells is to subtract a constant fluorescence value that represents the average of the fluorescence value of the neuropil for the entire recording trial. I considered this to not be conservative enough for the aim of tonotopy mapping, where small difference in the detected signals may affect the tonotopy map.

Most importantly, it is never the case that all cells show the tuning for the same frequency in deeper layers.

The second, even more conservative method which may be used is making use of the same single background ROI, and taking the best fit between each cell somata and this background ROI in order to perform the subtraction. We called this the linear fitting background subtraction method. This reduced the number of tuned cells to around 70%.

The third and most conservative background subtraction method we experimented with is called the weighted baseline correction method which automatically makes a ROI around each cell somata and subtracting the nearby ROI from each somata.

Since none of these background subtraction methods are correct nor incorrect, it is worth mentioning their advantages and disadvantages. The single ROI background subtraction method has the advantage of subtracting a neuropile ROI dynamically. Since we could observe experimentally that the AM version of Cal520 can stain the tufts of the AM loaded cells, it follows that it may also invade other subcellular compartments, such as the basal dendrites and axons of cells found below the imaged field of view.

Subtracting, therefore, a background ROI may already be very conservative, as the dendrite and axonal calcium signals that are intermingled in the neuropil may well be larger than those recorded in the actual somas. This may mean that part of the somatic signal is extracted from the somatic signal. On the other hand, a background ROI made in a nonstained area of the AM-loaded region might not be sufficient to exclude the neuropil contribution, and therefore artificially generate more similarly tuned cells in the imaged field of view.

This background subtraction method was used however also in calculating the somatic calcium trace corresponding to the spiking activity. The second, linear fitting method of background subtraction is based on the idea that the neuropil contribution may be different in different areas of the recorded field of view, and therefore calculates the best fit between the neuropile and the somatic activity in order to perform the subtraction. This may be a good point, but like the previous method it may be overconservative and remove a large part of the actual somatic activity.

Finally, the third method which uses actual ROIs that are subtracted from their neighboring somatic ROIs seems to be most appropriate, but it is the subtraction method that most likely subtracts trunk and basal dendrite signals out of the recorded somatic signals, thereby potentially eliminating most of the real somatic signals recorded.

Because the choice for any of these methods is somewhat arbitrary, but rather have different advantages and disadvantages, we decided to perform an experiment that would give us the true tone responses without any contribution from the neuropil.

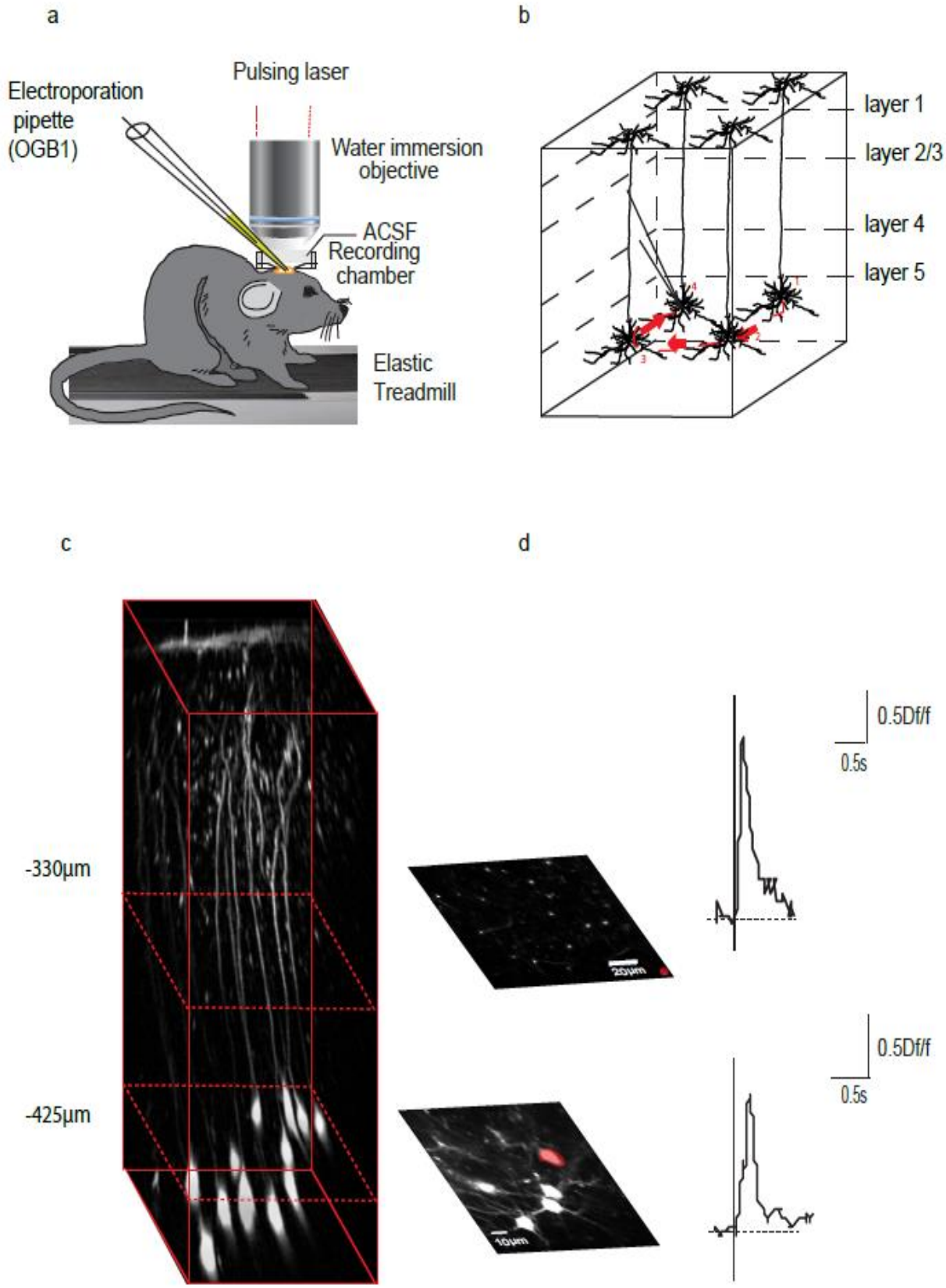

Fig.26. Schematic of the procedure for Targeted Multi-Cell Electroporation (TMCE). a. Experimental setup for two-photon guided electroporation of mul-

tiple cells. b. Schematic of experimental procedure for targeted multi-cell electroporation showing the sequence of cell electroporation. C. z-stack projection of multiple electroporated cells in layer 4. On the right side, average images (n=1000 images from a recording trial) of recording location at the soma and the apical trunk sites, respectively. d. Example single calcium transients recorded from the somas and the trunks, respectively.

The experiments consisted of electroporating multiple cells in the same field of view in either layer 4 or layer 5 with the salt version of OGB1, which is a variation of the electroporation procedure for single cells. Since the dye is designed to remain in the cell, there was no need for any background subtraction.

We called this method targeted multi-cell electroporation (TMCE). Up to 30 cells could be electroporated with up to 100% survival rate in deeper layers. After electroporation, the trunks of these cells were all imaged in one field of view and the same sound stimulation was performed as in the case of AM-loaded cells.

The reason why we decided to image the trunks and not the somas is that electroporation often leads to dye saturation at the level of the cell somata, while the OGB1-6K-loaded trunks of these cells give the best one action potential resolution and follow the spiking activity linearly, based on the extensive data set acquired with single cell electroporation and cell-attached recordings. As Fig.32d shows, the calcium transients recorded in the apical trunks show faster rise times and higher Df/f. The fast rise times are particularly important for tonotopy mappins, as a fast response (in the range of a few ms from the stimulus onset) is, in the case of the auditory cortex, a good indication that the recording site is indeed in the primary auditory cortex of the mouse and not in the belt areas, where response times would be 10-fold longer.

The number of cells which can be electroporated in a single cluster with the TMCE method depends on many factors. One of them is that the field of view which allows for the simultaneous recording of trunk signals is smaller than for AM-loaded cell somata, due to the difference in size between trunks and cell somata. Second, multi-cell electroporation implies a certain amount of movement in all directions, which may lead to brain displacement should these movements be too wide. Therefore, electroporating a much larger number of cells may actually cause enough mechanical damage to kill cells in the immediate vicinity that were previously electroporated.

Finally, deep imaging implies raising the laser power in order to penetrate the brain tissue, which is the case in layers 4 and 5 of the cortex. Therefore, applying a large amount of laser power on cells right after they are elec-

troporated and therefore physiologically recovering may destabilize their activity irreversibly. Importantly, mechanical damage due to electroporation would only generate a linear increase in the spiking activity of the cells, by only lowering the cell's threshold for firing an action potential. This was avoided by using the same procedure that was optimized during single cell electroporation and having a waiting time of 1h for the dye to load into the

cells.

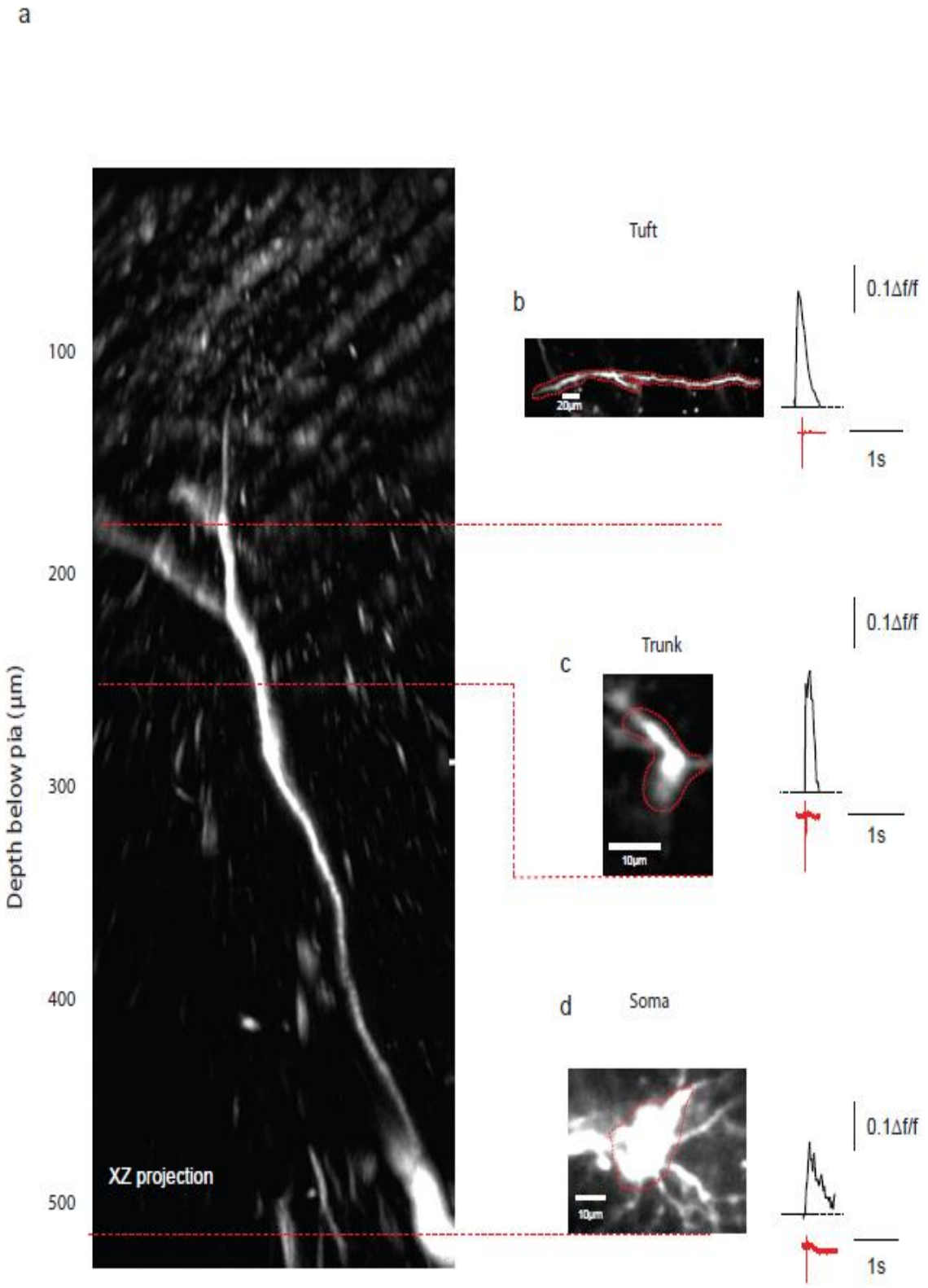

Fig. 27. Combined electroporation and cell-attached recordings. a. z-stack projection of a single electroporated layer 5 cell. Scale bar = 70µm. b. Image at

high magnification of tuft dendritic segments as indicated in b. Left, single action-potential-induced calcium transients in the three dendritic segments. c. Image at high magnification of the trunk of the cell depicted in b. Left, action-potential induced calcium transients in the the trunk. d. Image of high magnifi--cation of the soma of cell depicted in b. Left, single action-potential induced calcium transients in the soma.

Fig.27 shows that single action potentials can be reliably detected as calcium transients in electroporated cells in all compartments of a single cell. An important observation we made was that the detected single-action potential-induced calcium transients are larger and have faster rise times in the apical trunk, and this could therefore be a good imaging location if more cells are electroporated.

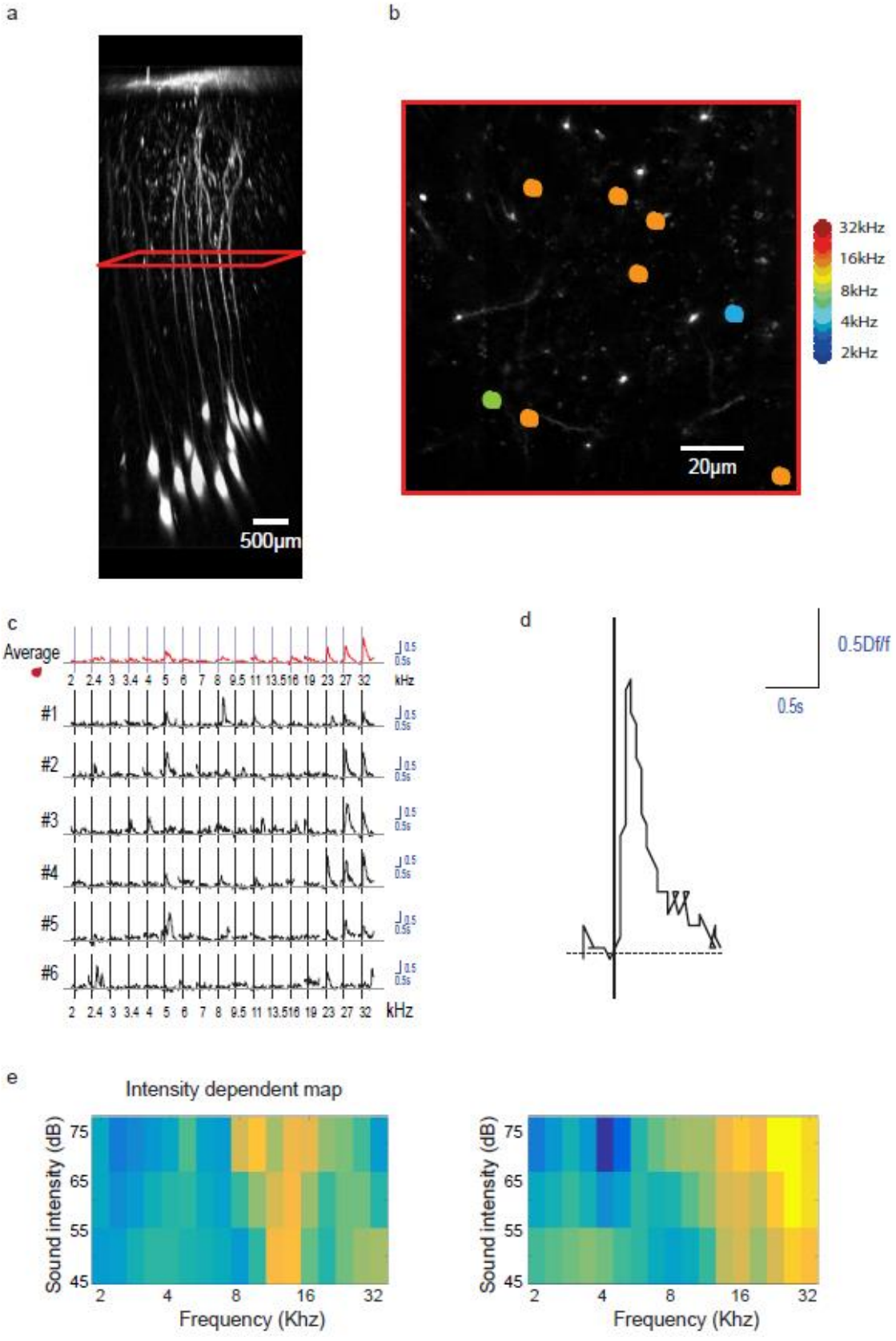

Fig.28. Fig. 4. L4 maps in awake mice. a.z-stack of cells in layer 5 electroporated with the TMCE method. b. Merged high-resolution image of imaged

trunks of layer 4 cells (average of 500 images) showing tuned responses to pure tones (right, color code for frequency range). c. Average and single trial responses to pure tones of a ROI marked in b. Red trace shows the average responses, and black traces show single trial responses to pure tones. d. Example single trial response to a given tone as shown in c. scale bar=0.5s. e. Examples of intensity dependent maps for two cells marked in b.

The results obtained with trunk imaging of electroporated cells had the major advantage of not having any neuropile contribution due to the nature of the dye, and threrefore gave us undeniable proof that tonotopy at the imaged scale we used has a relatively heterogeneous nature, but does show clusters of similarly tuned neurons (Fig. 32b). The imaged field of view that includes the trunks of up to 30 electroporated cells in the same field of view in layer 4 (Fig. 32a) is around 150x150 µm. One of the first observations which could be made in layer 4 and is consistent across imaging methods was that a large number of cells showed tuning for more frequencies, and which showed clear responses around the (most) preferred frequency. This is consistent to a large extent with the literature based on electrophysiological studies of tonotopy of the mouse auditory cortex[4041]. Importantly, both trunk and AM-based population imaging reveal that although there is a tendency for nearby cells to have similar tuning properties, it is definitely not the case that all or most cells in layer 4 respond to the same frequency as the data of Winkowski et al would suggest.

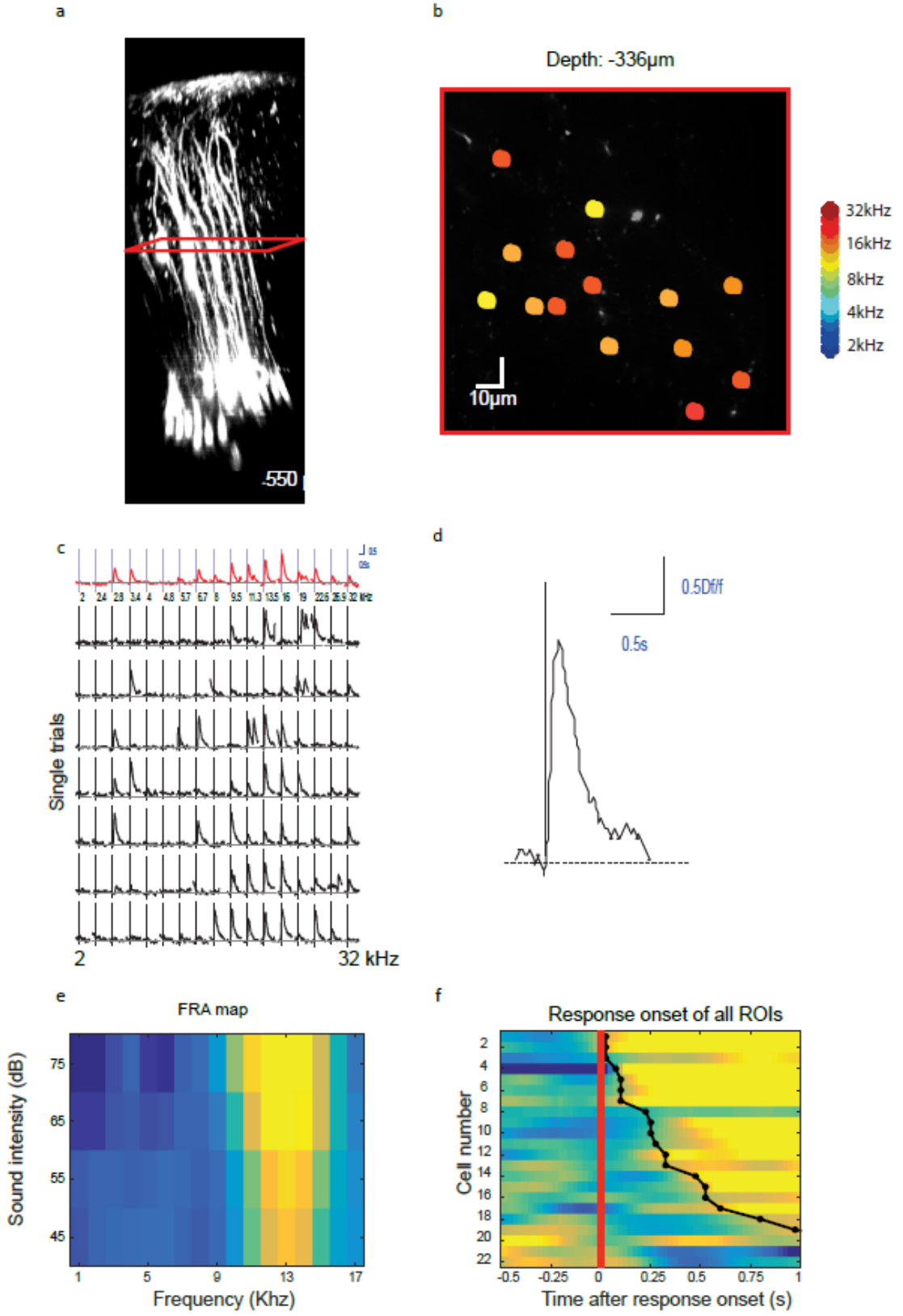

Fig. 29. Fig.7. L5 maps. a. z-stack of cells in layer 5 electroporated with the TMCE method. b. Merged high-resolution image of imaged trunks of layer 5 cells (average of 500 images) showing tuned responses to pure tones (right,

color code for frequency range). c. Average and single trial responses to pure tones of an ROI marked in b. Red traces shows the average responses, and black traces show single trial responses to pure tones. d. Example single trial response to a given tone as shown in c. scale bar=0.5s. e. Intensity-dependent FRA map for the cell described in c. f. Response onset of all cells marked in b.

As in the case of layer 4, trunk imaging of layer 5 neurons reveals clustering of similarly tuned trunks. As in layer 4, many cells show fairly wide tuning curves, with clear responses around the preferred frequency. In the case of layer 5, however, the clustering appears to be somewhat stronger, with stronger single-cell responses to individual pure-tone trials. Since this is the data showing tonotopy in layer 5 of the mouse auditory cortex, it is very important to account for potential distortions of the calcium transients due to previous depth limitations. The trunk imaging results obtained with the MTE offer proof of heterogeneity with a tendency for clustering that is stronger in layer 5 than in layer 4.

Layer 5 of the mouse auditory cortex is dominated by large pyramidal neurons[42]. In terms of connectivity, it is known that lemniscal thalamic input ends in the middle layers of the A1, the major cortico-cortical connections arise in layers 2 and 3, and the subcortical projections should originate primarily in layer 5, with layer 6 sending feedback projections to the thalamus. Feedback to the auditory thalamus (MGB) originates predominantly in layer 6 but also in layer 5, with projections to the inferior colliculus originating in layer 5. [434445]

The layer 4 trunk imaging data includes 96 trunks out of which 31 were found to be significantly tuned, while the layer 5 trunk imaging data includes 108 cells out of which 47 were found to be tuned. The slight increase in tuned cells also matches the frequency of calcium transients found in the trunks of layer 5 neurons.

To conclude on the data presented above as well as the studies on tonotopy mentioned so far, it appears that there is stronger heterogeneity in deeper layer of the A1 than previous imaging experiments would suggest. The reasons for disagreement between tonotopy studies could stem from the different types of stimuli used, the different types of anesthesia and their effect on cortical state, the lack of spatial information in electrophysiological studies, but also, as I have stressed in this chapter, the amount of neuropil contamination in AM loading studies, which can switch a tonotopic map from being highly homogeneous to looking highly heterogeneous. I hope that I have shown in this chapter that this issue is extremely important and should be controlled for. The targeted multi-cell electroporation method is therefore the most reliable for performing population imaging in deeper cortical layers, by complete-

ly removing the problem of neuropil contamination. Further AM loading tonotopy studies can therefore profit from this method and design the analysis as to fit the results of the TME.

5) Discussion

The main achievement of my doctoral work has been to develop a method that allows for improved single cell and population imaging that would help in getting a more accurate picture of cortical integration ranging from single spines to neuronal circuits. This method involved the combination of the LOTOS procedure with electroporation of single cells which was combined with cell-attached recordings (EC) or with targeted multicell electroporation (TMCE). The applications of these methods allowed for reliable recordings of subthreshold calcium transients in dendrites and spines during sensory stimulation as well as population imaging of trunks of electroporated cells which generated heterogeneous tonotopy maps in the mouse auditory cortex.

When performing single spine and dendrite imaging with the EC, we were able to record subthreshold dendrite and spine calcium transients in tuft dendrites of layer 3 neurons in the mouse auditory cortex. Moreover, we were able to obtain very reliable responses to white noise stimulation in tuft dendrites of these neurons. These results suggest that tuft dendrites do have an important role in functional integration and that there is no need for simultaneous action potential firing in these cells. By combining the method of single cell electroporation with bolus loading of the AM version of Cal520, we were able to confirm these results in unanesthetized animals.

The auditory system is one of the most well understood physiological systems, ranging from how sound waves are produced by vibrating objects, to the vibration these waves produce in the cochlea, to it being transduced into an electrical signal, which propagates through the thalamus and arriving into the primary auditory cortex. Despite the clarity of the sound wave-electric signal transformation, and many decades of research on what exactly the auditory cortex does, it is not clear how exactly it is that we process these sound waves. This made the auditory cortex particularly interesting for me, as a physical understanding of a large part of sound processing may help in finding a general principle for integration.

The issue of tonotopy, as illustrated by the Indian parable, includes many different methods and approaches and has led to very contradictory results so far. In the case of the auditory cortex, this decade-long debate has

started with multi-unit electrophysiological mapping[46474849] studies. These studies have the advantage of recording the electrical activity directly, but lack spatial information both in terms of the recorded area and cortical depth, as well as in terms of distinguishing between different cells, in the case of LFP and multi-site electrode recordings. Furthermore, as Issa et al and Rothschild et al point out, these studies may be amplifying the responses of highly active neurons and ignoring the contribution of less active ones. Population imaging studies have the advantage of single cell resolution and can provide single-cell based tonotopic maps, but are however limited by the quality of the calcium measurement as an indirect reporter of electrical activity. Bolus loading (Stosiek et al) has been used for tonotopy mapping (Rothschild et al) of the mouse A1. These results suggest that at least within layer 2/3, the maps are quite heterogeneous. These results were later on to a large extent contradicted by the findings of Issa et al, which show that multiscale tonotopic mapping allows for reliable measurement of similarly tuned neurons within the same frequency area of the A1, as previous electrophysiological studies would suggest. We have addressed this issue in our AM loading experiments in unanesthetized mice, and have found that even without much background subtraction the tonotopy maps observed look more heterogeneous than expected. The discussion on whether the tonotopy of the auditory cortex is homogeneous or heterogeneous has been examined with different kinds of electrophysiological recordings (multi-site electrode studies, LFP, cell-attached recordings etc.), different imaging methods and different calcium indicators (genetically encoded or chemical, having more or less neuropil contribution) as well as very different auditory stimulation paradigms (pure tones, white noise, click trains, natural sounds, SAM tones all with different durations and intensities).

The auditory cortex of the mouse is known to have 5 subregions. The largest one is the primary auditory one (A1), and has a tonotopical gradient going to low, high and then again low frequency-tuned areas. The anterior auditory field or AAF is the second largest and also has a tonotopic map but this time with the order of frequency tuned areas reversed. The second auditory field (A2), dorsoposterior field (DP) and the ultrasonic fields are smaller and do not show a clear tonotopy. The main inputs to the auditory cortex come from the thalamic medial geniculate body (MGB), arriving at cortical layers 3 and 4. The auditory cortex itself projects back into the thalamus from layers 5 and 6.[50]

After looking at integration from the perspective of a single cell, I noticed a strong gradient ranging from a complete lack of tuning to sensory stimuli either in an entire cell or in dendrites or spines, up to perfect tuning to a single frequency of an entire cell and all its inputs. Based on my previous experience with the mouse auditory cortex and its high number of cells respond-

ing to sound stimulation, I decided use the technical advantages that come with fast two-photon imaging in order to look at the deep cortical tonotopy at the population level in layers 4 and 5 of the mouse auditory cortex.

There have been several papers showing the need to understand computation in the A1 at the population level. In the auditory cortex, there has been a debate lasting over 4 decades on the nature of cotuning of nearby neurons[51] . On the one hand, electrophysiological studies have shown a clear tonotopic gradient in the A1, ranging from the low-frequency responsive area to the high frequency responsive area. On the other hand, most in vivo imaging studies seem to suggest that there is strong heterogeneity at the level of single cells. The long-lasting debate on the tonotopy of the mouse visual cortex bears its similarities to an Indian parable about six blind men. Although all men were ''To learning much inclined'' and had high hopes ''That each by observation/ Might satisfy his mind.''[52], each went to examine a different part of an elephant's body with their hands, such as the tail, the trunk and a leg, and individually come up with very different descriptions (either a wall, a spear, a snake, a tree, a rope etc.).

At first glance, it would appear that electrophysiology and imaging studies in the mouse A1 show a perfect contradiction. The first set of studies claim that there is quite some homogeneity, and the other one reveals a strong homogeneity.

However, there are a large number of considerations that need to be taken into account. Firstly, most of these studies use very different kinds of auditory stimulation: SAM tones vs. pure tones, static vs. different amplitudes, sound durations ranging from a few dozen miliseconds to a few hundred miliseconds, and different frequency ranges which sometimes don't even overlap.

Population imaging studies also have their contradictions: while Rotschild et al suggest that tonotopy is broken down at the level of single cells, Issa et al argue that multiscale tonotopy mapping allows for locating areas within the A1 which include very similarly tuned neurons. There are a number of reasons which might account for this contradiction: The Rothschild et al study was made in anesthetized, while the Issa et al study was made in unanesthetized animals, although Rothschild et al point out that wakefulness might in fact lead to a less tonotopical map than that observed in anesthetized animals. Secondly, the first study uses short pure tones, while the latter uses long SAM tones. Thirdly, the large scale imaging method might have cause less variability in the recording site, and therefore yield confusing results. In fact, multiscale imaging might yield some of the most controlled experiments in the mouse A1, given its small size (1x3 square mm), and the fact that its neighbouring areas, such as the A2, DP and AAF also show some frequency tuning. The findings of Issa et al do seem to be in agreement, howev-

er, with previous microelectrode mapping studies of A1[535455]. However, as mentioned by Rothschild et al, electrophysiological studies of A1 tonotopy also have their limitations. Single unit recordings might favor the most active neurons, and so do multiunit recordings. Two-photon Ca^{2+} imaging may include a large number of weakly active neurons. Furthermore, two-photon imaging studies on A1 tonotopy had focused mostly on layer 2/3 neurons due to depth limitations of two photon imaging, while many of multielectrode studies focus on deeper layer 4, where the tonotopy is expected to be stronger. Anesthesia might affect A1 tonotopy negatively but also positively, as Issa et al show. In short, there is a strong contradiction related to A1 tonotopy, and there are many factors which may contribute to these contradictions.

To summarize, the studies of Rothschild and Issa et al are both based on the idea of exploring tonotopy in layer 2/3 of the mouse auditory cortex. They show fairly different results, in that the latter confirms a reasonable amount of cotuning, while the first argues for heterogeneity at the fine scale. It is now obvious that it is necessary to compare the anesthetized with the awake condition.

To conclude on the studies presented so far, the moral of the case of understanding tonotopy in the mouse auditory cortex is quite similar to that of other questions related to cortical integration and is summed up very nicely by the Indian parable: ‘’*So oft in theologic wars,/The disputants, I ween,/Rail in utter ignorance/Of what each other mean./ And prate about an Elephant/Not one of them has seen!*’’

Winkowski et al have performed two-photon imaging in layer 2/3 and layer 4 of the mouse auditory cortex and concluded that while layer 2/3 neurons exhibit strong heterogeneity (in accordance with Rothschild et al and in contradiction with Issa et al), layer 4 shows a striking tonotopy. In fact, layer 4 neurons appeared to be tuned mostly to one single frequency. This discrepancy is striking but at the same time possible considering the fact that layer 4 should be the main thalamorecipient layer, and given the limitations of deep two-photon imaging. I have therefore decided to examine a new part of the elephant with the hope of gaining new insight on the full picture.

Given all this existing information, it makes sense to further examine cortical A1 tonotopy more deeply using improved two-photon imaging techniques and the LOTOS standard of 1-action potential resolution, unanesthetized animals, thereby perform high-quality two photon deep imaging with a focus on layers 4 and 5 of the mouse auditory cortex.

The first in vivo population imaging study in the anesthetized mouse A1 that was made by Rothschild et al revealed the heterogeneity of its layer 2/3 tonotopy. The FRA maps obtained in their study reveal very different best frequencies among nearby cells. In this study, only 42% of the imaged neurons

appeared to be responsive to the stimulation (376 out of 895), while only 16% of neurons showed frequency tuning. These data were contradicting electrophysiological studies in the mouse A1 made in the mouse[56], rat[57] and monkey[58]. The authors speculate that this could be due to limitations in electrophysiological recordings: multi-site recordings may amplify some stronger signals in the detriment of others through averaging responses of many neurons. Other studies which have examined tonotopy using intrinsic optical imaging[59] or voltage-sensitive dyes[60], the authors claim, also failed to extract information from single neurons.

Despite the local heterogeneity, the authors did point out some structures within the A1 organization. They found that nearby neurons were more similarly tuned on average compared to distant neurons, suggesting a tendency for forming the large-scale tonotopic maps observed so far only with electrophysiology. This tendency for tonotopy became apparent at distances larger than 250 µm, and very little tonotopy was observed at scales below 100 µm.

Another important study on the tonotopy of layer 2/3 mouse A1 came from Issa et al, who showed reasonable cotuning in layer 2/3 in the unanesthetized mouse A1. Before doing two photon imaging, the team first performed camera-based imaging of large GCaMP-labeled areas while stimulating with low, medium and high-frequency SAM tones, respectively.

By imaging the presumed A1 area with a regular CCD camera during the presentation of low-, middle-, and high- frequency SAM tones respectively, the authors noticed specific areas showing strong fluorescence in response to each of these three categories of stimuli, and then performed two-photon-based population imaging in the previously mapped area. After finding the low-frequency responsive area they could find reliable responses to the low-frequency tones in unanesthetized animals, which is now similar to the tonotopy map given by multi-electrode recordings. These tonotopy maps could be adapted to different mice and kept, to some extent, a general structure throughout all animals imaged.

Issa et al showed clearly co-tuned clusters of neurons in areas pre-identified as low-, middle- or high-frequency mouse primary auditory cortex. These findings clearly show a much stronger homogeneity in in tuning in the mouse layer 3 of the primary auditory cortex. The authors also compared their results with those of Rothschild et al and show that while in Rothschild et al the distribution of best frequencies does not show a dependence on the distance between neurons, in the present study, most neurons within 100 µm for each other appear to be less than 0.5 octaves apart in terms of their best frequency. Therefore, at this point, it seems not only that Issa et al had found much stronger homogeneity in the tonotopy of the mouse A1 than Rothschild

et al, but that the two studies would lead to opposite hypotheses: one says the tonotopy is broken down at the small scale, and the other one says it is clearly not.

Meanwhile, electrophysiological studies have shown a large number of cells which are strongly tuned to specific frequencies, and a very clear tonotopic gradient, and therefore a columnar arrangement in the mouse auditory cortex, at least at the large scale. On the other hand, population imaging studies[61] revealed a tonotopy map that remains homogeneous at the large scale but it broken down at single-cell level.

It was therefore clear that it is important to understand: first, which method is closest to the truth, and second, how exactly heterogeneous circuits at the fine scale produce a homogeneous tonotopical organization at the large scale. Single cell and population imaging studies have shown strong evidence for disorder and heterogeneity in the mouse auditory cortex, somewhat similarly to the salt-and-pepper organization of the visual cortex. From the perspective of single cells, Chen et al show that nearby spine inputs on a single cell in the mouse A1 can be tuned to very different frequencies, showing that nearby cells are tuned to very different frequencies themselves. The small distance between differently tuned spines shown by Chen et al 2010 further strengthens the notion that nearby neurons have different tuning properties in layer 2/3 of the mouse auditory cortex. Winkowski et al[62] have shown that while this is indeed the case in layer 2/3 of the A1, revealing a strong heterogeneity at a fine scale, the thalamorecipient layer 4 shows strong homogeneity and a large number of cotuned cells next to each other. The disorder and lack of homogeneity suggested by population imaging studies are is based on recordings made mostly in layer 2/3 of the mouse auditory cortex, with little information about deeper cortical layers of the A1. It is important to mention at this point that deep imaging has its limitations, and this has been one of the reasons we decided to revisit mouse A1 tonotopy in deeper layers with an improved technique for two photon imaging, unanesthetized animals, improved dye loading, and background subtraction that matches single cell results. This curiosity was also fueled by the study of Winkowski et which al suggests with AM-based population imaging that layer 4 should be far more homogeneous than layer 2/3.

By applying the TMCE to deeper layers of the mouse auditory cortex during pure tone stimulation, we observed that layers 4 and 5 have rather heterogeneous tonotopic maps. However, this only one of the many potential applications of the method.

Both single cell and targeted multi-cell electroporation can be easily applied to other systems, awake behaving animals and different calcium dyes, such as genetically encoded calcium indicators. These methods can be com-

bined with deep imaging methods, such as that of using a prism or a microendoscope in order to reach deeper brain structures, and can be used to assess the linearity of newly developed dyes. An important step forward for exploring cortical integration would be to also combine voltage dyes with electrophysiology in order to get a direct measurement of the voltage changes in subcellular compartments such as spines and dendrites. Blind electroporation could also be used to image layer 6 cells of the mouse cortex, and trunk imaging could be performed in order to obtain a tonotopic map of these cells. Another important future direction is to mark specific populations of neurons within an imaged population, such as 5-HT3 receptors with the 1-(m-Chlorophenyl)-biguanide (mCPBG) 5-HT3 receptor agonist and assess the contribution of specific interneuron subpopulations to the overall tuning.

The contribution of different cellular subpopulations can be assessed by using optogenetic stimulation of either particular interneuron subtypes, for example, to assess their contribution to tonotopy maps in the mouse auditory cortex. This method can also be used for exploring the contribution of different brain areas to these maps, since it is known that layer 4 of the A1 is the major thalamorecipient layer, while layers 5 and 6 should project to the thalamus themselves.

Moreover, imaging single neurons can be done also in 3D, either by using a compact acousto-optical lens[1] or by simply reducing the optical sectioning via underfilling of the back aperture. This would help in obtaining a larger picture of single cell integration.

Since the topic of integration is extremely wide and complex, the results presented above are by no means exhaustive and only serve to illustrate some applications of these methods. Hopefully, I have shown that one can get closer to a causal understanding of single cell integration by not affecting intracellular signaling and simultaneously recording the output and inputs in different cellular subcompartments. Going back to the Indian parable about the 6 blind men examining an elephant, the aim of these studies is to show that the animal can be examined from different parts and that this can give a clearer picture of what the animal may be.

Regarding the issue of finding the ideal unit for cortical computation of sensory inputs, I have found that this unit can be either a single neuron, a dendrite or spine, an entire network, a cortical layer and even entire brain areas and all of these can be considered to be a computational unit depending on the scientific question. Moreover, I hope I have convinced you that the same scientific question can be addressed by looking at multiple units at the same time, thereby removing the boundaries between functional modules. For example, I have used both single cells and neuronal populations in order to explore tonotopy, and I have made use of imaging multiple tuft dendrites

of layer 4 and 5 neurons in order to see whether layer one of the mouse auditory cortex can indeed respond reliably to white noise stimulation. These results can help in understanding what the function of the tuft really is or how tonotopy looks like in a given layer.

What I hope to have shown in these studies is that a scientific question can be approached by examining different units at the same time and that their advantages can be combined in order to obtain a more accurate picture of neuronal integration ranging from single spines to entire neuronal populations.

4) Summary

To summarize on the results shown so far, we have used the LOTOS procedure for two-photon calcium imaging in vivo on electroporated neurons in different cortical layers and brain areas in order to explore input integration in physiological conditions, with the aim of getting a more causal understanding of subcellular calcium signaling and the firing output in both spontaneous conditions and during sensory stimulation. In doing so, we have found subthreshold single dendritic calcium transients as well as single spine calcium transients both spontaneously and during auditory stimulation. When applying this method to layer 3 tufted neurons in the auditory cortex, we could observe reliable subthreshold responses in tuft dendrites, and these results were confirmed in unanesthetized animals. Furthermore, these effects can be modulated by local application of Muscimol, showing that these sound-evoked calcium transients can be observed in tuft dendrites in the absence of backpropagating action potentials.

At the population level, we have explored tonotopy in deeper layers of the mouse auditory cortex by means of a two-photon guided local application of the calcium dye Cal520. We were able to observe large and isolated calcium transients in single neuronal somata at depths varying between 450 and 700 µm, corresponding to layers 4 and 5 of the mouse auditory cortex, in both anesthetized and unanesthetized animals. In order to account for the issue of neuropil contamination in AM loading experiments, we have developed a new method called Targeted Multi-Cell Electroporation (TMCE) which allowed us to examine tonotopy in conditions where there is no neuropil contribution.

To conclude, the studies presented so far show the applications of the combined electroporation and cell-attached method and the Targeted Multi-Cell Electroporation (TMCE). On the single cell level, these results show that there are many modes of integration in single cells and that subthreshold calcium transients can be detected reliably in vivo, that tuft and basal dendrites behave very differently, and that tuft dendrites can be reliably activated by

sound stimulation, and finally that this effect can be modulated without affecting intracellular calcium concentration. At the population level, these results show that there is strong heterogeneity in deeper layers of the mouse auditory cortex, and that layer 5 neurons behave differently from layer 4 neurons in terms of tuning.

6) Acknowledgements and contributions

I would like to thank my supervisor, Prof. Arthur Konnerth, for day-by-day supervision as well as the detailed design of the studies and experiments. Within the 4 years of my Phd in his lab, I have had the opportunity of interacting and teaming up, either as a trainee or a trainer with people from different fields, such as Biophysics, Medicine, Physics, and Engineering. Together, we have explored the brain with state-of-the-art techniques and amazing technical support. This allowed me to develop my own perspective on Neuroscience, and these friendships have also sculpted my view of the world. I have learned a lot about science and life and have experienced science from its most frustrating lows to levels of exaltation that are only meant for poets.

I have started out in the lab as the trainee of Dr. Nathalie Rochefort who was extremely patient and kind and has taught me my most basic experimental skills, as well as helping me implement electroporation and cell-attached recordings as a method for exploring input-output computation in single neurons. She therefore contributed experimentally to the data obtained in the visual cortex and most importantly to my crossover into Neuroscience by teaching me the basics of cellular physiology. Other people in the lab, such as Christine Grienberger, Hongbo Jia, Valerie Bonfardin and Thomas Wegehaupt have also contributed to this study, and, again, to my conceptual . I would estimate my contribution to this dataset to be around 60% for this first study. I would also like to thank Xiaowei Chen for allowing me to contribute to the LOTOS method and to follow up on it.

Later on, I have continued working in a team with Antje Birkner and explored the limits of single cell imaging as well as deep imaging in the mouse auditory cortex. I would like to thank her especially for continuous technical and moral support. She has learned from me and contributed to the applications of the electroporation and cell-attached recordings in layer 3 tufted neurons by helping with implementing auditory stimulation and endless technical support. I would estimate my experimental contribution to this study to be around 60%.

In the last phase of my Phd, I have worked in a team with Takashiro Noda, whom I would like to thank for his vital contribution in terms of concep-

tual understanding of the mouse auditory cortex and for teaching me how to conceptualize and analyze scientific data. His contribution to deep imaging of cortical integration in the A1 has been the most important of them all. I would estimate my contribution to this project to be 60%.

I would also like to thank Christian Obermeyer, Felix and Dietmar Beyer and Andreas Fohr for excellent technical assistance and friendly atmosphere, as well as Helmuth Adelsberger and Israel Nelken for long-distance guidance and substantial help with understanding auditory cortex data. Prof. Thomas Misgeld has delivered one of the best courses I have ever attended and made me like microscopy. I want to thank everyone in the Institute for the great atmosphere. I can only hope to find more people like them in the future, and that I can inspire the people around me to be as genuine and sharp as they are.

Finally, I have been lucky enough to be surrounded in my spare time by people whom I love and who have inspired me, including my family and my friends. This work would not have been possible without them.

7) Publications and related activities

1. Langfelder A, Okonji E, Deca D, Wei WC, Glitsch MD. Extracellular acidosis impairs P2Y receptor-mediated Ca(2+) signalling and migration of microglia. Cell Calcium. 2015 Apr;57(4):247-56. doi: 10.1016/j.ceca.2015.01.004.

2. Deca D, Koene RA. Experimental enhancement of neurphysiological function. Front Syst Neurosci. 2014 Oct 8;8:189. doi: 10.3389/fnsys.2014.00189.

3. Charest I, Kievit RA, Schmitz TW, Deca D, Kriegeskorte N. Unique semantic space in the brain of each beholder predicts perceived similarity. Proc Natl Acad Sci U S A. 2014 Oct 7;111(40):14565-70. doi: 10.1073/pnas.1402594111.

4. Kriegeskorte N, Walther A, Deca D. An emerging consensus for open evaluation: 18 visions for the future of scientific publishing. Front Comput Neurosci. 2012 Nov 15;6:94. doi: 10.3389/fncom.2012.00094.

5. Chen X, Leischner U, Varga Z, Jia H, Deca D, Rochefort NL, Konnerth A. LOTOS-based two-photon calcium imaging of dendritic spines in vivo. Nat Protoc. 2012 Oct;7(10):1818-29. doi: 10.1038/nprot.2012.106.

6. Deca, D. Available tools for whole-brain emulation. Int. J. Mach. Conscious., 04, 67 (2012). DOI: 10.1142/S1793843012400045

7. Koene, R., Deca, D. Whole Brain Emulation seeks to Implement a Mind and its General Intelligence through System Identification. Journal of Artificial Intelligence Research 12/2013; 4:1-9. DOI:10.2478/jagi-2013-0012

In preparation: first-author manuscript on TMCE.

References

[1] Rochefort, N. and Konnerth, A.,Dendritic spines: from structure to in vivo function, EMBO Reports, Volume 13, Issue 8, pages 699–708, 2012

[2] García-López P, García-Marín V, Freire M. The discovery of dendritic spines by Cajal in 1888 and its relevance in the present neuroscience. Prog Neurobiol 2007 83: 110–130

[3] Shepherd, G. The dendritic spine: a multifunctional integrative unit. J Neurophysiol 1996 75: 2197–2210

[4] Chen, X., Leischner, U., Rochefort, N.L., Nelken, I., Konnerth, A.. Functional mapping of single spines in cortical neurons in vivo. Nature. 2011 ;475(7357):501-5. doi: 10.1038/nature10193.

[5] Chen, T.W., Wardill, T.J., Sun, Y., Pulver, S.R., Renninger, S.L., Baohan, A., Schreiter, E.R., Kerr, R.A., Orger, M.B., Jayaraman, V., Looger, L.L., Svoboda, K., Kim, D.S. Ultrasensitive fluorescent proteins for imaging neuronal activity. Nature. 2013;499(7458):295-300. doi: 10.1038/nature12354.

[6] Grienberger, C., Chen, X., Konnerth,A. Dendritic function in vivo, Trends in Neurosciences January 2014, Vol. 38, No. 1.

[7] Bading, H. Nuclear calcium signalling in the regulation of brain function. Nat. Rev. Neurosci. (2013) 14, 593–608

[8] Spruston, N. Pyramidal neurons: dendritic structure and synaptic integration. Nat. Rev. Neurosci. 9, 2008 206–221

[9] Yuste R. Dendritic spines and distributed circuits. Neuron, 2011, 71: 772–781

[10] Stuart,G., Spruston, N., Häusser , M. Dendrites., Oxford University Press, 2008, ISBN 978-0198566564

[11] Larkum, M.E. et al. Synaptic integration in tuft dendrites of layer 5 pyramidal neurons: a new unifying principle. Science 2009 325, 756–760

[12] Larkum, M.E. et al. A new cellular mechanism for coupling inputs arriving at different cortical layers. Nature, 1999, 398, 338–341

[13] Mel, B.W. Synaptic integration in an excitable dendritic tree. J. Neurophysiol. 70, 1993, 1086–1101

[14] Polsky, A. et al. Computational subunits in thin dendrites of pyramidal cells. Nat. Neurosci. 7, 2004, 621–627

[15] Jia, H., Rochefort, L. N., Chen, X., Konnerth, A. Dendritic organization of sensory input to cortical neurons in vivo. Nature, 2010, 464, 1307–1312, doi:10.1038/nature08947

[16] Palmer, L. M., Shai, A.S.,Reeve,J.E., Anderson, H.L., Paulsen, O., Larkum, M.E. NMDA spikes enhance action potential generation during sensory input. Nature Neuroscience 2014, 17, 383–390 doi:10.1038/nn.3646

[17] Xu, N.L., Harnett, M.T., Williams, S.R., Huber, D., O'Connor, D.H., Svoboda, K., Magee, J.C. Nonlinear dendritic integration of sensory and motor input during an active sensing task. Nature, 2012 Dec 13;492(7428):247-51. doi: 10.1038/nature11601.

[18] Smith, L.S., Smith, I.T., Branco, T., Häusser, M. Dendritic spikes enhance stimulus selectivity in cortical neurons in vivo. Nature, 2013, 503, 115–120, doi:10.1038/nature12600

[19] Longordo, F., To, M.S., Ikeda, K., Stuart, G.J. Sublinear integration underlies binocular processing in primary visual cortex. Nat Neurosci. 2013 Jun;16(6):714-23. doi: 10.1038/nn.3394.

[20] Cichon, J., Gan, W.B. Branch-specific dendritic Ca(2+) spikes cause persistent synaptic plasticity. Nature., 2015;520(7546):180-5. doi: 10.1038/nature14251.

[21] Hagenston, A. M. , Bading, H. Calcium Signaling in Synapse-to-Nucleus Communication. Cold Spring Harb Perspect Biol., 2011,;3(11):a004564. doi: 10.1101/cshperspect.a004564.

[22] Andermann, M.L., Gilfoy, N.B., Goldey, G.J., Sachdev, R.N.S., Wölfel, M., McCormick, D.A., Reid, C.A., Levene, M.J. Chronic cellular imaging of entire cortical columns in awake mice using microprisms. Neuron. 2013; 80(4): 10.1016/j.neuron.2013.07.052. Published online 2013 October 17. doi: 10.1016/j.neuron.2013.07.052

[23] Jennings, J.H., Ung R.L., Resendez S.L., Stamatakis A.M., Taylor J.G., Huang, J., Veleta, K., Kantak, P.A., Aita M., Shilling-Scrivo, K., Ramakrishnan, C., Deisseroth, K., Otte, S., Stuber, G.D.. Visualizing hypothalamic network dynamics for appetitive and consummatory behaviors. Cell., 2015;160(3):516-27. doi: 10.1016/j.cell.2014.12.026.

[24] Bandyopadhyay, S., Shamma, S.A., Kanold, P.O.. Dichotomy of functional organization in the mouse auditory cortex. Nat Neurosci. 2010;13(3):361-8. doi: 10.1038/nn.2490. Epub 2010 Jan 31.

[25] Issa, J.B., Haeffele, B.D., Agarwal, A., Bergles, D.E., Young, E.D., Yue, D.T.. Multiscale optical Ca^{2+} imaging of tonal organization in mouse auditory cortex. Neuron., 2014,;83(4):944-59. doi: 10.1016/j.neuron.2014.07.009.

[26] Yuste, R., and Denk, W. 1995. Dendritic spines as basic functional units of neuronal integration. Nature,1995, 375, 682–684.

[27] Helmchen, F., and Denk, W. , 2005, Deep tissue two-photon microscopy. Nat. Methods, 932–940.

[28] Chen, X., Leischner, U., Varga, Z., Jia, H., Deca, D., Rochefort, N.L., Konnerth, A. LOTOS-based two-photon calcium imaging of dendritic spines in vivo. Nat Protoc., 2012;7(10):1818-29. doi: 10.1038/nprot.2012.106.

[29] Denk, W., Strickler, J. H. & Webb, W. W. Two-photon laser scanning fluorescence microscopy. Science 248, 1990, 73–76

[30] Berridge, M.J., Bootman, M.D., Roderick, H.L. Calcium signalling: dynamics, homeostasis and remodelling. Nat Rev Mol Cell Biol. 2003 (7):517-29. Review.

[31] Paredes, R.M., Etzler, J.C., Watts, L.T., Zheng, W., Lechleiter, J.D. Chemical calcium indicators. Methods. 2008 Nov;46(3):143-51. doi: 10.1016/j.ymeth.2008.09.025. Epub 2008 Oct 16.

[32] Tada, M. , Takeuchi, A., Hashizume, M., Kitamura, K., Kano, M. A highly sensitive fluorescent indicator dye for calcium imaging of neural activity in vitro and in vivo. Eur J Neurosci. 2014 (11):1720-8. doi: 10.1111/ejn.12476.

[33] Kitamura, K., Judkewitz, B., Kano, M., Denk, W., Häusser, M. Targeted patch-clamp recordings and single-cell electroporation of unlabeled neurons in vivo. Nat Methods., 2008 Jan;5(1):61-7.

[34] Judkewitz, B., Rizzi, M., Kitamura, K., Häusser, M. Targeted single-cell electroporation of mammalian neurons in vivo. Nat Protoc., 2009;4(6):862-9. doi: 10.1038/nprot.2009.56

[35] Oyama, K., Ohara, S., Sato, S., Karube, F., Fujiyama, F., Isomura, Y., Mushiake, H., Iijima, T., Tsutsui, K. Long-lasting single-neuron labeling by in vivo electroporation without microscopic guidance. J Neurosci Methods., 2013 Sep 15;218(2):139-47. doi: 10.1016/j.jneumeth.2013.06.004.

[36] Stosiek, C., Garaschuk, O., Holthoff, K., Konnerth, A. In vivo two-photon calcium imaging of neuronal networks. Proc Natl Acad Sci U S A. 2003 Jun 10;100(12):7319-24.

[37] Grienberger, C., Chen, X., Konnerth, A. NMDA receptor-dependent multidendrite Ca(2+) spikes required for hippocampal burst firing in vivo. Neuron. 2014 Mar 19;81(6):1274-81. doi: 10.1016/j.neuron.2014.01.014. Epub 2014 Feb 20.

[38] Larkum, M.E., Nevian, T., Sandler, M., Polsky, A., Schiller, J. Synaptic integration in tuft dendrites of layer 5 pyramidal neurons: a new unifying principle. Science. 2009 Aug 7;325(5941):756-60. doi: 10.1126/science.1171958

[39] Mouse Brain Atlas, mouse coronal slice - http://atlas.brain-map.org/atlas?atlas=1&plate=100960301#atlas=1&plate=100960224&resolution=11.16&x=6289.95556640625&y=3834.13330078125&zoom=-3&structure=735

[40] Sakata, S., Harris, K.D. Laminar structure of spontaneous and sensory-evoked population activity in auditory cortex. Neuron. 2009;64(3):404-18. doi: 10.1016/j.neuron.2009.09.020.

[41] Guo, W., Chambers, A.R., Darrow, K.N., Hancock, K.E., Shinn-Cunningham, B.G., Polley, D.B. Robustness of cortical topography across fields, laminae, anesthetic states, and neurophysiological signal types. J Neurosci. 2012 Jul 4;32(27):9159-72. doi: 10.1523/JNEUROSCI.0065-12.2012.

[42] Winer, J.A. The functional architecture of the medial geniculate body and the primary auditory cortex. In: The mammalian auditory pathway: neuroanatomy (Webster DB, Popper AN, Fay RR, eds), 1992 ,pp. 222–409. New York: Springer-Verlag.

[43] Huang, C.L., Winer, J.A. Auditory thalamocortical projections in the cat: laminar and areal patterns of input. J Comp Neurol 2000 427:302–331.

[44] Mitani, A., Shimokouchi, M. Neuronal connections in the primary auditory cortex: an electrophysiological study in the cat. J Comp Neurol, 1985 235:417–429.

[45] Mitani A, Shimokouchi M, Itoh K, Nomura S, Kudo M, Mizuno N (1985) Morphology and laminar organization of electrophysiologically identified neurons in the primary auditory cortex in the cat. J Comp Neurol 235:430–447.

[46] Stiebler, I., Neulist, R., Fichtel, I., Ehret, G. The auditory cortex of the house mouse: left-right differences, tonotopic organization and quantitative analysis of frequency representation. J Comp Physiol A. 1997 Dec;181(6):559-71.

[47] Linden, J.F., Liu, R.C., Sahani, M., Schreiner, C.E., Merzenich, M.M. Spectrotemporal structure of receptive fields in areas AI and AAF of mouse auditory cortex. J Neurophysiol. 2003 Oct;90(4):2660-75.

[48] Joachimsthaler, B. , Uhlmann M. , Miller, F. , Ehret, G., Kurt, S. Quantitative analysis of neuronal response properties in primary and higher-order auditory cortical fields of awake house mice (Mus musculus). Eur. J. Neurosci., 2014, pp. 904–918

[49] Hackett, T.A. , Barkat, T.R. , O'Brien, B.M. , Hensch, T.K. , Polley, D.B. Linking topography to tonotopy in the mouse auditory thalamocortical circuit. J. Neurosci.,2011, pp. 2983–2995

[50] Llano, D.A., Sherman, S.M. Evidence for nonreciprocal organization of the mouse auditory thalamocortical corticothalamic projection systems. J Comp Neurol. 2008;507(2):1209-27. doi: 10.1002/cne.21602.

[51] Kanold, P.O., Nelken, I., Polley, D.B. Local versus global scales of organization in auditory cortex. Trends Neurosci. 2014;37(9):502-10. doi: 10.1016/j.tins.2014.06.003.

[52] Saxe, J. G. The Poems of John Godfrey Saxe, Complete edition; Boston: James R. Osgood and Company, (1873)

[53] Guo, W. , Chambers, A.R. , Darrow, K.N., Hancock, K.E., Shinn-Cunningham, B.G., Polley, D.B. Robustness of cortical topography across fields, laminae, anesthetic states, and neurophysiological signal types. J. Neurosci., 32 (2012), pp. 9159–9172

[54] Hackett, T.A., Barkat, T.R., O'Brien, B.M., Hensch, T.K., Polley, D.B. Linking topography to tonotopy in the mouse auditory thalamocortical circuit. J. Neurosci., 2011, pp. 2983–2995

[55] Stiebler, I., Neulist, R., Fichtel, I. , Ehret, G. The auditory cortex of the house mouse: left-right differences, tonotopic organization and quantitative analysis of frequency representation. J. Comp. Physiol. A Neuroethol. Sens. Neural Behav. Physiol., 181 (1997), pp. 559–571

[56] Stiebler, I., Neulist, R., Fichtel, I. & Ehret, G. The auditory cortex of the house mouse: left-right differences, tonotopic organization and quantitative analysis of frequency representation. J. Comp. Physiol., 1997, 181, 559–571.

[57] Kilgard, M.P. & Merzenich, M.M. Distributed representation of spectral and temporal information in rat primary auditory cortex. Hear. Res., 1999, 134, 16–28.

[58] Philibert, B. et al. Functional organization and hemispheric comparison of primary auditory cortex in the common marmoset (Callithrix jacchus). J. Comp. Neurol., 2005, 487, 391–406.

[59] Nelken, I. et al. Large-scale organization of ferret auditory cortex revealed using continuous acquisition of intrinsic optical signals. J. Neurophysiol., 2004, 92, 2574–2588.

[60] Chakraborty, S., Sandberg, A. & Greenfield, S.A. Differential dynamics of transient neuronal assemblies in visual compared to auditory cortex. Exp. Brain Res., 2007, 182, 491–498.

[61] Rothschild, G., Nelken, I., Mizrahi, A. Functional organization and population dynamics in the mouse primary auditory cortex. Nat Neurosci. 2010 Mar;13(3):353-60. doi: 10.1038/nn.2484

[62] Winkowski, D.E., Kanold, P.O. Laminar transformation of frequency organization in auditory cortex. J Neurosci. 2013 Jan 23;33(4):1498-508. doi: 10.1523/JNEUROSCI.3101-12.2013.